CAVITY OPTOMECHANICS

WITH HIGH Q MECHANICAL RESONATORS

by

Tolga Bagci

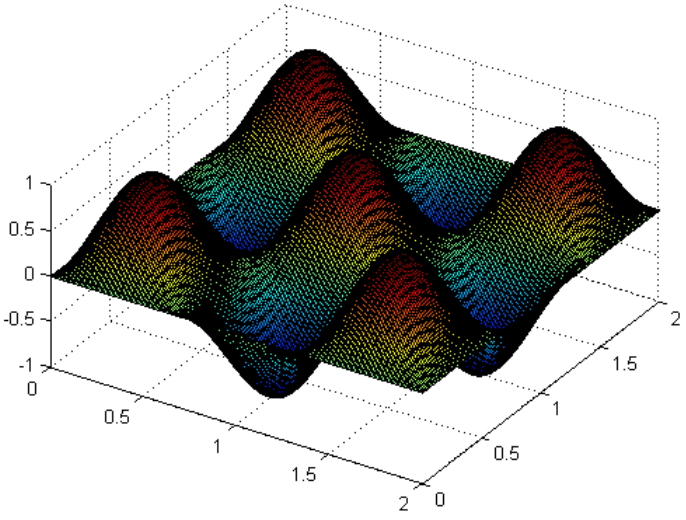

Master of Science

Niels Bohr Institute/QUANTOP

University of Copenhagen

September 2010

under the supervision of Prof. Eugene Simon Polzik

ABSTRACT

The thesis presented here deals with the optomechanical interaction between a mechanical resonator(membrane) and radiation pressure. A two color-probing scheme is proposed for reading out the displacement of a membrane sitting inside a high-finesse cavity, in order to eliminate technical noise as a common-mode signal. In pursuit of a long-term goal in which we hope to see quantum correlations between light and a high Q micromechanical resonator cooled down to the ground-state, an experimental work has been carried out to characterize the eigenfrequencies and Q-factors of the vibrational modes for SiN(stoichiometric form) and GaAs membranes. Both thermal spectrum and mechanical ringdown measurements were performed and the results were compared. The author reports impressive Q-factors(dominantly dependent on clamping loss) for SiN membranes, exceeding 10^6 at room temperature, at frequencies in MHz regime. For the GaAs membrane, measurements yielded Q values exceeding 10^5 in $\approx$ 20 kHz-70 kHz frequency range, including one outstanding mode with a Q-factor of $\approx 10^6$ and rendering the possibility for more interesting experiments due to the unique properties of GaAs. The master thesis is rather focused on the characterization measurements on two different SiN membranes which can be regarded as prerequisite steps for our prospective optical experiments with mechanical resonators.

ACKNOWLEDGMENTS

The experimental work submitted to the Faculty of Science herein, has been carried out at the Danish Research Foundation Center for Quantum Optics, QUANTOP Laboratories, at the Niels Bohr Institute in Copenhagen. Along with the courses, during the first year of my master study, I was given the opportunity to familiarize myself with the basic optical measurements and later on in the second year, I started to carry out my master project at the laboratory.

First of all, I would like to thank my supervisor Eugene Polzik for giving me the opportunity to work in this world-renowned research center and for his guidance throughout the project. I am grateful to Koji Usami, who had taught me everything about the optical table from scratch in a very patient way. His guidance for my master thesis and his ideas for the experiment have been very significant. I would like to thank Bo Melholt Nielsen for being very willing to help me in the laboratory, especially on technical issues. Thanks to Andreas Næsby Rasmussen for the times we have spent struggling with the setup and for our fruitful discussions. I would like to thank Jürgen Appel for his contributions to the idea of the two-color scheme and for the discussions he was engaged in. Thanks to Jörg Helge Müller for his willingness to join our discussions and for his suggestions in general. As a whole, QUANTOP has provided me a very friendly and warm atmosphere, so I thank all the individuals who have been a part of this environment.

I would also like to thank our collaborators at the Quantum Photonics group at DTU, Søren Stobbe, Jin Liu and the group leader Peter Lodahl for their efforts to fabricate the GaAs membrane for us and for the fruitful discussions we had during our visits to DTU.

Finally, I thank The Faculty of Science (University of Copenhagen) for funding my master study as an international student and therefore giving me the opportunity to study at the historical Niels Bohr Institute. I also thank QUANTOP for funding our experimental project.

Contents

Chapter 1

Introduction

The thesis presented here was part of an experimental project with a long-term goal of observing quantum signatures in a cavity optomechanical setup. High Q-factor nanomechanical resonators are promising candidates for this goal, given that sufficiently strong coupling of the mechanical resonator to radiation-pressure in a high-finesse cavity can be realized and this can be furthermore combined with cyrogenics and radiation-pressure cooling to reach the ground state of the mechanical resonator. The thesis will consist of a proposal for two-color probing of a mechanical resonator and mainly the mechanical characterization results of high Q membranes that are aimed to be used in our future experiments. The logical flow of the thesis is laid forth in such a way that first the big picture and the long term goals are introduced to the reader and then the characterization measurements are discussed as the main content of the experimental work. In the conclusive part, the aim is to get back to the idea and the big goal in mind with a feedback from the experimental results and challenges encountered on the way.
Chapter 2 is intended to outline the fundamentals of resonator optics and mechanical resonators in a way where the goal is to have an understanding of the optomechanical coupling realized in cavity optomechanical systems. The main goals like reaching high position sensitivites, cooling to the ground state and observing quantum signatures, are discussed.
In Chapter 3, I introduce to the reader the proposal for the two-color probing scheme where a micromechanical resonator(membrane) sits at a specific point ($\lambda/8$) inside a two-mirror cavity. The goal is to analyze that situation and convince the reader in an intuitive way, on how this method helps in reducing the technical noise in displacement readout and eliminates classical radiation pressure fluctuations. Estimation of the shot-noise limited sensitivity(based on PDH locking method) is also provided.
Chapter 4 lays the basics of membrane's motion derived from a simple rectangular drum model. Eigenfrequencies of our square membranes are estimated and a short analysis for thermally-induced and radiation-pressure induced vibrations is performed.
The experimental setup for eigenfrequency and Q-factor characterization of our two SiN membranes is discussed in detail in Chapter 5. Thermal spectrum and ringdown measurements are seperately treated with the specific elements used.
Chapter 6 can be regarded as the main work of the master thesis. It includes eigenfrequency and Q-factor determinations of two SiN membranes. Two different methods, namely thermal spectrum and mechanical ringdown, are compared in terms of their performance for

high Q-factor measurements. Apart from that, a comparison for the Q-factors of two SiN membranes which were glued differently to the support structure, has been performed in order to have an understanding of possible damping sources.
Chapter 7 is intended to show our first Q-factor results with a GaAs membrane. The chapter provides a brief discussion about the so-called 'magical' properties of GaAs which makes it an interesting candidate for future optomechanics experiments. I also touch upon the prospects with GaAs membranes.
Finally in the conclusive part, the importance of mechanical characterization is emphasized for future experiments and the main ideas and goals are recapitulated to converge to the big picture.

Chapter 2

Theoretical foundations of cavity optomechanics

This chapter of the thesis is intended to give an introduction to the basic concepts in Cavity Optomechanics. We will mainly focus on a typical system where a mechanical resonator is coupled to a single-mode field in a high-finesse cavity. Section 2.1 will outline the principles of basic resonator optics, namely of Fabry-Perot cavities. This will provide the foundation for understanding the conditions under which the optical modes can be sustained inside the cavity. Section 2.2 will introduce the conventional cavity optomechanical setups where one of the mirrors of the cavity is movable and therefore acts as a mechanical oscillator interacting with the light field. The section will touch upon the main motivations in cavity optomechanics, including high-sensitive position detection, investigation of thermal noise of the resonators and finally the figure of merits that determine the observibility of quantum radiation pressure effects. Section 2.3 will deal with the optomechanical interaction in such systems and will provide the theoretical basis by outlining the equations of motion that determine the dynamics of a cavity optomechanical system.

2.1 Basics of resonator optics

As its name suggests, the field Cavity Optomechanics deals with the interaction of a mechanical resonator coupled to light field inside a cavity. Cavities to be investigated are usually referred to as Fabry-Perot resonators that are basically composed of two partially transmissive mirrors. In this regard, it would be nice to find out the basic properties of such cavities, namely their transmission and reflection properties as a function of input beam frequency. Throughout this section, I shall follow the treatment in *Fundamentals of Photonics by Saleh and Teich* [1] with basically a similar notation.

2.1.1 The allowed modes inside an optical resonator

We will first start by writing the field amplitudes inside the resonator and then try to find the resonance condition which renders it possible to have self-sustaining solutions inside the cavity at the steady state. Here I prefer to implement the travelling wave approach where we will be seeking for self-reproducing waves. Of course one could in principle also

use the standing wave approach and apply the boundary conditions to the solution of the well-known Helmholtz equation.

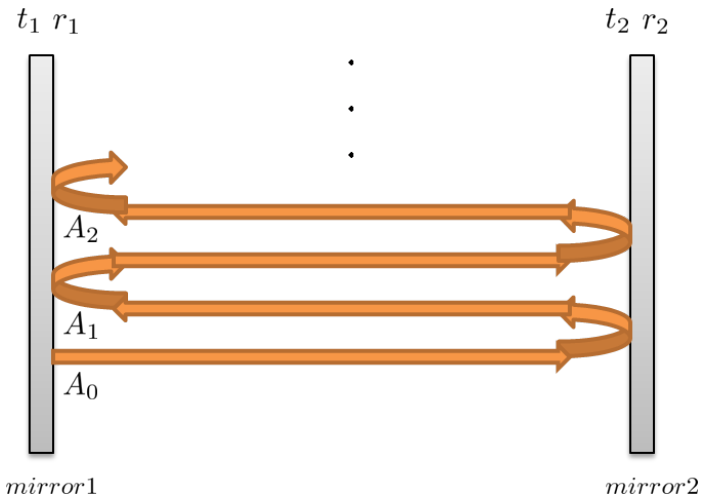

Figure 2.1 The first mirror and the second mirror have amplitude transmittances and reflectivities of t_1, r_1 and t_2, r_2 respectively. If the appropriate resonance condition is satisfied, the initial field inside the cavity builds up power as it bounces back and forth between the reflective mirrors.

As can be seen in Figure 2.1, we can envision the cavity modes as bouncing back and forth inside the cavity mirrors. In order to have self-reproducing waves, we impose the condition that after a single round trip, the phase shift imparted by the propogation distance of $2d$(between two mirrors) should be an integer multiple of 2π,

$$\phi = k2d = n2\pi, n = 1, 2, 3... \tag{2.1}$$

From the well-known relation between the angular frequency and the wave number, we have $\omega = ck$ and therefore we find the resonance frequencies as

$$\nu = n\frac{c}{2d} \tag{2.2}$$

A conceptual way to understand the phase matching condition is to treat the system as composed of field amplitudes where the output is fed back in phase with the input in a positive manner [1]. In the simple case where there is no loss within the system, the initial wave A_0 propogates and reflects back from the second mirror and then also reflects back from the first mirror. This continues ad infinitum and the resultant wave amplitude is actually a sum of all these, lets say infinitesmall waves,

$$A = A_0 + A_1 + A_2... \tag{2.3}$$

As a basic argument, one can say that only when the phase matching conditions occurs (equivalently the resonance frequency match), the monochromatic wave amplitude inside the cavity can reach up to a finite value since only this condition satisfies the appropriate feedback. A more realistic case would be to include the losses associated with the two mirror

reflection and the absorption in the medium. At this point, for the notation of the total amplitude attenuation factor, I stick to [1] where we shall denote it by r. Therefore, the intensity attenuation factor becomes r^2. It is obvious now that the amplitudes add up in a geometrically reduced manner as follows,

$$A = A_0 + hA_0 + h^2A_0 + h^3A_0... \tag{2.4}$$

where $h = re^{-i\phi}$ includes both the amplitude reduction and the phase information. The geometric series is nothing but the well-known result yielding $A = A_0/(1-h)$. Therefore the total intensity that builds up in the resonator is given by,

$$\begin{aligned} I = |A|^2 &= |A_0|^2/(|1 - re^{-i\phi}|^2) \\ &= I_0/[(1 - r\cos\phi)^2 + (r\sin\phi)^2] \\ &= I_0/[(1-r)^2 + 4r\sin^2(\phi/2)] \end{aligned}$$

With a bit of manipulation it is possible to write the intensity in a more compact manner,

$$I = \frac{|A_0|^2}{[(1-r)^2(1 + (2\mathcal{F}/\pi)^2\sin^2(\phi/2))]} \tag{2.5}$$

where we define the parameter $\mathcal{F}$ as the finesse of the resonator. It will be a crucial figure of merit for a cavity optomechanical system for the very fact that finesse shows the strength of the field confinement inside the cavity. Therefore high-finesse cavities are desirable to increase the interaction between light and the mechanical resonator.

$$\mathcal{F} = \frac{\pi r^{1/2}}{1-r} \tag{2.6}$$

If we look into the equation we found for the intensity in the resonator, it is easy to see that it is a periodic function of the frequency since phase is related to the frequency in a manner where $\phi = 4\pi\nu d/c$. Thus we may write the intensity in a frequency dependent way which will actually give us the spectral response of the Fabry-Perot cavity,

$$I = \frac{|A_0|^2}{[(1-r)^2(1 + (2\mathcal{F}/\pi)^2\sin^2(\pi\nu/\nu_f))]} \tag{2.7}$$

where $\nu_f = c/2d$ represents the free spectral range of the cavity.

2.1.2 Transmission properties of a Fabry-Perot resonator

So far we have concentrated on the intensity inside the resonator and our analysis was based on the picture where we had self-reproducing waves circulating between the two reflective mirors. Equation 2.7 tells us at which frequencies we have the resonances and therefore the highest response. Yet, what is more fruitful for us, would be to determine the transmittance properties of such a resonator where we send some monochromatic wave into the cavity and look at the response from the other side. As can be guessed, the result is not different from the one we found before. The transmittance properties of the cavity follows the same manner as the self-reproducing waves and the intensity profile inside the cavity. The approach is basically the same as we have followed so far. The only difference is that now we come with

some initial amplitude(entering the cavity from the first partially transmissive mirror) and denote the bouncing wave amplitudes with respect to that incoming amplitude. Since the algebra is the same, there is no need to show them in detail here and I shall directly write the spectral response function giving the ratio of I_t/I_i where respectively they refer to the transmitted intensity through the second mirror and the initial intensity of the incoming light. Thus in this case, the transmittance of such a cavity is given by,

$$\mathcal{T} = \frac{|t|^2}{(1-r)^2(1+(2\mathcal{F}/\pi)^2\sin^2(\pi\nu/\nu_f))} \tag{2.8}$$

where $t = t_1 t_2$ and $r = r_1 r_2$.

If one plots the dependance of transmittance with respect to the frequency, one would see peaks at the integer multiples of the free spectral range of the cavity. If the finesse is high, there will be sharp resonance peaks and as finesse gets worse(which means that loss increases) then the resonance peaks get broadened. Assuming that $\mathcal{F} \gg 1$ which is usually the case with the optical resonators used in the experiments, the FWHM(full width at half maximum) of the peaks is found to be,

$$\delta\nu = \nu_f/\mathcal{F} \tag{2.9}$$

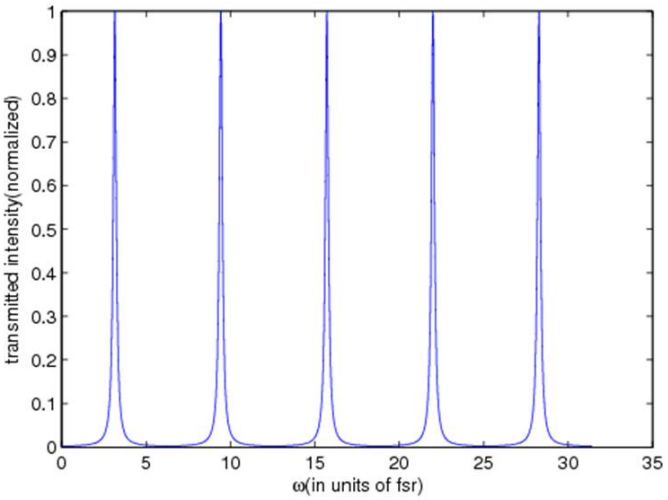

Figure 2.2 The transmission profile of a lossy resonator is plotted with respect to the frequency of the incoming light. As can be seen, the resonance lines have a certain width and the maximim points are distanced equally far from each other which is determined by the fsr(free spectral range) of the cavity. Exploiting such a frequency dependent behaviour, high-finesse Fabry-Perot cavities are widely used as sensitive devices to measure tiny frequency shifts due to the change in the length of the resonator.

At this point it will be a nice idea to zoom into one of the resonance peaks and define the Quality Factor of the optical resonator which is of course closely related to the finesse.

Here I shall write it as defined in [1],

$$Q = 2\pi \frac{\text{stored energy}}{\text{lost energy per cycle}} \tag{2.10}$$

To make more clear what the Q-factor is I shall define L as the loss factor coming from the finite reflectivities of the mirrors and the absorption in the medium for which I do not go into the details right now. This way the loss per unit time in the resonator becomes cL where c is the speed of light. The loss per cycle is then equal to cL/ν_0. Then by utilizing the relation between resonator loss and the spectral linewidth broadening which is given by $\delta v = cL/2\pi$ we reach a rather compact formula for the Q-factor,

$$Q = \frac{\nu_0}{\delta v} \tag{2.11}$$

Furthermore, by using the relation given by Equ.2.9

$$Q = \frac{\nu_0}{\nu_f}\mathcal{F} \tag{2.12}$$

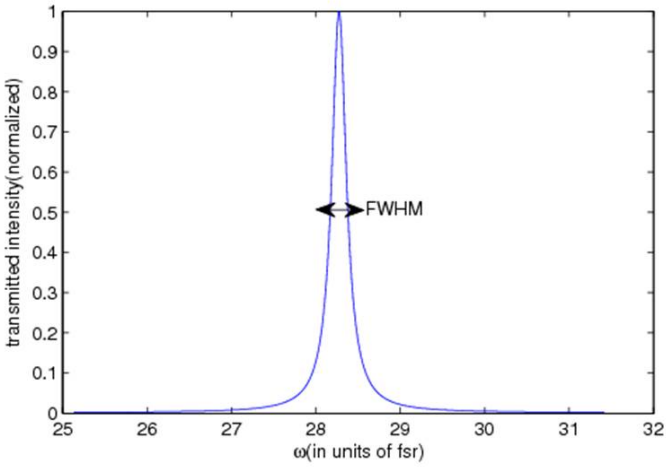

Figure 2.3 The figure shows a zoom-in profile of a single resonant peak. The finesse and correspondingly the Q-factor strongly depends on the loss inside the resonator.

To wrap up the section, what we have done so far was to determine the basic properties of an optical resonator consisting of two highly reflective mirrors. Our goal was to look at the transmission spectrum of such a structure and on the way we have defined important properties like finesse, free spectral range and quality factor of the resonator. In the following sections, it will become more clear why achieving high finesse (low loss) resonators is a crucial concern for people working in the field of Cavity Optomechanics. Furthermore we will refer to the relations we have seen in this section, later in the following chapters, especially for the analysis of the Pound-Drever-Hall signal in a high-finesse cavity.

2.2 Conventional cavity optomechanical systems

2.2.1 A basic optomechanical setup and displacement measurements

In this part, I shall introduce the idea for the conventional optomechanical setup that is mainly implemented in the experiments. As we have seen in the previous section, Fabry-Perot cavities are suitable canditates for highly sensitive position measurements. This is of course mostly due to the high-finesse that makes the readout signal stronger. The basic idea in these conventional optomechanical system is to use one of the mirrors as a movable mechanical object and look at the response of the cavity which will carry the mechanical information.

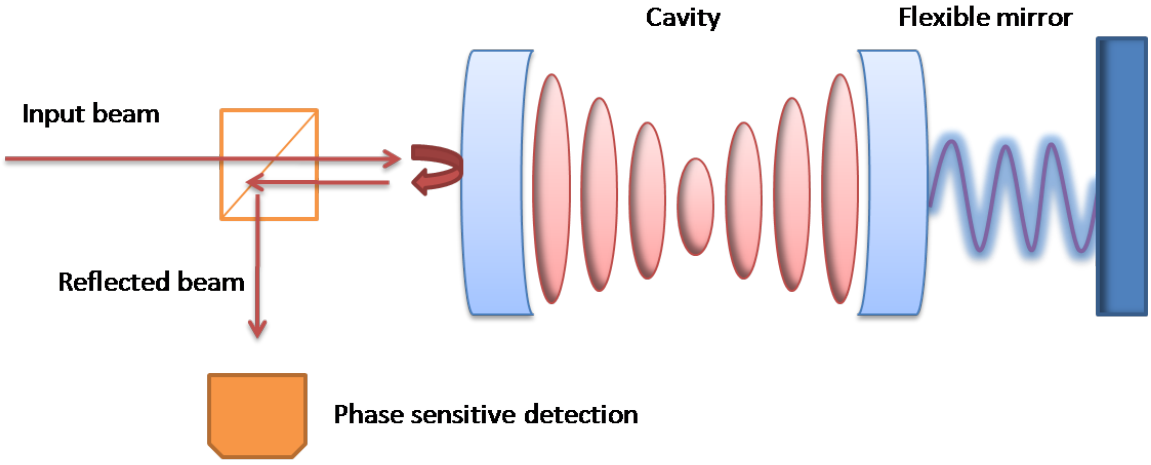

Figure 2.4 A typical optomechanical setup is shown. In principle it is possible to monitor the transmitted light through the cavity, however there is a more sophisticated scheme where one can look at the reflected light as well. The incoming beam passes through the first mirror and resonates inside the cavity(kept on resonance). As the flexible mirror fluctuates, the phase of the reflected beam becomes altered due to the path length change. Thus the mechanical motion becomes imprinted on the reflected beam signal. By making a phase-sensitive detection of the reflected beam, one can monitor the motion of the mechanical oscillator in a precise manner.

To be more clear about how the mechanical fluctuations of the movable mirror can be detected, it would be better to look at the amplitude and phase change of the reflected light.The picture can be clearly envisioned as depicted in Figure 2.5. In that case the reflected phase is altered by the motion of the movable mirror and this change is enhanced by the finesse of the cavity since the beam makes multiple reflections inside the cavity. Simply put, the phase is related to the displacement in a manner as follows [2],

$$d\phi \approx \frac{\mathcal{F}}{\lambda} dx \tag{2.13}$$

where λ is the wavelength of the incoming beam.

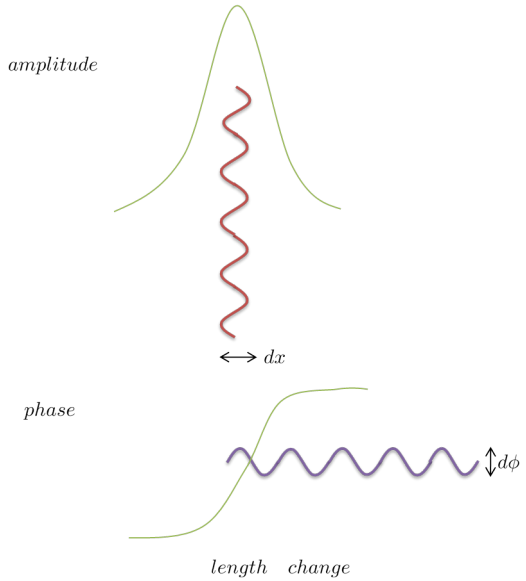

Figure 2.5 Both the amplitude and phase information of the light field are depicted in the figure. In the case of resonant probing, the amplitude of the reflected light does not change. However, if we look at the phase information, one can see that it gives the highest slope on resonance. Therefore the phase information is quite sensitive to the mirror motion around this region.

Highly sensitive displacement measurement is one of the main goals in the field of Cavity Optomechanics. Especially for the Gravitational Wave Detectors, it is of utmost importance to achieve high sensitivty in order to be able to see the tiny fluctuations caused by the passing of a supposedly gravitational wave. The basic idea is to combine a two-mirror cavity system in a Michelson type interferometer configuration to detect the relative length change between the two arms of the interferometer as in LIGO(Laser Interferometer Gravitational Observatory) in USA [3]. On the other hand, cavity optomechanical systems are also being extensively used by especially Quantum Optics groups. The main idea is to utilize the nice optical properties of cavities(high finesse) in both determining the properties of a mechanical resonator and investigating the interaction between light and the resonator, namely due to radiation pressure. As one further possibility, once the coupling is strong enough, detuned light itself can change the dynamics of the mechanical resonator significantly leading to radiation-pressure cooling. From another point of view, high finesse and high Q-factor of the mechanical resonator make cavity optomechanical systems ideal environments for fundamental quantum optics experiments where quantum phenomena like radiation-pressure back-action, entanglement, generation of squeezed states etc may be observable [2]. Also in the case of strong coupling, those sytems might be utilized for Quantum Information protocols as well [4]. However, strong coherent control of an optomechanical system implies the requirement for reaching the quantum noise-dominated regime and this has not been achieved so far in optomechanical systems. The main requirements for seeing quantum effects is the careful elimination of technical noise(intensity, phase, frequency noise of the laser etc) and cooling the resonator close to its ground state for the very reason that thermal

fluctuations tend to mask the quantum properties. Reaching ground state is a formidable task and recently a lot of groups have been working on cooling of the resonator by utilizing radiation pressure [5–8]. Actually, ground state cooling has recently(2010) been achieved in rather an electromechanical setup where coherent control between a superconducting qubit and a mechanical resonator(6GHz) was realized [9].

The main motivations in the field become more clear when we actually ask the question of " What is the ultimate sensitivity of such a cavity optomechanical system?". At this point, one has to consider all the possible noise sources. The first obvious source would of course be the classical noise which comes from the intensity, phase and frequency fluctuations of the probe laser and vibrations coming from the environment. In principle this type of noise can be eliminated totally, however this is not easy to achieve practically. We will come back to this point of course for the very fact that eliminating the classical noise to a large extent is one of the motivations in our prospective experiments. Yet now we shall assume that it is perfectly eliminated. Then, resolving tiny displacements means that achieving very low temperatures is also a requisite. Thermal excitations from the environment would always give random kicks to the mechanical resonator, therefore masking to a large extent the tiny oscillations at the quantum scale. I shall also discuss thermal noise briefly in the following section. So presuming that classical noise and thermal noise are eliminated to a large extent, then it is possible to see the quantum noise effects which is of course one of the main goals in the field.
Noise of quantum origin basically comes from two sources, namely shot noise and quantum back-action noise [2]. Shot noise is basically related to the detector noise. Due to the quantum nature of photons, they arrive in random time intervals to the detector which causes an uncertainty for the measurement. Since the fluctuations are proportional to $\sqrt{n}$ where n is the number of photons, the relative noise would be $\sqrt{n}/n$ which makes shot noise,

$$\Delta\phi = \frac{1}{\sqrt{n}} \tag{2.14}$$

and considering the enhancement of the intracavity photon number by the finesse and therefore using the relationship between phase and position (phase becomes our signal of interest in our case)

$$\phi = 4\mathcal{F}\frac{x}{\lambda} \tag{2.15}$$

then Δx representing the position measurement accuracy becomes

$$\Delta x = \frac{\lambda}{4\mathcal{F}}\frac{1}{\sqrt{n}} \tag{2.16}$$

As can be seen at first sight, it seems possible to increase the measurement accuracy arbitrarily by increasing the power, therefore the number of photons inside, however this itself causes another source of imprecision(for continuous position readout) which is referred to as the measurement back-action. Once we increase the power, we at the same time increase the effect of random momentum kicks on the mechanical object exerted by radiation pressure. It is easy to show that the momentum back-action imparted by radiation pressure is,

$$\Delta p = 2\hbar k \frac{\mathcal{F}}{2\pi}\sqrt{n} \tag{2.17}$$

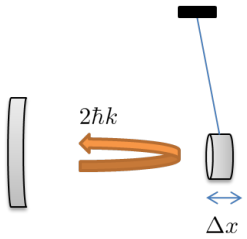

Figure 2.6 The figure depicts the radiation pressure back-action on the movable mirror, the motion of which is to be investigated. As light bounces back from the mirror it exerts a stoachastic force stemming from radiation pressure fluctuations of the field. This noise in principle can be free of classical contribution, however there is unavoidable quantum part as well.

The discussion here comes to the well-known point which is referred to as the Heisenberg Microscope. As Fig 2.6 shows, increasing the optical power results in the contribution of the back-action noise. If we use equations 2.16 and 2.17 and multiply the two uncertainties, we obtain the Heisenberg limit:

$$\Delta x \Delta p = \frac{\hbar}{2} \tag{2.18}$$

At this level people have defined the so-called Standard Quantum Limit (SQL) where both detector shot noise and quantum back-action noise contibute equally to the uncertainty product. To circumvent this limit, injection of squeezed light [10] and back-action evading schemes [11] have been proposed.

2.2.2 Thermal noise

In the previous part, we had outlined the basic sources of noise that would mask our signal of interest,namely of the mechanical resonator. As was shown, the ultimate sensitivity of an interferometer is fundamentally limited by the laws of Quantum Mechanics and reaching that regime where one can see the quantum radiation-pressure effects, already requires the elimination of classical noise and thermal noise. Thermal noise so far has been a basic limiting factor in Gravitational Wave Detectors by masking the real signal [12]. Yet from another point of view, one can investigate the mechanical properties of a mechanical oscilator by looking at the thermal spectrum at room temperature. For example utilizing a phase sensitive detection method, one can get the data of a broadband scan where individiual peaks corresponding to the internal mechanical eigenmodes, are visible. We shall at this point follow the approach in [12]. Let $u(r,t)$ be our displacement, namely the internal deformation of our movable mirror which obeys the elasticity equation. In principle, one can write any displacement as a linear combination of all modes which means that;

$$u(r,t) = \sum_n a_n(t) u_n(r) \tag{2.19}$$

where $a_n(t)$, as the amplitude of a specific mode, follows the equation of motion for a simple forced harmonic oscillator as follows,

$$\frac{d^2}{dt^2}a_n(t) + {\omega_n}^2 a_n(t) = \frac{\langle F(r,t), u_n(r)\rangle}{M_n} \tag{2.20}$$

Here M_n denotes the effective mass of the corresponding mode, ω_n is the eigenfrequency and $\langle F(r,t), u_n(r)\rangle$ is the spatial overlap of the force and the acoustic mode. One can go into the frequency domain and write the equation of the harmonic oscillator in the following manner,

$$a_n(\omega) = \chi_n(\omega)[\langle F(r,\omega), u_n(r)\rangle] \tag{2.21}$$

where we shall define an important parameter, namely the effective susceptibility of the resonator as follows,

$$\chi_n(\omega) = \frac{1}{M_n({\omega_n}^2 - \omega^2)} \tag{2.22}$$

Note that we did not include any damping in the equation of motion for the harmonic oscillator. However we can readily insert such a term in the case of a Langevin force representing the thermal bath and then the effective susceptibility becomes modified,

$$\chi_n(\omega) = \frac{1}{M_n({\omega_n}^2 - \omega^2 - i\frac{{\omega_n}^2}{Q_n})} \tag{2.23}$$

where Q_n is the quality factor of the specific mode which is actually given by,

$$Q = \frac{\omega_n}{\gamma} \tag{2.24}$$

γ being the decay rate of the mode which is related to the power decay time by $\mathcal{T} = 2\pi/\gamma$,

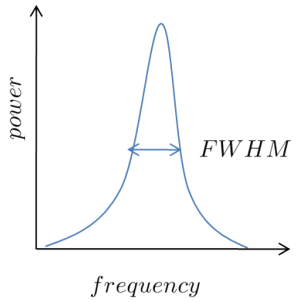

Figure 2.7 The zoom-in depiction of a hypotethical single resonant peak where a specific mechanical mode of the resonator is excited by thermal fluctuations. The spectrum is actually a Lorentian profile with a FWHM corresponding to γ .

We can then denote the force coming from thermal bath as a Langevin Force and use the fluctuation-dissipation theorem to write its spectrum. It is related to the imaginary part of the mechanical susceptibility as follows;

$$S_{T,n}(\omega) = -\frac{2k_BT}{\omega} Im(\frac{1}{\chi[\omega]}) \tag{2.25}$$

where $\mathcal{T}$ is the temperature of the thermal bath and k_B is the Boltzmann constant. We can at this point also drop the mode number n because we are interested in a single frequency near one of the resonances. Then the thermal spectrum becomes more clear,

$$S(\omega_{res}) = 2M\gamma k_BT \tag{2.26}$$

By reminding ourselves the equation 2.21, it is easily seen that the displacement spectrum due to the thermal force is a Lorentzian function with a linewidth of γ as also shown in Figure 2.7.

2.2.3 Figure of merits for an optomechanical setup

In this short section, I would rather wrap up the important parameters in a typical optomechanical system and show them in a formulized manner. As we have seen so far, the finesse of the optical resonator is crucial in increasing the coupling of light to the mechanical resonator and therefore enhancing the position sensitivity and the chance of seeing quantum effects. On the other hand, the mechanical Q-factor of the mirror is crucial because the higher it is, the less coupling it has to the environment and this again paves the way for reaching the quantum ground state as well as the observibility of various quantum phenomena.
At this point I shall write the interaction Hamiltonian for the optomechanical coupling between light and the mirror as in [4],

$$H_{int} = -\hbar g_0 n_c X_m \tag{2.27}$$

where $X_m = (a_m + a_m{}^\dagger)$ denotes the position quadrature and n_c is simply the intracavity photon number. g_o , the coupling rate is given by,

$$g_0 = \frac{\omega_c}{L}\sqrt{\frac{\hbar}{m\omega_m}} \tag{2.28}$$

Here L, w_c, w_m and m being the cavity length, optical frequency, mechanical frequency and the effective mass respectively. Derivation of this optomechanical coupling is provided in Appendix A. Usually a strong laser beam is used in the experiments and it is valid to make a mean-field expansion. Then the optomechanical interaction can be written in a form,

$$H_{int} = -\hbar g X_c X_m \tag{2.29}$$

where $X_c = (a_c + a_c{}^\dagger)$ is the optical quadrature. Within this approximation, now the effective coupling rate becomes $g = g_0\sqrt{\langle n_c\rangle}$ which means that the single photon coupling is enhanced by the intracavity photon number.
Many groups working in the field are interested in achieving coherent quantum control over the optomechanical system and in this regard, reaching the regime of strong coupling turns out to be a requisite for such a goal. To formulize it simply, the strong coupling regime

is usually defined so as to bear the condition $g \gg \kappa, \gamma$ where κ and γ denote the cavity decay rate and the mechanical decay rate, respectively. Strong coupling between light and a micromechanical resonator has already been observed recently [4]. As can be seen from the strong coupling condition, there are two decoherence mechanisms, namely the optical and the mechanical decay, which would work against the coherence of the sytem. In fact the strong coupling condition can also be translated into the statement that high finesse and high mechanical Q are requisites for an optomechanical setup.
The importance of high F and high Q can also be realized by considering the ratio of the radiation-pressure shot noise and the thermal power spectral densities. As we have touched upon before, in order to be able to see the quantum effects coming from radiation-pressure coupling, one has to eliminate the masking effect of the thermal Brownian motion. In this regard, I find it useful to refer to the figure of merit which gives a comparison of the radiation-pressure effects over thermal fluctutations as formulated in [13],

$$\frac{S_f(radiation \quad pressure)}{S_f(thermal)} = \frac{16\hbar P_{in} Q \mathcal{F}^2}{\lambda c \pi k_B T m \omega_m} \tag{2.30}$$

where P_{in} is the input power and λ is the wavelength of the light and m is the motional mass of the mechanical resonator. As can be seen from this formula, while high laser power and high $\mathcal{F}$ enhance the optical properties, high Q and small mass improve the mechanical properties of the optomechanical system.

2.3 A closer look at the optomechanical interaction, QLE and cooling

In this section, we shall try to have a closer look at the Hamiltonian of a conventional optomechanical system. In this way, I aim to outline the basic mathematical description of the optomechanical interaction, namely the coupling between radiation pressure and the mechanical resonator. Here, I will follow the paper [5]. The main motivation is to write the equations of motion for the quadratures of light and mechanical resonator and try to get the expressions for the fluctuations, revealing also how they are coupled. This will provide us the dynamical picture through which, later on, we can touch upon the issue of radiation pressure cooling which is an important tool to reach ground-state cooling. Throughout the section, I will give the key results rather than the derivations, so the details can be found in [5].

2.3.1 Quantum Langevin Equations

We start with the Hamiltonian describing the optomechanical system in which a single optical mode inside a cavity is coupled to a mechanical resonator(movable mirror) through radiation pressure. We impose that coupling between meachanical modes is negligible and we are only interested in a single mechanical mode(bandpass filter detection). Then the Hamiltonian is given by [5] as follows,

$$H = \hbar\omega_c a^\dagger a + \frac{1}{2}\hbar\omega_m(p^2 + q^2) - \hbar G_0 a^\dagger a q + i\hbar E(a^\dagger e^{-i\omega_0 t} - a e^{i\omega_0 t}) \tag{2.31}$$

where a and $a^\dagger$ are annihilation and creation operators of the single mode optical field at frequency ω_c. For the second term, q and p refer to the position and momentum operators of the mechanical mode at frequency ω_m. G_0 is the coupling term as defined in the previous sections and the last term reads as the optical driving term with frequency ω_0 and intracavity amplitude E.
In the interaction picture with respect to the driving field, taking the time derivatives results in a set of equations as follows,

$$\begin{aligned}
\dot{q} &= \omega_m p \\
\dot{p} &= -\omega_m q - \gamma p + G_0 a^\dagger a + F_{brownian} \\
\dot{a} &= -(\kappa + i\Delta)a + iG_0 aq + E + \sqrt{2\kappa}a^{in}
\end{aligned} \tag{2.32}$$

here detuning is denoted by $\Delta = \omega_c - \omega_0$, γ and $F_{brownian}$ represent the mechanical damping rate and the stochastic thermal force respectively. Cavity decay rate is given by κ.
After this point, one can characterize the system as a semi-classical state where the cavity mode amplitude is high ($|\alpha_s| \gg 1$) and we have stable solutions around the equilibrium points. Then one can claim to write the Heisenberg operators in the previous set of equations as c-number steady state values plus fluctuating terms. As a result, one gets the Quantum Langevin Equations as follows,

$$\begin{aligned}
\delta\dot{q} &= \omega_m \delta p \\
\delta\dot{p} &= -\omega_m \delta q - \gamma \delta p + G_0(\alpha_s \delta a^\dagger + \alpha_s^\dagger \delta a) + \delta a^\dagger \delta a + F_{brownian} \\
\delta\dot{a} &= -(\kappa + i\Delta)\delta a + iG_0(\alpha_s + \delta a)\delta q + \sqrt{2\kappa}a^{in}
\end{aligned} \tag{2.33}$$

At this point it would be valid to drop the terms $\delta a^\dagger \delta a$ and $\delta a \delta q$ since the steady state amplitude is larger than 1. It is then possible to write the equations of motion in a simpler form, namely linearized Quantum Langevin Equations,

$$\begin{aligned}
\delta\dot{q} &= \omega_m \delta p \\
\delta\dot{p} &= -\omega_m \delta q - \gamma \delta p + G\delta X + F_{brownian} \\
\delta\dot{X} &= -\kappa\delta X + \Delta\delta Y + \sqrt{2\kappa}X_{in} \\
\delta\dot{Y} &= -\kappa\delta Y - \Delta\delta X + G\delta q + \sqrt{2\kappa}Y_{in}
\end{aligned} \tag{2.34}$$

where as in ref [5], the cavity field quadratures and the vacuum radiation noise operators are defined to be,

$$\begin{aligned}
\delta X &= (\delta a + \delta a^\dagger)/\sqrt{2} \\
\delta Y &= (\delta a - \delta a^\dagger)/i\sqrt{2}
\end{aligned} \tag{2.35}$$

and also $G = G_0\alpha_s\sqrt{2}$ is defined as the effective optomechanical coupling which absorbs the intracavity amplitude.

2.3.2 Radiation pressure cooling

The previous equations we have dealt actually shows us how the field fluctuations and the mechanical resonator quadratures are coupled via radiation pressure. By this coupling, as long as it is strong, it is possible to change the dynamics of the microresonator in a predictable way which would result in either amplification or cooling of the motion. To get a quantitative picture, one has to calculate the variances of motion, basically $\langle \delta q^2 \rangle + \langle \delta p^2 \rangle$ for the very fact that the energy of the oscillator in the steady state is given by the simple relation,

$$U = \frac{\hbar \omega_m}{2} (\langle \delta q^2 \rangle + \langle \delta p^2 \rangle) = \hbar \omega_m (n_{eff} + \frac{1}{2}) \tag{2.36}$$

By solving the linearized QLE given in the set of equations set beforehand, switching to the frequency domain and integrating the result, one gets the relationship between the variances and the position spectrum. As we have seen before, the position spectrum is related to the expression which includes two terms(thermal and readiation pressure), through the susceptibility. Writing the radiation pressure and the thermal spectrum explicitly, one gets the effective susceptibility of the oscillator, which in another words, appears as the effective damping rate and effective frequency of the oscillator. Here it is worth to note them in their mathematical expression,

$$\omega^{eff}{}_{(\omega)} = \sqrt{\omega_m^2 - \frac{G^2 \Delta \omega_m (\kappa^2 - \omega^2 + \Delta^2)}{(\kappa^2 + (\omega - \Delta)^2)(\kappa^2 + (\omega + \Delta)^2)}} \tag{2.37}$$

$$\gamma^{eff}{}_{(\omega)} = \gamma_m + \frac{2G^2 \Delta \omega_m \kappa}{(\kappa^2 + (\omega - \Delta)^2)(\kappa^2 + (\omega + \Delta)^2)} \tag{2.38}$$

These two equations provide us a clear view of how the dynamics can be affected by the radiation pressure. Apparent from the first equation is that, when the detuning is nonzero, the mechanical eigenfrequency is modified. This is known as the optical spring effect in literature [14]. However for high frequency oscillators(typically around 1 MHz) which is also relevant to our experiment, the optical spring effect is negligible. And if we look at the second equation , we can see that the damping rate is also modified by coupling of radiation pressure to the mechanical resonator. This is actually the basis of radiation pressure cooling which is a so-called dynamic-back action effect [2]. Given that the coupling constant is high and the detuning is positive, it is possible to cool the resonator to consirably low temperatures. Recently, people have achieved to reduce the mean phonon number to a few tens with different types of resonators [6, 7].
We keep on the mathematical description to reach the result for the final phonon number. Imposing the stability condition, the integrals for the variances become exactly sovable. The details for the lengthy expressions can be found in [5]. At this point, it will be nicer to define the Stokes and anti-Stokes scattering rates;

$$A_+ = \frac{G^2\kappa}{2(\kappa^2 + (\Delta + \omega_m)^2)} \tag{2.39}$$

$$A_- = \frac{G^2\kappa}{2(\kappa^2 + (\Delta - \omega_m)^2)} \tag{2.40}$$

where the two expressions refer to the absorption and emission of a phonon, respectively. One can then also define the net cooling rate (for $\Delta > 0$) $\Gamma = A_- - A_+$. For small γ_m (which means the thermal coupling rate is smaller than the cooling rate) and imposing these limits $\omega_m \gg \bar{n}\gamma_m, G$ and $\kappa \gg \gamma_m, G$ which are satisfied in the experimental case, one reaches the final equation which is one of the most crucial results in the field;

$$\langle \delta p^2 \rangle \approx \langle \delta q^2 \rangle = n_{eff} + 1/2 \tag{2.41}$$

and the effective phonon number being ;

$$n_{eff} = \frac{\gamma_m \bar{n} + A_+}{\gamma_m + \Gamma} \tag{2.42}$$

To be able to reach the ground state, one should find the optimum values for the parameters in equ. 2.42. Of course one way is to make the detuning exactly at the value of the mechanical resonance($\Delta + \omega_m$). This maximizes the anti-Stokes sideband energy transfer. Also G should be large but not so large that the stability condition is maintained. The laser cooling rate Γ should be smaller than κ for the very fact that the cavity should respond faster than the oscillator response time. Basically it is well-known that this way of dynamic back-action cooling is more effective in the good cavity limit where $\kappa < \omega_m$ which translates into the statement that the photon lifetime in the cavity should be larger than the period of mechanical oscillation. In other words, this dynamic back-action effect results from a delayed response of the cavity field to the mechanical motion. There is also an alternative cooling scheme, called cold-damping method, namely an active way of cooling where the motion is monitored in real time and then an appropriate feedback signal, proportional to the velocity, is applied to the resonator in order to damp the motion as in [8]. For this cooling scheme, the most efficient regime turns out to be the bad cavity limit where $\kappa > \omega_m$ in contrast to the passive cooling method we have mentioned here [5].
The phonon number equation can also be grasped in a simple physical manner as well. First, one can make use of the assumption that the cooling rate is much larger than the mechanical decay rate $\Gamma \gg \gamma$ which is easily achieved in the experiments due to the large number of photons. Then the effective phonon number in equ. 2.42 can be seperated into two terms that read as,

$$n_{eff} \approx \frac{\gamma_m \bar{n}}{\Gamma} + \frac{A_+}{\Gamma} \tag{2.43}$$

The expression on the left comes from the competition between the rethermalization rate(which is enhanced by the initial photon number) and the cooling rate. In principle this term can be made as small as possible with a high Q mechanical resonator and a low initial temperature

but this has been the limiting factor in cooling in terms of its experimental realization so far. The right hand term simply comes from the Stokes scattering, namely the absorption of phonons which is funtamentally a quantum back-action term.
Lets now briefly discuss dynamic back-action cooling in a rather intuitive way. In the time domain picture, dynamic back-action cooling as mentioned before, was a time- lag related phenomenon causing the radiation pressure response to the mechanical motion . This phenomenon can be understood better in the Fig 2.8. Basically when we have positive (red) detuning, we are on the positive slope of the radiation pressure curve with respect to the position and on this curve radiation pressure extracts work from the mechanical resonator which corresponds to cooling. On the other hand, when we are on the blue detuned part, radiation pressure imparts work on the resonator therefore leading to mechanical amplification, which means simply heating [2]. Another way of grasping this phenomenon is

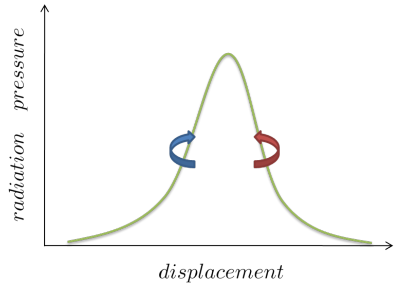

Figure 2.8 Radiation-pressure cooling and heating due to dynamic back-action are depicted in the figure. Radiation pressure force is maximum when driving laser light is on resoance. When we send red-detuned light, work curve is clockwise resulting in work extraction while when blue-detuned, the curve is counter-clockwise resulting in amplification of motion [15]. This is a time domain picture of radiation pressure effect.

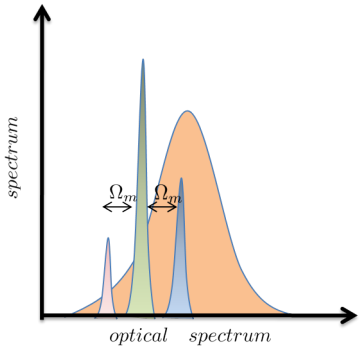

Figure 2.9 Depiction of sideband cooling(in frequency domain) where the laser light is red detuned with respect to the cavity resonance peak(orange field) . This way, cavity favors the blue resonance line over the pink one because of the assymetry in the density of modes [15]. Therefore, the mechanical resonator effectively emits a phonon to the cavity mode which acts as a cooling reservoir.

to switch to the frequency domain which is sort of a quantum mechanical analogue of the time-domain explanation. The idea is that one can envision the cavity spectrum being modulated by the mechanical motion, resulting in sidebands in the output spectrum. This is mainly due to two competing mechanisms supported in the cavity, which are the Stokes and anti-Stokes processes. In case of a perfectly tuned light (with respect to the cavity resonance), these two processes are balanced. However, when one comes with a detuned light, the balance is broken and either Stokes or anti-Stokes process is favored. If the laser is red-detuned, then the Stokes line takes over the other which means that effectively a mechanical quanta(phonon) is removed from the resonator, resulting in cooling. When $\omega_m \gg \kappa$, this is called the resolved sideband regime where cooling is most efficient [2]. This side-band cooling is depicted in Fig 2.9.

To wrap up the theory section, what we have done was basically to write the fundamental equations of motion for the light and mechanical resonator quadratures and investigate the dynamics of the system under certain assumptions and limits. The aim was to give an insight and intuition on the optomechanical interaction between the resonator and light which is of course the main driving theme for the physical foundations behind the position readout and radiation-pressure cooling that are two of the big motivations in the field .

Chapter 3

Membrane in a cavity and two-color probing scheme

In this chapter, I will introduce to the reader the idea of using a membrane as a mechanical resonator in a two-mirror high-finesse cavity as proposed in [13]. I will first give the transmission and reflection properties of such a cavity and then the expression for detuning due to the motion of the dielectric membrane. Having understood the optical propertes of this cavity, I will mention our proposal of two-color probing, where instead of using one color to probe the fluctuations of the membrane, we plan use two colors exactly one fsr away from each other and show that this is a promising method to eliminate classical noise.

3.1 Membrane in the middle approach

In the previous chapter, I had introduced the concept of optomechanical coupling between a cavity field and a mechanical resonator and how it is possible to make a sensitive position measurement or either achieve a strong coherent interaction, where one might be able to see quantum effects. However, as has been stated, this requires that both the mechanical properties and optical properties of the cavity be of high quality. In conventional optomechanical systems, one of the mirror is free to move and this acts as one end of the mirror as well as the mechanical object under investigation. But one big problem with this conventional method is that it is very difficult to find a material that has both good optical properties(high reflectivity leading to high finesse) and good mechanical properties(low mass, high Q-factor etc). Therefore one has to find a compromise between these two properties. Yet a nice idea has been proposed to circumvent this limit in a recent paper [13]. The main point is to use two highly reflective mirrors to form the high finesse cavity and then put a high Q mechanical object in the middle of the cavity. In this way, the good optical properties come from the two end mirrors while high mechanical Q of the resonator comes only from the membrane itself, thus removing the constraint of seeking a compromise between optical and mechanical properties in a single element. The difference from the conventional optomechanical coupling is that the detuning of the cavity depends on the position of the membrane with respect to the nodes or antinodes of the field in a periodic manner, whereas in the conventional system the motion of the mirror would change the length of the cavity and to first order it simply gives a linear detuning in the resonance frequency of the cavity.

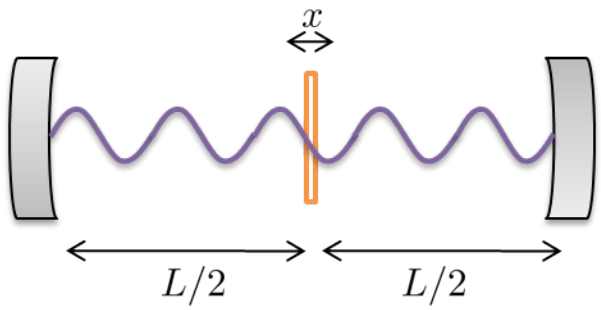

Figure 3.1 The figure shows the simple sketch of the membrane in the middle geometry. The cavity is formed by the two rigid end mirrors which dominantly determine the finesse of the cavity. On the other hand, the mechanical object which is free to move, is a transmissive membrane with a high mechanical Q-factor. The membrane interacts with the field which shows a simple periodic standing wave pattern inside the resonator.

One other advantage of the membrane in the middle approach over the conventional methods is that it provides a much richer playground for the manipulation of the optomechanical coupling. Depending on where excatly one puts the membrane with respect to the nodes or antinodes of the cavity field, one can realize a linear coupling for a position measurement or one can as well achieve a quadratic coupling which renders a phonon number measurement possible. This was the main motivation in [13]. However our main direction is to operate in the linear coupling regime where we want to eliminate technical noise in the position readout of the membrane by utilizing the two color probing approach.

3.1.1 Membrane sitting at a specific point inside the cavity and the detuning expression

Here I shall give the mathematical description of the cavity frequency detuning as the membrane moves. Due to the fluctuations of the membrane, just like in the case of conventional optomechanical coupling, the cavity eigenfrequency is no longer the same but rather altered. It is this detuning difference that is imprinted in the transmitted or reflected light. For example if one monitors the cavity at resonance (by some locking mechanism) and looks at the reflected light, he will see that the membrane's motion will modulate the phase of the reflected light at the mechanical eigenfrequencies. Our main task later on would be to elaborate on how the error signal(Pound-Drever-Hall scheme) from this cavity looks like. But before that, let us understand how detuning works.

Let us make our analysis for a general case of a membrane sitting at some arbitrary place inside the cavity. We base our analysis on the picture depicted in Fig. 3.2. Now I shall write the electromagnetic field amplitude equations for each of those amplitudes with their phases they acquire along their path, in parallel with the set of equations as stated

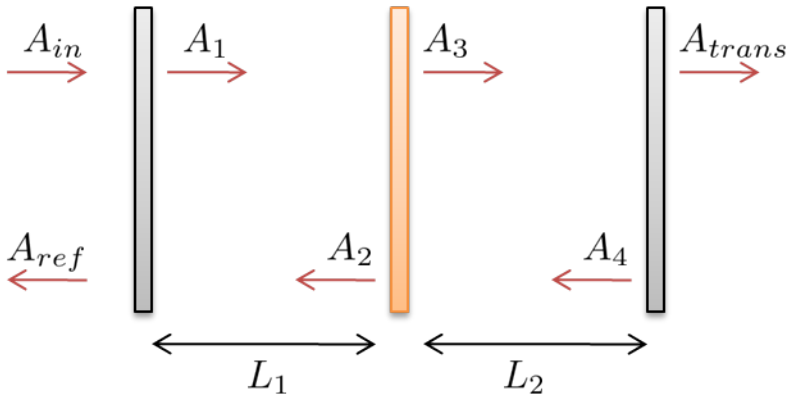

Figure 3.2 Depiction of the membrane sitting at a spesific point inside the cavity. The total cavity length is $L_1 + L_2$, the membrane reflectivity and transmittance(field) are r_m and t_m respectively. They are set to be r and t for the two rigid mirrors. The amplitudes with the arrows are the electromagnetic field amplitudes at the corresponding position of the cavity.

in [16].

$$\begin{aligned} A_1 &= tA_{in} - rA_2e^{ikL_1} \\ A_2 &= r_mA_1e^{ikL_1} + t_mA_4e^{ikL_2} \\ A_3 &= t_mA_1e^{ikL_1} - r_mA_4e^{ikL_2} \\ A_4 &= rA_3e^{ikL_2} \\ A_{ref} &= rA_{in} + tA_2e^{ikL_1} \\ A_{trans} &= tA_3e^{ikL_2} \end{aligned} \tag{3.1}$$

where k refers to ω/c , namely the wave number of the incident light. One has to find A_{trans} and A_{ref} in terms of the input field A_{in} to find out the transmission and reflection properties of this cavity as a whole. The solution to those 6 equations are straightforward but extremely lengthy and cumbersome to show here, so instead I shall write what comes out as a result,

$$A_{trans} = \frac{t^2t_me^{ik(L_1+L_2)}}{1 + rr_m(e^{ik2L_1} + e^{ik2L_2}) + r^2e^{ik2(L_1+L_2)}}A_{in} \tag{3.2}$$

for the transmission coefficient given that we have no loss ($r^2 + t^2 = 1$ and also $r_m^2 + t_m^2 = 1$) . We have also introduced the total length of the cavity $L = L_1 + L_2$. In a similar way (through solving those equations) we get the following relation between the reflected amplitude and the input amplitude,

$$A_{ref} = \frac{1}{r}[1 - \frac{t^2(1 + rr_me^{ik2L_2})}{1 + rr_m(e^{ik2L_1} + e^{ik2L_2}) + r^2e^{ik2(L_1+L_2)}}]A_{in} \tag{3.3}$$

At that point, we have to find the eigenfrequency of that cavity, namely of the allowed modes that satisfy the boundary conditions and render it possible to have self-sustaining solutions. The eigenfrequency of the cavity might be found out by imposing the condition that the denominator goes to zero at resonance, yielding the highest transmission out of the cavity. We are rather interested in power ratios, so more strictly we impose the condition that $|denominator|^2 = 0$. In our case it means that,

$$[1+rr_m(e^{ik2L_1}+e^{ik2L_2})+r^2e^{ik2(L_1+L_2)}][1+rr_m(e^{-ik2L_1}+e^{-ik2L_2})+r^2e^{-ik2(L_1+L_2)}] = 0 \quad (3.4)$$

So what we have to do now is to find the roots of this equation. This again requires manipulation of some lengthy algebra which the reader would not be so interested in. So I will show the result again, but before that, it is worth to note that we have to make some assumptions to make the algebra look simpler. This is that we take the reflectivities of the end mirrors rather large which translates into the statement $r \to 1$. One then has to make use of trigonometric relations to be able to solve the equations. Finally, one reaches the result that gives the eigenfrequencies of the allowed modes inside this cavity as,

$$\omega(x) = \frac{c}{L} arccos(r_m cos[2\frac{\pi}{\lambda}(L_1 - L_2)]) \quad (3.5)$$

To make things make more sense, let us say that the membrane is put at some point x away from the center of the cavity, then L_1 becomes $L/2 + x$ whereas L_2 becomes $L/2 - x$ .So their difference is then 2x and when put into the equation above, we reach,

$$\omega(x) = \frac{c}{L} arccos[r_m cos(\frac{4\pi x}{\lambda})] \quad (3.6)$$

Here λ is the wavelength of the incident light.That is a key result showing that depending on where we put the membrane with respect to the nodes of the cavity, the resonance frequency shows a periodic behavior. In principle there should be a factor stating the mode number as well (n+1/2) to refer to the higher order solutions, however for simplicity I shall not write it. At this point we shall remind ourselves that r_m is the amplitude reflectivity of the membrane and in principle one can calculate this, given that he knows the refractive index and the thickness of the dielectric stab. The derivation for the reflectivity can be performed following the approach described in [17]. Here I would rather give the result,

$$r_m = \frac{(n^2 - 1)sin(knd)}{2incos(knd) + (n^2 + 1)sin(knd)} \quad (3.7)$$

where n is the refractive index and d is the thickness of the dielectric membrane.

3.1.2 Transmission and reflection with respect to membrane's position

In this section I will try to to figure out how the transmission and reflection transfer functions of a membrane in the cavity look like. For our purposes now, the analysis will be based on just one color. It is worth to note here that our main interest is the $\lambda/8$ point where we expect to see a linear coupling between the membrane position and detuning signal. So this point will be our operating point to see the displacement of the membrane and in the later sections, I will specifically show how the linear detuning comes out at this specific point.

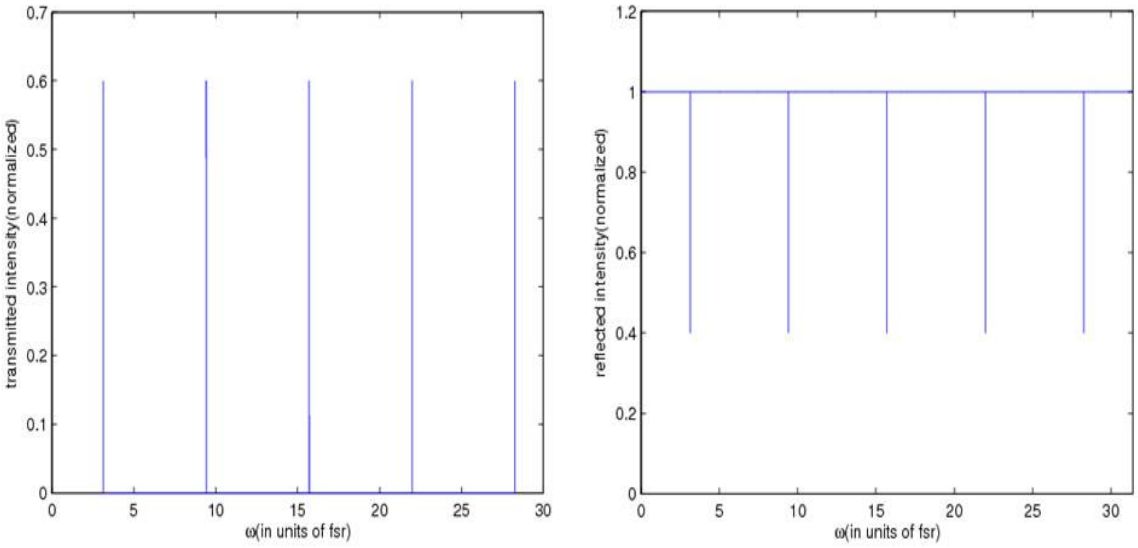

Figure 3.3 The normalized transmitted power with respect to the frequency of the incoming light in case the membrane sits at $\lambda/8$ position. The two mirror reflectivities are chosen to be close to 1 and they have the same values. Membrane reflectivity(power) is set to 0.4 . Cavity length is 2.3 cm(left). The corresponding reflected power(right).

Now let us turn back to our simple purpose and visualize how the transmission looks at the $\lambda/8$ point when we scan the frequency of the incident light. Our configuration is the same in Fig 3.2 and the membrane is displaced by a distance of $\lambda/8$ from the middle point of the cavity. The transmisson and reflection functions are modeled based on the equations 3.2 and 3.3. In Fig 3.3 , the results with certain cavity parameters are shown. There are a few things worth to note in the figure. First of all, at the $\lambda/8$ point, we see that the free spectral rangle is a constant value for any two of the adjacent modes. However, it is not the same case for different operation points like $\lambda/4$. Another thing is that in the symmetric-two mirror cavity case, the reflected power seen by the detector should almost be zero but in our case the existence of the membrane breaks the symmetry of the cavity. The promptly reflected beam and the leakage beam are no longer equal in amplitude, so we have a nonzero coherent sum of reflected beams. Assuming no loss, transmitted and reflected intensities add up to unity as expected.

3.2 Introduction to the two-color probing scheme

I shall first start by introducing the idea behind two-color probing for the membrane at $\lambda/8$ position. The basic proposition is that we aim to send two colors to the cavity instead of one color and look at the differential error signal from these two colors to eliminate common-mode technical noise as shown in Fig 3.4.

This scheme then in principle should help in increasing the sensitivity of the position measurement due to noise elimination to a large extent. The two colors should of course

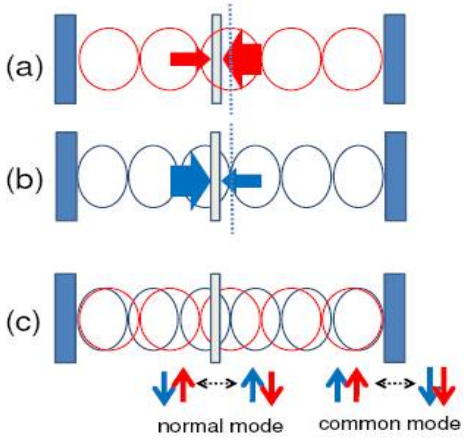

Figure 3.4 The figure depicts how the two colors, which are exactly one fsr away from each other, look like inside the cavity. It turns out that the standing wave pattern of the blue and red light satisfy a special condition at $\lambda/8$ point yielding an optomechanical coupling which is quite advantageous for technical noise elimination. Note also that the radiation pressure from the red beam is balanced by the one from the blue beam so it is possible to null the radiation pressure effect.

come from the same laser source and be both resonant with the cavity. It turns out that when there is exactly a frequency difference of one fsr between the two colors, one can realize the same optomechanical coupling for the two colors but having negative signs if we operate around the $\lambda/8$ point. In this way one both assures that the two colors are resonant with the cavity and also that they have linear detuning due to the membranes motion which is crucial for the displacement readout. If one looks at the error signal from both colors and subtract them by a differential circuit then in principle all common-mode noise like intensity, frequency and phase fluctuations and cavity length change should be eliminated. For this part, I think that introduction is enough for I will give a more detailed account of the detuning in the upcoming sections.

3.2.1 Detuning for two colors at $\lambda/8$ point

Now based on the Fig 3.4 , we will try to find out a linear expression of the detuning for both colors. We first start with the red color. Now supposing that our membrane sits at $\lambda/8$ away from the center of the cavity and plotting the detuning for both colors, we will have a picture as depicted in Fig 3.5.

I shall start the analysis for the determination of the frequency detuning with the red color which has a positive slope. Our detuning function was, as derived before, is given by,

$$\omega(x) = \frac{c}{L} arccos[r_m cos(\frac{4\pi x}{\lambda})] \tag{3.8}$$

At this point, we can make a simple assumption that would make our job easier. Since we

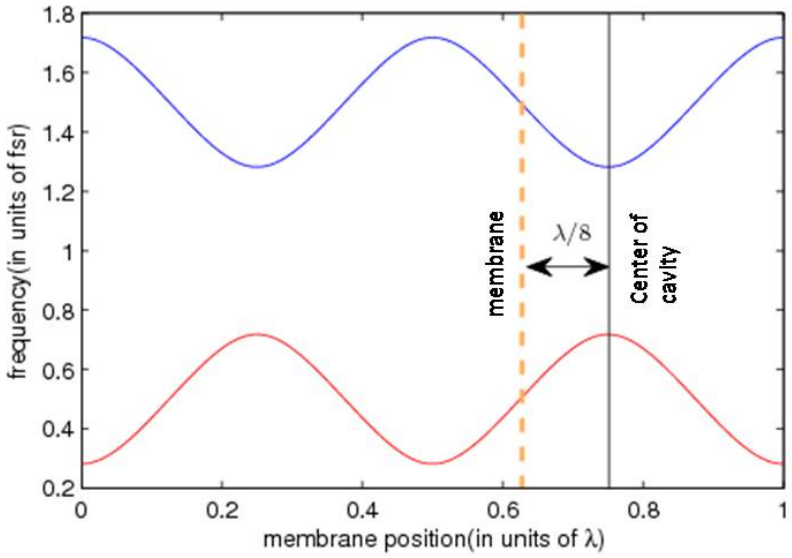

Figure 3.5 The figure corresponds to the case as shown in Fig 3.4 but showing the detuning this time. Blue curve gives the detuning of the higher order mode which is one fsr larger than the other color, that is represented by the red curve. The curves are described by the equation 3.6. Lets say that the black line represents the middle point of the cavity. Then at $\lambda/8$ away from the center, the blue color has a negative slope whereas the red color has a positive slope.

are interested in tiny fluctuations of the membrane around its initial position, we Taylor expand the detuning function around that point and look at the first and second order perturbative terms in the expression.

$$\omega(\frac{\lambda}{8}+x) = \omega(\frac{\lambda}{8}) + \frac{d\omega(\frac{\lambda}{8})}{dx}x + \frac{d^2\omega(\frac{\lambda}{8})}{dx^2}x^2... \tag{3.9}$$

If one calculates the first and second derivatives of the periodic detuning function,one obtains the results below,

$$\frac{d\omega}{dx} = \frac{c}{L}\frac{4\pi}{\lambda}\frac{r_m sin(\frac{4\pi x}{\lambda})}{\sqrt{1-r_m^2 cos^2(\frac{4\pi x}{\lambda})}} \tag{3.10}$$

$$\frac{d^2\omega}{dx^2} = \frac{c}{L}\frac{-16\pi^2}{\lambda^2}\frac{r_m(r_m^2-1)cos(\frac{4\pi x}{\lambda})}{[1-r_m^2 cos^2(\frac{4\pi x}{\lambda})]^{3/2}} \tag{3.11}$$

After finding those derivatives, the rest is just to put $\lambda/8$ for x since we have decided to operate at this point. Then the derivatives become,

$$\frac{d\omega}{dx} = \frac{c}{L}\frac{4\pi}{\lambda}r_m \tag{3.12}$$

wheres the second derivative vanishes at that point yielding,

$$\frac{d^2\omega}{dx^2} = 0 \tag{3.13}$$

Equation 3.12 is very simple and intuitive. The detuning signal is linearly proportional to the tiny membrane displacements around this equilibrium point and it also scales linearly with the reflectivity of the dielectric membrane. For the red color which we have analyzed so far, the signal is positive as expected. So than we can write the detuning term including a constant term which comes from the value of the function at the $\lambda/8$ point. Calculating the detuning function at this point, our equation for the detuning of the red light becomes,

$$\omega_{red} = \frac{c\pi}{2L} + \frac{c}{L}\frac{4\pi r_m}{\lambda}x \tag{3.14}$$

Now let us do the same thing for the higher frequency which is namely the blue light entering the cavity. To write the detuning function for the blue beam, one has just to make a small trick which is to add a phase of $\lambda/4$ to the argument of the cosine in the detuning function. Because this way, we mathematically imitate our figure which means that when one of the beams has its antinode at a certain position, the other color has its node at that same point. Therefore we write the frequency for the blue color in that way as follows,

$$\omega(x) = \frac{c}{L} arccos[r_m cos(\frac{4\pi(x + \lambda/4)}{\lambda})] \tag{3.15}$$

If one now calculates the derivatives for the blue color, one will easily see that the results are the same except for a sign change. And no surprise that this comes from the phase difference we added. So jumping ahead, I directly write the detuning expression for the blue light,

$$\omega_{blue} = \frac{c\pi}{2L} - \frac{c}{L}\frac{4\pi r_m}{\lambda}x \tag{3.16}$$

So just as we expected, the detuning term again linearly scales with the membranes displacement but this times appears as a negative term. Thus we have confirmed that when our membrane is put $\lambda/8$ from the center of the cavity and if it moves around that point, we will get signals with opposite signs for the red and blue beam.

3.2.2 Error signal from the two colors based on the PDH method

In this section I will try to show how the error signal coming from our two colors will look like with respect to the displacement of the membrane. Throughout this section, I will construct the analysis based on a locking-method called the Pound-Drever-Hall lock. So I will basically follow the famous paper [18] which is a very nice source due to the authors pedagogical approach. I will mainly pull out the key results from the paper, so I would suggest the reader to refer to the original paper for the details and derivations.
Before I move on to the analysis part, I shall briefly discuss what the PDH method is. It is an extensively used technique for locking a laser's frequency to a cavity or vice versa. The

idea is simply as follows; lets say we try to keep our frequency at a point with respect to the resonance defined by the cavity length and we want to apply a feedback to the laser to do this. Basically what we need is an error signal that would tell us where our laser frequency is sitting with respect to the resonance and how much it is away from that point. One can do this by simply sitting at the slope of the transmission signal and lock around this point, however the PDH method, in which we look at the phase of the reflected beam(on resonance), proves to be more sophisticated since it decouples the intensity fluctuations of the laser from the frequency fluctuations(the reflected beam intensity should be zero at resonance). In this method, one has to modulate the laser frequency as a means for measuring the derivative of the intensity since we need to have a sign change to know which side of the resonance our laser is. If we think of our case where we want to measure the tiny fluctuations of our membrane, we would in principle be able obtain the mechanical information coming purely from the membrane, by utilizing this PDH lock setup.
Now I shall refer to our reflection coefficient in equation 3.3 which we derived for our membrane in the middle of our cavity. Suppose that we modulate the phase of our laser. Then what we see would actually be an electric field oscillating at the carrier laser frequency ω_c plus two more fields oscillating at $(\omega_c+\Omega)$ and $(\omega_c-\Omega)$ which are called sideband frenquencies where Ω is the modulation frequency. Neglecting higher order sidebands, if we look at the reflected beam power, we would see many terms due to the interference of the carrier beam and sidebands with each other. It would be nice to write the reflected beam to see the components of the signals we are interested in as in [18].

$$\begin{aligned} P_{ref} &= P_c|F(\omega_c)|^2 + P_s(|F(\omega_c+\Omega)|^2 + |F(\omega_c-\Omega)|^2) \\ &+ 2\sqrt{P_cP_s}\{Re[F(\omega_c)F^*(\omega_c+\Omega) - F^*(\omega_c)F(\omega_c-\Omega)]cos(\Omega t)) \\ &+ Im[F(\omega_c)F^*(\omega_c+\Omega) - F^*(\omega_c)F(\omega_c-\Omega)]sin(\Omega t)\} \\ &+ (2\Omega \quad terms) \end{aligned} \tag{3.17}$$

where P_c and P_s refer to the carrier power and the sideband power respectively.
From that point on, we will be interested in the terms that are oscillating with sine and cosine becasue they will be the relevant signal bearing the phase of the reflected carrier. One can get rid of the higher order terms (2Ω) by using a low pass filter in principle. We shall also make our job easier by making some reasonable assumptions. First of all, we will have a relatively fast modulation (our experimental parameters would be 16 MHz and 24 MHz for the seperate modulation frequency of the two colors). At that condition, we can safely say that when our carrier is close to resonance, sidebands will be mostly reflected making $F(\omega_c \mp \Omega) \approx -1$ so our expression containing $[F(\omega_c)F^*(\omega_c+\Omega) - F^*(\omega_c)F(\omega_c-\Omega)] \approx -i2Im\{F(\omega_c)\}$ is then imaginary. Then the real term with cosine does not contribute to the result and omitting the constant terms, finally the error signal of interest takes the simple form below,

$$\epsilon \approx -4\sqrt{P_cP_s}Im\{F(\omega_c)\}sin(\Omega t) \tag{3.18}$$

One can in principle extract this signal by using a mixer and adjusting the phase correctly. Then it is possible to get a DC component which carries information about the frequency shift. Now let us see how this works in our special case with two mirrors and a membrane

sitting at the $\lambda/8$ position. To see how the error signal looks in our case for the two colors, a Matlab code was written to calculate the reflected power spectrum for each frequency component and compute the error signal from that. The cavity is of course modelled to be frequency-detuned due to the membrane motion. The detuning term due to this motion is exactly the one as found in equation 3.12. Note that the term for the red and blue beams bear opposite signs.

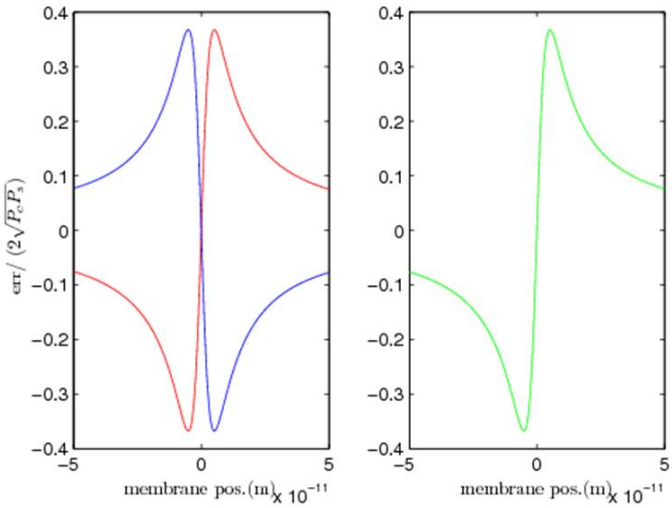

Figure 3.6 The error signal coming from the blue and red beams are shown seperately. They show the same behaviour but the slopes have different signs. Recall that our approach was only valid in the close vicinity of the $\lambda/8$ point. The error signal is only well aproximated as a linear function of x within this limit. Beyond a certain point the error signal drops down as a sign of getting completely away from resonance. Sideband frequencies are 24 MHz for blue beam and 16 MHz for red beam. Carrier power is set to be 1 milliwatt . Reflectivities of the mirrors are close to 1 and power reflectivity of the dielectric membrane is 0.4 (left). The differential error signal of the blue and red beams. In our experimental scheme, we will subtract the two signals by a differential circuit. So the figure shows the final signal that comes from differentiation. As a result, the membrane motion results in a cavity frequency detuning and consequently we see this frequency detuning by looking at the error signal from the reflected beam (right).

3.2.3 Shot-noise limited resolution of two-color probing

This section will deal with the estimation of our resolution for the position measurement. I will try to find an approximate expression for the shot-noise limited sensitivity of our two-color scheme. The idea is as follows; we regard the detuning due to the membranes displacement as a small perturbation on a two-mirror cavity system. So I just add a frequency term to the resonant frequency and see how the error signal is affected by this small frequency change. Finally we convert this frequency change to membrane's displacement because it is, as derived before, a linear function of membrane motion. Thus we can cal-

culate the shot-noise limited signal and see how small we can resolve. However, we should be aware that this is a limited approximation. It is actually a very nice approximation on the limits where the reflectivity of the membrane goes to 0 or 1 because at those limits the system very much looks like a two mirror cavity. But at intermediate values of membrane reflectivity, the system rather resembles a two-coupled cavity combination instead of one, which might make things more complicated. This is apparent from the reflection coefficient expression in equation 3.3. The equation does not look so intuitive in this form and not easy to linearize with respect to the frequency. Instead, what we look for, is a simple linearizable expression from which we can easily switch to a dependance of displacement. In this regard, I assume that the linear response we get from a detuning due to the displacement of the membrane does not make much difference whether I use the reflection coefficient expression for the two mirror plus membrane picture or only the two mirror case. Our approach is also justified by the fact that the existance of the membrane does not alter the finesse(therefore sensitivity) in a dramatic manner for finesses of a few thousands [16]. So then I take the well-known two-mirror cavity reflection coefficient from [18], which is much more easily linearizable with respect to the frequency and treat the membrane detuning as a small perturbation on that expression. The expression is given as follows,

$$F(\omega) = \frac{r(e^{(i\frac{\omega}{fsr})} - 1)}{1 - r^2 e^{i(\frac{\omega}{fsr})}} \tag{3.19}$$

Our aim is to make this expression simpler so that we can directly insert it in the error function equation 3.18 to find the sensitivity. Then the idea is to get rid of the exponential term and rather have linear dependence of the angular frequency. First of all, the angular frequency ω in the above equation can be written in that form,

$$\omega = 2\pi N fsr + \delta\omega \tag{3.20}$$

The first term in the frequency represents the resonant term (an integer multiple of the free spectral range) and the second term is some small detuning. In our case, of course this corresponds to the membrane's displacement. As can be easily seen, the first resonant term does not bring any change to the equation because the exponent is a multiple of 2π yielding 1. From this point on, we have to make several assumptions. Here I will give the main results and the reader can see the full derivation of the linearized equation in Appendix B. After some algebra and assuming that $r \to 1$, the finesse is high and the detuning is small with respect to the cavity bandwidth ($\delta\omega \ll \delta\nu$) which are all sound arguments for our experimental scheme, then we reach a very simple expression for the reflection coefficient as given in [18],

$$F(\omega) \approx \frac{i\delta\omega}{\pi\delta\nu} \tag{3.21}$$

where of course $\delta\nu = fsr/\mathcal{F}$ with $\mathcal{F}$ referring to the finesse of the cavity. Next we have to insert the reflection coefficient into the expression for the error signal in equation 3.18. At this point we make use of the fact that $\nu = fsr/\mathcal{F}$. Then the error signal for one of the colors (omitting negative signs) would be given by(sharing the power to two colors equally is taken into account)

$$\epsilon = \frac{4}{\pi}\frac{\sqrt{P_s P_s}}{c} L\mathcal{F}\delta\omega \tag{3.22}$$

After putting in the detuning term we have derived for the two colors (equ. 3.12) which depends linearly on membrane displacement, and then subtracting the two signals from each other, we finally reach for the error signal the expression below,

$$\epsilon = 32\sqrt{P_c P_s}\mathcal{F}\frac{r_m}{\lambda} \tag{3.23}$$

Now to find the shot-noise limited sensitivity, we assert that we are only limited by the shot-noise of photons hitting our detector, the noise spectrum of which is given by [18] as,

$$S_{shot} = \sqrt{\frac{2hc}{\lambda}2P_s} \tag{3.24}$$

The reason why we put $2P_s$ for the power is simply because that in our case the detector will mainly collect the sidebands which are mostly reflected from the cavity. Finally to find the sensitivity reached in this limit, one has to divide the shot noise spectrum by the error signal. Thus the length sensitivity becomes,

$$S_L = \frac{\sqrt{hc}}{16 r_m \mathcal{F}}\frac{\sqrt{\lambda}}{\sqrt{P_c}} \tag{3.25}$$

The expression makes sense ; the resolution increases as we increase the membrane reflectivity (because the detuning signal is linearly proportional to the reflectivity) and it also increases with the input power and the finesse. To get a feeling of how small one can resolve with such a cavity, I inserted in realistic parameters similar to be realized in our experiment. For $\lambda = 810$nm, $r_m = 0.5$, finesse of 1000 and an input power of 1 mW, it is possible to reach a shot-noise limited resolution of approximately on the order of $10^{-18}m/\sqrt{Hz}$.

3.3 Common-mode noise rejection and experimental considerations

So far we have performed a mathematical analysis of the error signal given that we had two colors coming from the same laser source. As stated before, the main goal of using the two color approach is to eliminate classical noises as common mode signals to both colors. It is quite easy for eample to see the cancellation for the intensity noise. Since both blue and red colors come from the same laser source, the fluctuations would be the same for both and when we subtract the two error signals we would in principle cancel that noise to a large extent. This is a method extensively used on electronic circuits which is called Common Mode Rejection. That is also valid for frequency noise, phase noise and the vibrational noise of the cavity. Let us take the case where the cavity length increases; then if we consider the probing position for blue and red colors, they will both be displaced to the blue side of the resonance peak. And if the cavity length decreases, they will both be displaced to the red side of the resonance curve. Therefore the net effect would be zero if we subtract those two signals. The same model holds for the frequency noise as well.
There is noise cancellation if we also think of the radiation pressure effects. If one has only one probing color inside the cavity, this color would actually drive the membrane with a stochastic force due to the intensity fluctuations. This would then heat the membrane by setting it into a driven motion. However, with the two color scheme, since the coupling of

blue and red colors to the membrane is with opposite sign, this effect cancels in principle. This advantage can be utilized in experimental setups where one wants to see the quantum correlations between light and the membrane position. This requires that (apart from thermal noise), the classical noise coming from radiation pressure should be eliminated so that the quantum behaviour is not screened by the classical fluctuations. The idea has actually been proposed in a recent paper [19].

Now I shall comment on the experimental realization of such a scheme. We have actually been at the construction stage of the two color scheme along with the membrane characterization and one can say that the requirements of the setup is achievable even though there are some practical difficulties. The crucial idea behind the experimental realization of that two color probing scheme lies in the generation of two colors that are exactly one fsr away from each other in the frequency space. And one should also note that these two colors should come from the same laser source so that the noise is common to both colors. This idea can in practice be achieved by splitting the main beam into two paths and using AOMs (Acousto-Optical Modulators) to shift the frequency of both colors in a double-pass configuration. The scheme can be realized in such a way that while the frequency of one color is up-shifted(blue), the other one is down-shifted(red) and when they pass through the AOM second time, they are again shifted with the same amount. This way one can achieve a huge frequency seperation between the colors. Our design of the cavity requires that our free spectral range is 3.26 GHz and this frequency seperation is achievable with high bandwidth AOMs.

The other concern is the detection of the signal from the two colors. The scheme requires that we should be able to distinguish the two colors when we detect them and then through a subtraction circuit, we look at the difference of the two signals. To implement this, one can use two EOMs (Electro-Optic Modulators) for modulating each color at a different frequency so that after demodulation of the signals, we can see which signal corresponds to which color. The use of EOM is anyway a must for the realization of the PDH method as well. So we basically aim to phase modulate one color at 16 MHz and the other at 24 MHz. Then one needs a fast photodetector and an electronic circuit that produces the differential signal of the two colors.

The two-color scheme would of course bear technical difficulties that might deteriorate the ideality of the perfect noise cancellation. This may in principle come from different sources which would result in signals that are not of common-mode origin for both colors. One immediate non-common source of errors would of course be the different responses of the two AOMs and EOMs used seperately for the red and blue colors. Yet another issue might be path length changes of the two seperate beam passes. Based on this logic, one should take care of the elements like amplifiers used in the setup. It would always be a better idea to use such elements in a way that would feed the signal to two colors in a common mode. However given that we will be interested in relatively high frequencies (MHz range), those uncommon noises still seem to be unlikely to have a strong deteriorating effect on the noise cancellation.

On the whole, we laid down the mathematical foundation behind the two-color probing scheme where the membrane sits at $\lambda/8$ position inside the cavity. We derived the detuning term which linearly scales with the membrane motion and we estimated the shot-noise limited sensitivity of the two-color probing. Finally I touched upon the experimental realization of the idea. It would be one of our future goals to investigate this two-color probing scheme

and whether it really helps reducing the noise significantly. For this, of course we have to construct the cavity with two mirrors and be able to find a way of precisely controlling the membrane position since it might be tricky in a high-finesse cavity. Later on, the two color scheme might be utilized for radiation-pressure noise cancellation and seeking for quantum correlations of light and the membranes we have(and will have) characterized.

Chapter 4

A model for membrane's eigenmodes and motion

This chapter is intended give the theoretical background for the mechanical characterization of the specific membranes that we aim to use in our prospective Quantum Optics experiments. Mechanical characterization, namely the eigenfrequency and Q-factor determination, is an essential task before proceeding to any optomechanics experiment with those membranes. But apart from that, it can be regarded as a seperate field of research where fabrication of high Q(low loss) resonators is one of the main goals. As I have touched upon the importance of having high Q resonators before, it has been of great interest to investigate the trend of Q-factor in specific conditions of temperature and different ways of mounting. The flow of this chapter is organized as follows; I shall first start with the theory behind the mechanics of a rectangular membrane. I will introduce the simple model that explains the modes with which the membrane oscillates. With this simple approach, we will try to estimate the eigenfrequencies of such a resonator. Then I will introduce our Fabry-Perot Cavity composed of a membrane and a mirror and will show briefly how the membrane responds to thermal fluctuations and to an external radiation-pressure force. This way we can understand how one can actually monitor the membrane's mechanical response by a cavity-assisted interferometric measurement.

4.1 Modelling the oscillations of a rectangular membrane

The SiN(Silicon Nitride) membranes we are going to work with are almost perfect square membranes(Norcada) of 1mm x 1mm size and 50 nm thickness. This special geometry renders our task of determining the eigenfrequencies very easy as I will now show. The membrane is made of a thin SiN film and we have tried two high stress(Si_3N_4) membranes. The SiN membrane is surrounded by a Si support window which can be few hundred microns.

Before starting the derivation, we shall make certain simplifications about the motion of the membrane. First of all, we have a 3 dimensional membrane and we restrict our analysis of motion to a single dimension where the wave travels around the surface of the membrane(x,y) and we look at the displacement in the z direction which is a function of x and y. In other words we are interested in the displacement in the z direction where for example a laser beam passes through. This will also allow us in the future to treat the interaction of

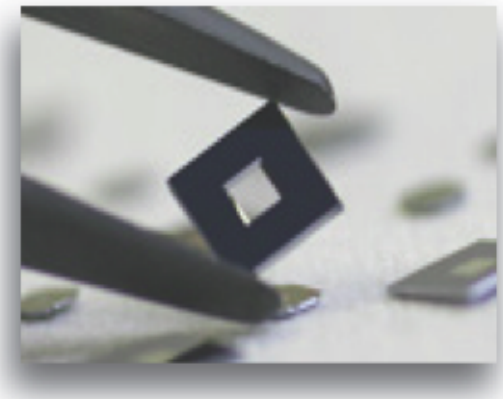

Figure 4.1 A typical square Si membrane. For our SiN membrane the lenghts L_x and L_y are 1 mm x 1mm and the thickness is around 50 nm. The picture is taken from the Norcada website [20].

the probe beam with the membrane in a single direction.

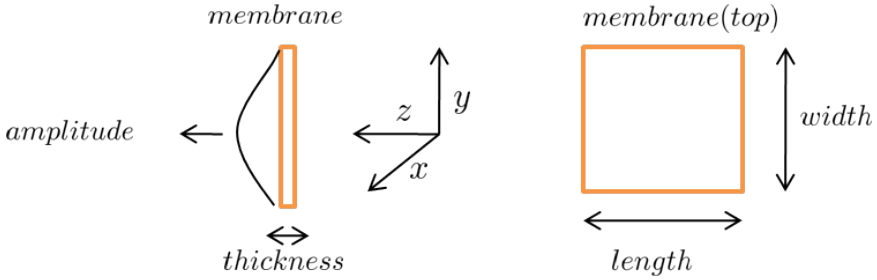

Figure 4.2 The figure depicts the simple motion of a rectangular membrane for a specific dimension here being the z dimension. As the membrane fluctuates ,we observe a displacement in the z direction ; it streches back and forth as a consequence of excitation of a specific mechanical mode.

Our way of treating the membrane motion becomes clearer if we look at the Figure 4.2. For the time being , we treat the membrane as a rectangular structure of length L_x and L_y and derive a rather general formula for the eigenfrequency. As having done our simplifications, we start the derivation by writing down the well-known 2D wave equation,

$$\frac{\partial^2 z}{\partial^2 x} + \frac{\partial^2 z}{\partial^2 y} = \frac{1}{\nu^2}\frac{\partial^2 z}{\partial^2 t} \tag{4.1}$$

As I have mentioned before, here $z(x, y, t)$ is the vertical displacement of the membrane which is a function of x,y coordinates and also time. We should note that ν refers to the speed of the wave propogating in the medium. We proceed by assuming a solution which is seperable to X , Y and Z [21],

$$z(x, y, t) = X(x)Y(y)T(t) \tag{4.2}$$

Once we insert this form of solution back to the wave equation and take the corresponding derivatives, the equation readily turns into the form as below,

$$YT\frac{d^2X}{dx^2} + XT\frac{d^2Y}{dy^2} = \frac{1}{\nu^2}XY\frac{d^2T}{dt^2} \tag{4.3}$$

We now apply the usual trick and divide all the terms in the equation by XYT and also multiply by v^2. Then we reach the following equation,

$$\frac{\nu^2}{X}\frac{d^2X}{dx^2} + \frac{\nu^2}{Y}\frac{d^2Y}{dy^2} = \frac{1}{T}\frac{d^2T}{dt^2} \tag{4.4}$$

This equation has a solution only when both sides are equal to a constant value. Simply working on the right hand side of the equation, we may write,

$$\frac{1}{T}\frac{d^2T}{dt^2} = -\omega^2 \tag{4.5}$$

This equation has the well-known harmonic solution which oscillates at frequency ω. Then we can write $T(t)$ as,

$$T(t) = A\cos(\omega t) + B\sin(\omega t) \tag{4.6}$$

This is also true for the left-hand side of the equation so,

$$\frac{\nu^2}{X}\frac{d^2X}{dx^2} + \frac{\nu^2}{Y}\frac{d^2Y}{dy^2} = -\omega^2 \tag{4.7}$$

After dividing all terms by ν^2 and some manipulation, we have,

$$\frac{1}{X}\frac{d^2X}{dx^2} = -\frac{\omega^2}{\nu^2} - \frac{1}{Y}\frac{d^2Y}{dy^2} = -k_x^2 \tag{4.8}$$

where we have equated the terms to a consant k_x^2.

We can have yet another simplification because the term including Y dependent terms should also be equal to a constant. Thus we have the relation,

$$\frac{1}{Y}\frac{d^2Y}{dy^2} = k_x^2 - \frac{\omega^2}{\nu^2} = -k_y^2 \tag{4.9}$$

where the new constant we introduced satisfies the condition,

$$k_x^2 + k_y^2 = \frac{\omega^2}{\nu^2} \tag{4.10}$$

As a result we have the solution for the spatial coordinates x and y as follows,

$$\begin{aligned} X &= C\cos(k_x x) + D\sin(k_x x) \\ Y &= E\cos(k_y y) + F\sin(k_y y) \end{aligned} \tag{4.11}$$

After this point we have to apply the boundary conditions to this rectangular membrane problem. Of course the membrane is assumed to be fixed from its ends and in this case the wave should vanish at the boundaries. This actually fits well with the real world because our SiN membrane is supported by a silicon frame and we can at this point assume that the conditions $z(0, y, t) = 0, z(x, 0, t) = 0, z(L_x, y, t) = 0$ and $z(x, L_y, t) = 0$ hold. From the first two boundary conditions, we have C=0 and E=0 and moreover from the other two conditions we have $sin(k_x L_x) = 0$ and $sin(k_y L_y) = 0$ yielding,

$$\begin{aligned} k_x &= \frac{i\pi}{L_x} \\ k_y &= \frac{j\pi}{L_y} \end{aligned} \tag{4.12}$$

where i and j are integers.

Finally we are able to write the eigenfrequency ω at which the membrane follows an oscillatory motion. We just put the k constants in equation 4.10 yielding,

$$\omega = \nu\pi\sqrt{(\frac{i}{L_x})^2 + (\frac{j}{L_y})^2} \tag{4.13}$$

To be more clear again , i and j are the specific mode numbers and L_x and L_y are the dimensions of the membrane. Although derived from a very simple approach, this equation is very important for us in terms of comparing our experimentally found eigenfrequencies with theory. To be more specific , we take the square membrane case where the dimension is set to be L . Also dividing by 2π we get the frequency in a rather simpler form,

$$f = \frac{\nu}{2}\sqrt{\frac{i^2 + j^2}{L^2}} \tag{4.14}$$

which is actually the same as stated in [22] where the experiment is done again with SiN films. This equation gives us the frequency for the specific mode we want but one also has to know about ν which is the speed of the wave in the medium. From elasticity theory, this speed is given by the formula,

$$\nu = \sqrt{\frac{\mathcal{T}}{\rho}} \tag{4.15}$$

where $\mathcal{T}$ is the tensile stress and ρ is the density of the membrane. Given that we know these values , one can then easily calculate the expected eigenfrequency. In addition to that, we had better write the solution for the amplitude of the motion just by putting in the spatial and time dependent part of the solution we had for z(x,y,t) as follows,

$$z_{ij}(x, y, t) = [A_{ij}\cos(\omega_{ij}t) + B_{ij}\sin(\omega_{ij}t)]\sin(\frac{i\pi x}{L_x})\sin(\frac{j\pi y}{L_y}) \tag{4.16}$$

here A_{ij} and B_{ij} are of course the constants of motion depending on the initial conditions. Yet a more general solution for the motion would be,

$$z_{ij}(x,y,t) = \sum_{i=1}^{\infty}\sum_{j=1}^{\infty}[A_{ij}\cos(\omega_{ij}t) + B_{ij}\sin(\omega_{ij}t)]\sin(\frac{i\pi x}{L_x})\sin(\frac{j\pi y}{L_y}) \tag{4.17}$$

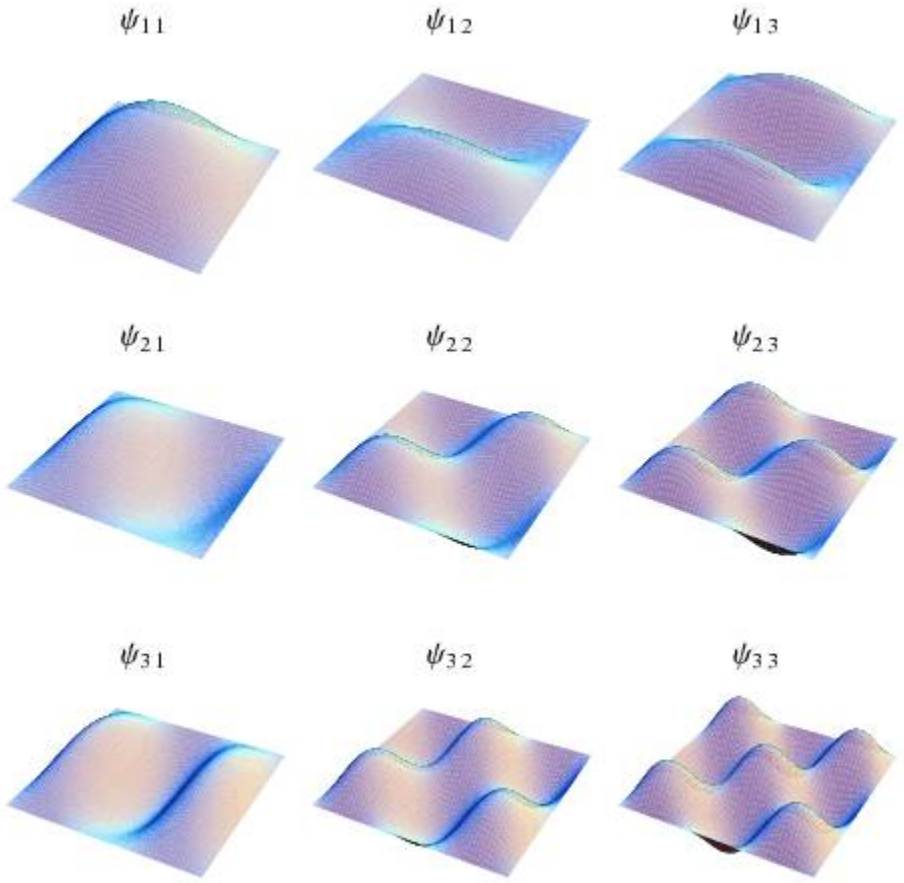

Figure 4.3 Spatial part of the modes for a rectangular membrane. The illustration is taken from Wolfram Mathematica website [21].

The spatial characteristics of the eigenmodes of the membrane will be important for us since in the experiment we will mainly be interested in exciting spesific modes and monitoring the amplitude of vibrations. In that sense, it would be nice to have an illustration of how several modes oscillate in space as in Fig 4.3. Later on in the following sections I will elaborate on how the amplitude of the mechanical response due to external excitation and the Q-factor may depend on the spatial feature of the specific mode.

4.2 Fabry-Perot Cavity formed by a membrane and a curved mirror

In this section, I will deal with the Fabry-Perot Cavity formed by a membrane and a curved mirror. In this configuration, the membrane functions as a movable mirror and our aim is to investigate this motion under the influence of thermal and radiation-pressure excitation for it will be the very phenomenon we will handle in our experiments for characterization. I will first start with the estimation of the amplitude for the thermally-induced vibration. Later in the subsequent subsection, I will outline the simple harmonic motion problem(with applied force) and derive the transfer function. Then I will show how the Q-factor comes into play and enhances the displacement. So this section will provide us an understanding of what we mean by the thermal spectrum of the membrane and external excitation by radiation pressure at a certain frequency. In the last part of the section, I will show what kind of signal we expect to see by monitoring the reflected light from a cavity formed by a membrane and a mirror.

4.2.1 Estimation of the amplitude for the thermally-induced vibration

To estimate the thermally-induced vibration at 300 K- room temperature (the condition we work in our experiment) I shall start by introducing the well-known displacement operator in the quantized picture,

$$x = \sqrt{\frac{\hbar}{2m\omega}}(a + a^\dagger) \tag{4.18}$$

where a and $a^\dagger$ are annihilation and creation operators for the phonons, m is the effective mass and ω is the eigenfrequency of the mechanical oscillator.
One has to take the mean value of the operator $\langle x^2 \rangle$ for a thermal state in order to calculate the thermal noise. (Taking the mean of x does not work since it gives zero for a thermal state). So we have,

$$\langle x^2 \rangle = Tr[x^2 \rho_{th}] \tag{4.19}$$

where we know that the density operator for a thermal state is as follows,

$$\rho = \sum_{n=0}^{\infty} \frac{\bar{n}^n}{(1+\bar{n})^{n+1}} \mid n\rangle\langle n \mid \tag{4.20}$$

with n being the number of phonons. So after plugging the density operator for the thermal state, one gets the following for $\langle x^2 \rangle$,

$$\langle x^2 \rangle = Tr[\frac{\hbar}{2m\omega}(a^\dagger a^\dagger + aa + aa^\dagger + a^\dagger a)\rho_{th}] \tag{4.21}$$

using the commutation relation $aa^\dagger - a^\dagger a = 1$, one further gets,

$$\langle x^2 \rangle = Tr[\frac{\hbar}{2m\omega}(a^\dagger a^\dagger + 2a^\dagger a + 1 + aa)\rho_{th}] \tag{4.22}$$

and performing the math with the raising and lowering operators, we reach the simpler form,

$$\langle x^2 \rangle = \frac{\hbar}{2m\omega}(2\langle n \rangle + 1) \tag{4.23}$$

$$\langle x \rangle = \sqrt{\frac{\hbar}{2m\omega}(2\langle n \rangle + 1)} \tag{4.24}$$

here $\langle n \rangle$ is of course nothing but the mean phonon number which depends on the frequency and temperature dictated by the Bose distribution. And the Bose distribution takes a rather simpler form since we can assume that $kT \gg \hbar\omega$ which translates into,

$$\langle n \rangle = \frac{1}{e^{\frac{\hbar\omega}{kT}} - 1} \approx \frac{1}{1 + \frac{\hbar\omega}{kT} - 1} = \frac{kT}{\hbar\omega} \tag{4.25}$$

Then inserting 300 K for T and 1MHz for ω(fundamental frequency for typical membranes), we reach $\langle n \rangle_{th} \approx 6\text{x}10^6$ for the number of phonons at room temperature. Finally the thermally-induced displacement becomes on the order of $x_{th} \approx 10^{-12} m$.
So this simple calculation so far gives us a feeling about how large the thermally induced displacement at room temperature should be for a membrane of our type. In the thermal spectrum measurements what we try to see, would be the peaks at the resonance frequencies of the membrane with the amplitudes being determined by the thermally-induced excitation.

4.2.2 Displacement under the influence of an external force

In this subsection, I will try to show how the Q-factor comes into play when we are talking about exciting the membrane with an external force. So we start with the simple harmonic oscillator problem, namely with the equation of motion where we have some damping and an external force, which in our case, is of course the radiation pressure. The equation in the time domain reads as,

$$m\ddot{x} + b\dot{x} + kx = F_{rad} \tag{4.26}$$

where b denotes damping and k denotes the spring constant associated with the motion. Applying the Fourier transform trick and dividing by m, the equation becomes,

$$-\omega^2 x + i\frac{b}{m}\omega x + \frac{k}{m}x = \frac{F_{rad}}{m} \tag{4.27}$$

Here we shall define the decay rate $\gamma = b/m$ and the bare resonance frequency $\omega_0^2 = k/m$. Then the equation for the displacement reads as,

$$x_\omega = \frac{1}{\omega_0^2 - \omega^2 + i\omega\gamma}\frac{F_{rad}}{m} \tag{4.28}$$

Now taking the absolute value and then the square of both sides would make it more meaningful as it will give the power spectrum,

$$|x(\omega)|^2 = \frac{1}{(\omega_0^2 - \omega^2)^2 + \gamma^2\omega^2} |\frac{F_{rad}}{m}|^2 \tag{4.29}$$

and imposing the condition that we are driving the excitation at the mechanical resonance which means $\omega = \omega_0$, the equation gets much simpler,

$$|x|^2 = \frac{1}{\gamma^2\omega_0^2} |\frac{F_{rad}}{m}|^2 \tag{4.30}$$

and finally taking the square root again yields,

$$|x| = Q\frac{1}{m\omega^2} F_{rad} \tag{4.31}$$

since Q can be written as ω/γ .This is a very simple result showing how the Q-factor enhances the effect of the excitation coming from the radiation pressure. Therefore it means that it is easier to get a high response from a high Q mode of a mechanical resonator. Later it will turn out that this is what we also observed for exciting our membrane during the experiment. What we basically do in the experiment is that we send an excitation laser beam on the membrane which is modulated at the mechanical resonance frequency and hope to kick it in a proper manner so that we can excite that specific mode.

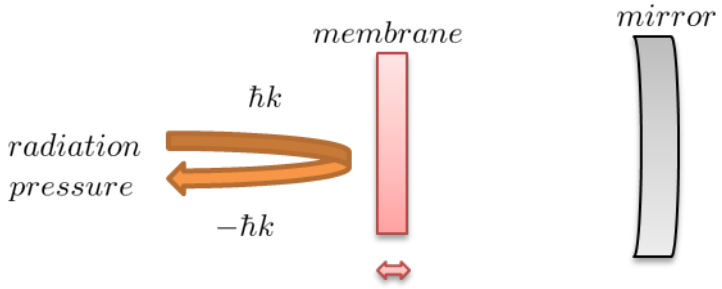

Figure 4.4 The figure is a simple depiction of how one can excite the mechanical mode of a membrane by just shining light on it. In this way radiation pressure couples to the membrane and exerts a momentum of $2\hbar k$ that results in a detectable response due to driven oscillations.

4.2.3 Reflected power from the membrane-mirror cavity

In this short subsection, I shall basically show what kind of signal we expect from a cavity formed by a membrane and mirror. In the previous chapter regarding the two color scheme we had already determined in detail how the signal looks like when we use the Pound-Drever-Hall locking scheme. However, in this case we actually have a rather bad cavity(low finesse) due to the poor reflectivity of membranes as mirrors. As a difference from the PDH method, we will try to operate around the linear slope position of the transmitted light and we will detect the amplitude modulation due to the membrane's fluctuations by monitoring the AC signal of the reflected light from the cavity.

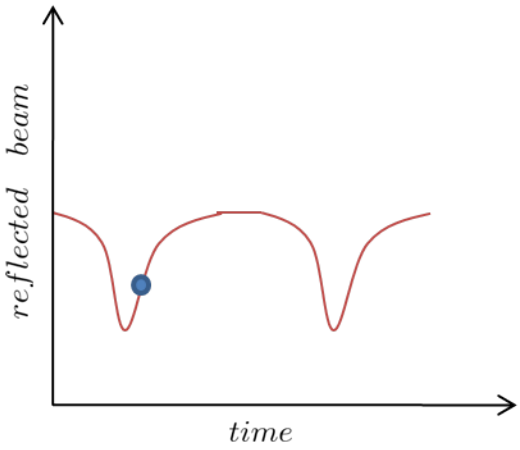

Figure 4.5 For characterizing the membrane's mechanical properties, we use a cavity assited interferometric setup where the membrane functions as the free end of the cavity. As the membranes moves at its eigenfrequencies, it modulates the intensity of the transmitted and reflected beam at those frequencies. We operate around the slope and look at the fast AC signal from the photodetector that collects the reflected light.

It is also better to mention the transfer function of such a membrane-mirror cavity. The cavity formed in this way is an assymetric one due to the different transmission and reflection coefficients of the two elements. Carrying out the calculation for the electromagnetic waves in the cavity and letting the amplitude and transmission coefficients be r_1, t_1 and r_2, t_2 for the membrane and the end mirror respectively, the reflection coeffcient for the cavity reads [18],

$$F = \frac{-r_1 + r_2(r_1^2 + t_1^2)exp(i\frac{\omega}{fsr})}{1 - r_1 r_2 exp(i\frac{\omega}{fsr})} \tag{4.32}$$

So the power reflected from the cavity is proportional to the absolute square of that function and the input power. Here ω is the frequency of the incoming light and as we did in the previous chapter, one can insert for the frequency a term consisting of probing frequency(depending on where you sit with respect to the fsr- in this case the steep slope) plus the fluctuating x dependent term due to the detuning from the membrane fluctuation. Then it is possible to derive an x dependent signal which would carry the membrane's oscillation information.
To summarize the chapter, we saw how the membrane motion can be simply modeled starting from the rectangular wave equation and how it responses under the influence of the thermally-induced and radiation pressure-induced excitation. We also touched upon the transmission and reflection properties of a Fabry-Perot cavity formed by a membrane and a fixed mirror and the expected response from this interferometric setup. I hope this theoretical section will provide us a basis for understanding the experiment in a deeper way. Also we will later see how succesful the simple model for estimating the eigenfrequencies of the membrane is, when we compare it to the experimental data.

Chapter 5

Experimental Setup

This chapter is intended to give the details of the experimental setup for characterizing our SiN membranes. We did both thermal spectrum and ring-down measurements on two SiN membranes so I will show two experimental schemes which are slightly different from each other. After having elaborated on the idea of exploiting the setup for our purposes, I will give information about the key elements of the experimental setup.

5.1 Overview of the setup

As stated in the previous chapter, we would like to investigate the mechanical properties of our membranes by using a Fabry-Perot cavity formed by the membrane and a curved mirror. I shall first start with the thermal spectrum measurement setup in which we try to see a bare thermally-induced signal from the membrane at 300 K. By looking at the spectrum analyzer one can then determine the eigenmodes of the membrane and compare the values with theory. Moreover one can also try to determine the Q-factor, namely by dividing the frequency to the width of the thermal peak.

5.1.1 Setup for thermal spectrum measurement

The idea of the thermal spectrum measurement (Fig 5.1) is as follows ; We formed a Fabry-Perot cavity from the SiN membrane and the curved mirror. The cavity was placed in a vacuum chamber with a pressure of around 10^{-7} Torr. The probe light from a TiS laser operating at 810 nm was directed into the cavity and mode matched. For this, we monitored the transmitted light from the mirror and aligned the mirrors so as to get a nice Gaussian $TEM_{0,0}$ mode which means that we had to minimize all the other modes. On the other hand, the curved mirror(piezo attached) was also driven by a function generator to scan the cavity length. For our experiment, we looked at the transmitted light and made sure that we could see a few resonance peaks due to the scan. Then the scan was turned off and by adjusting the offset, one can settle around the slope position of the transmitted beam. To detect the mechanical signal from the membrane, we monitored the reflected beam and extracted the AC signal from the photodetector. After some amplification, it was sent to the spectrum analyzer to record the mechanical response. Further details about how we made the measurement will be given in the Characterization Chapter. By this spectroscopy

method, one can find out the resonance frequencies of the membrane and estimate the Q value from the width of the resonance line. However, this method is not always reliable as we will see, for the very reason that we are working with quite large Q-factors. As it will turn out, mechanical ringdown measurement has some clear advantages over this method in terms of estimating the Q value correctly. But thermal spectrum measurement helped us considerably in locating the eigenfrequencies roughly and seeing the big picture.

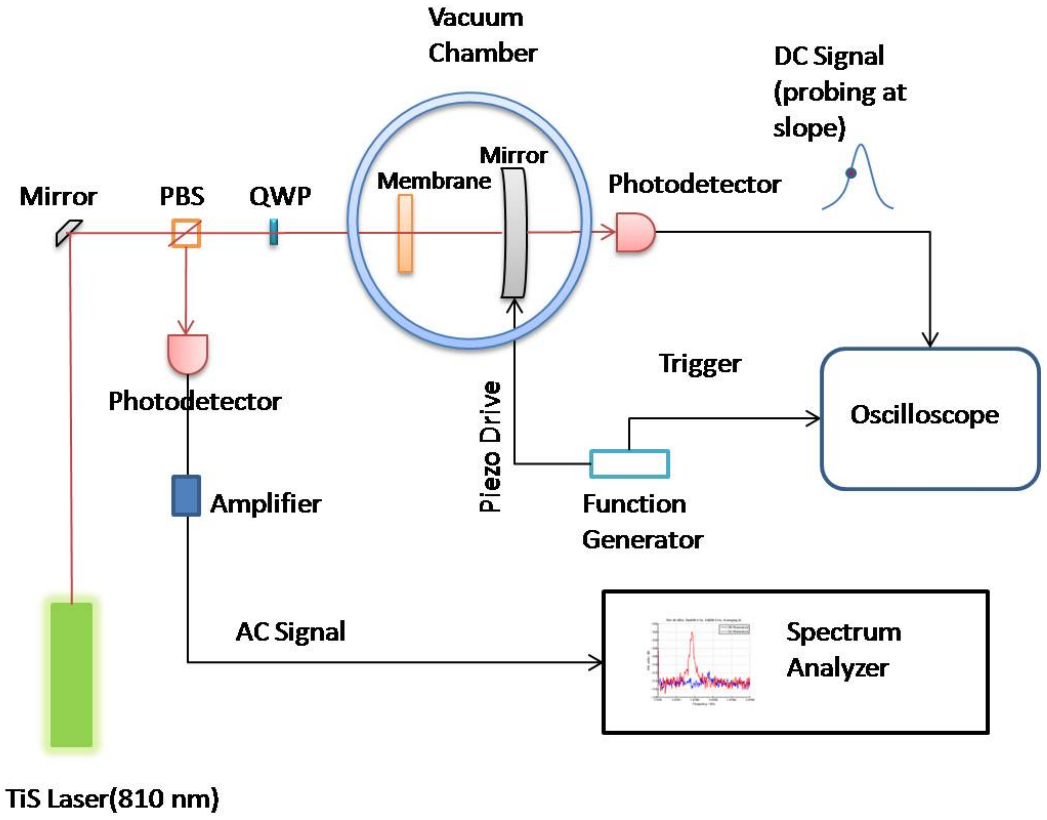

Figure 5.1 Experimental scheme for detecting thermally-induced displacement of the membrane. There are some additional elements like mirrors, waveplates, lenses and CCD but they are not shown here to keep the figure as clear as possible.(PBS: Polarizing Beam Splitter , QWP: Quarter Wave Plate)

5.1.2 Setup for mechanical ringdown measurement

As I mentioned in the previous subsection, we also performed ringdown spectroscopy of our membrane and estimated the high Q values from this measurement. The basic idea behind ringdown experiment is that one excites the membrane at the specific eigenfrequency of interest and then suddenly cuts off the excitation. Then the membrane loses its energy due to damping and decays to an amplitude of zero. One can assert that the energy decay is of exponential form so it follows,

$$Energy = |A_0|^2 exp(-\frac{t}{\tau}) \tag{5.1}$$

here τ denoting the decay time and A_0 is the amplitude. In the frequency domain, Q-factor is calculated by finding the ratio of the frequency to the full width at half maximum and in time domain, this corresponds to an exponential time decay of the energy as stated in the above formula. So if one monitors this decay time, one can easily get the Q-factor from the relation [13] below,

$$Q = \omega\tau \tag{5.2}$$

where ω is the eigenfrequency of the specific eigenmode and τ is the decay time observed. One should be a little bit careful here because we are interested in the energy decay. In my notation, I did not divide $\omega\tau$ by two as is done in [13]. If one talks about the amplitude decay time the above formula should of course be divided by two to find Q. However as we will see, in the experiment we look at the amplitude square of the signal(energy) so there is no need to divide by two.

The ringdown method can also be used to monitor the optical power decay that is transmitted through a cavity and it is extensively utilized in measuring the absorption coefficient of certain materials [23]. Since the absorption brings extra loss in the cavity, the decay time gets shorter and one can deduce the loss from that difference in a quite sensitive way(due to the huge effective path length). One main advantage of the ringdown method is that it is not influenced by intensity fluctuations since one looks at the decay information in time domain. Also for high-finess (narrow bandwidth) cavities, residual frequency noise of the laser with respect to the cavity, is strongly converted to amplitude fluctuations and therefore just looking at the transmitted intensity to measure the absorption turns out to be problematic when compared to time-domain measurements like ringdown [24].

Now I shall describe the mechanical ringdown method we applied in our experimental setup. Probing method is entirely same as the thermal spectrum experiment. We again used the 810 nm TiS laser to probe the mechanical fluctuations of the membrane. However, we needed an additional laser to excite the membrane motion by radiation-pressure force. For this purpose, we used a 852 nm TiS laser and amplitude modulated that light by an EOM(Electro-optic modulator). The function of modulation is to make this excitation light act as a sinosoidal force that is driven at the eigenfrequency of interest. The excitation light was misaligned so that it was not collected at the photodetector since we only wanted to look at the probe light. The rest of the task is to turn this excitation light on/off so that we can cut off the excitation quickly and look at the decay of the response on the scope. This was done by an electronic circuitry the details of which I keep for the Characterization Part. Basically we manipulated the modulation and switched it on/off appropriately. In order to capture the mechanical signature of the membrane, we again used a fast photodetector and extracted the AC signal. Then this signal was fed to a lock-in detection circuit. The reference signal(local oscillator input) was provided by the signal generator which was used to excite our membrane at the same time. So excitation and local oscillator were at the same frequency as they should be. The lock-in detection circuit therefore selects out a single frequency component of the signal. The circuit produces cosine and sine outputs of the signal and these two signals are then electronically converted to square summation, therefore yielding the power.

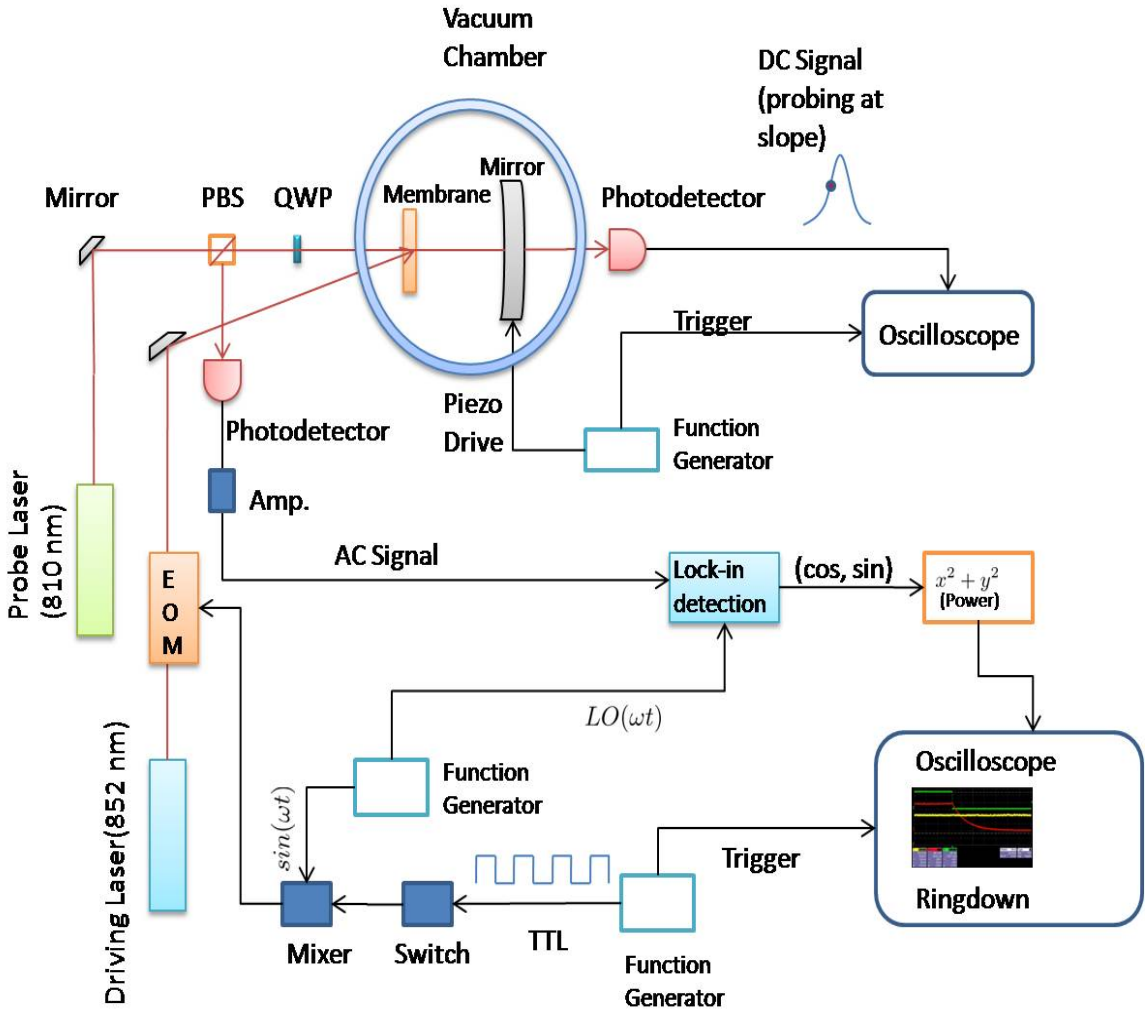

Figure 5.2 Experimental scheme for detecting the radiation-pressure induced mechanical excitation of the membrane(mechanical ringdown).

5.2 Elements used in the setup

5.2.1 Laser sources

For the thermal spectrum measurement we needed one probing laser source and for the ringdown measurment we needed an additional laser source since we had to excite a specific mechanical mode of the membrane. The laser we used for probing is a TiS laser operating at a wavelength of 810 nm. It is actually a tunable laser so we have the opportunity of changing our wavelength of operation. It turned out that the laser output was close to its maximum at around 810 nm so it was a suitable choice for us. The TiS laser is pumped by a 532 nm semiconductor Verdi laser. In order to use the TiS laser source we fiber coupled it to our table for the experiment(this also provides mode cleaning for the beam shape). To prevent reflecting light from disturbing the laser by inducing instability, we used an isolator

just after the output of the TiS laser(for the exciting laser as well). The linewidth of this TiS laser is roughly estimated to be around few MHz. We also used etalon-lock to prevent the mode hopping.
As for the excitation purpose for the ringdown measurement, we used yet another TiS laser which operates around 852 nm. That laser is also pumped by a semiconductor laser. Light from that laser source was modulated by an EOM to provide the sinosoidal driving force for exciting the membrane and after fiber coupling, we shined it on the membrane as shown in Fig 5.2.

5.2.2 Membrane-curved mirror cavity

Our cavity is formed by a membrane(acting as a flexible mirror) and a rigid curved mirror as in Fig 5.3. The free spectral rangel(fsr) of the cavity is calculated to be around 6 GHz from the simple relation $fsr = c/2d$ where our d(distance between the mirror and the membrane) is approximately 2.3 cm. The finesse of the cavity is actually quite low(≈ 3) due to the moderate reflectivity of the membrane and the mirror we used.

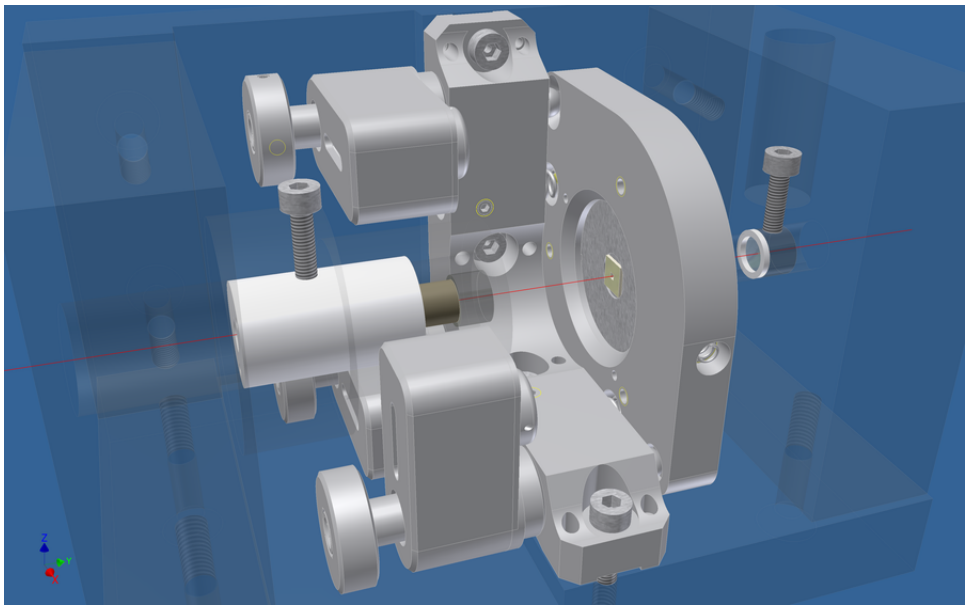

Figure 5.3 The schematic view of our cavity. One end of the cavity consists of the curved mirror which sits on a piezo tube. The other end is formed by the membrane mounted on a circular metal plate. Red line shows the optical beam pass. The cavity is supported by metal supports which are shown in a transparent way here. One can in principle put another mirror to the right side of the membrane and realize membrane in the middle geometry as well.

5.2.3 Curved mirror

The curved mirror is an M44 type mirror which has a radius of curvature of 50 mm. The mirror is in contact with a piezo tube in order to be able to scan the length of the cavity.

It is also surrounded by a teflon cylinder and the voltage cables to the piezo pass through the holes inside the teflon as shown in Fig 5.4.

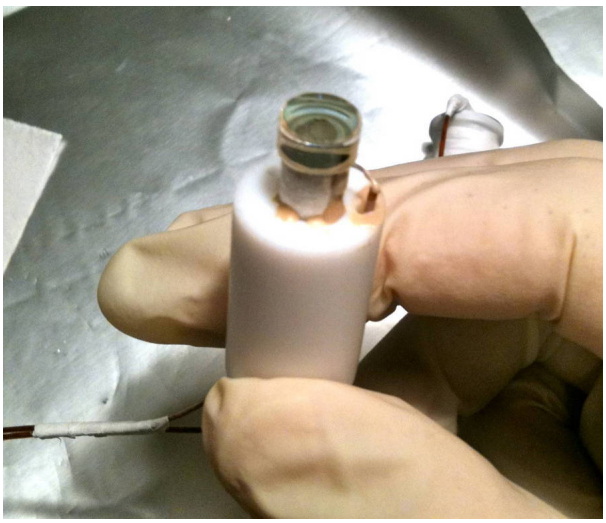

Figure 5.4 Our curved mirror that is attached to a piezo tube.

Our beam width for the probe light was determined by our cavity parameters, namely the mirror curvature and the length. The beam waist that fitted to this configuration was around 80 μm . The beam waist for the excitation light was as well close to that value. By this beam size we ensure that it is well within the membrane's dimensions. We also had to know the transmission properties of our curved mirror. Since the transmission was relatively high, it was easily measured by the conventional method where one looks at the input and transmitted beam and gets the ratio. The measurement yielded a power transmission of around 15 percent.

5.2.4 The SiN membrane and mounting

We had our high-stress commercial membranes(Si_3N_4) from Norcada and we used two different samples and characterized them. The membrane dimension is 1mm x 1mm (square) and the thickness is 50 nm. The membrane's transmission was also measured in the way as the curved mirror and the power transmission seemed to be 79 percent, therefore meaning a reflectivity of almost 20 percent. This way the membrane serves as a very bad mirror. We have not yet made an absorption measurement. It depends strongly on the wavelength and at 1064 μm wavelength, the absorption coefficient is very small(as low as 10^{-4}) as reported in [22] making these membranes desirable to be used in quantum optics experiments where one needs low loss.

Fig 5.5 shows how our membrane mount looks in real life. The empty circle in the middle is for the membrane holder(circular metal plate) which can be screwed to the structure. The mount is connected to three screws which are necessary for changing the membrane's position. The motors are attached to wires and the NewFocus Intelligent iPico driver is connected to a computer.It is controlled digitally by a Labview programme. By playing with the three motors we can tilt and displace the membrane to a certain amount. We

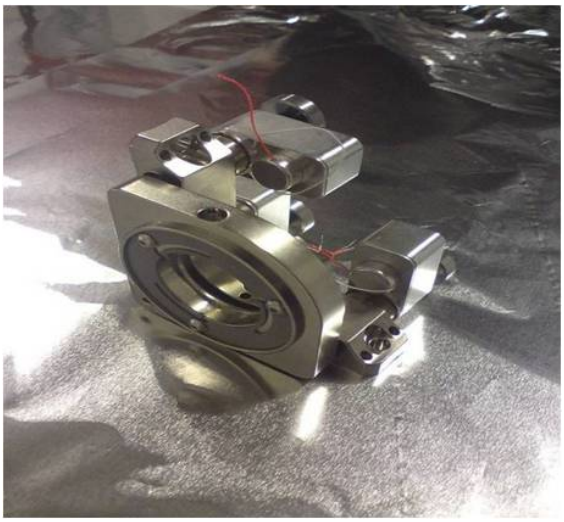

Figure 5.5 The membrane mount which is attached to three motors that can drive the screws to position the membrane.

confirmed an angular resolution of roughly 0.2 arcsecond by looking at the response with a split-diode photodetector. The control mechanism however needs to be developed for we will need a more flexible control of the membrane position for future experiments. The cables that carry the pulse to the motors are of course vacuum compatible. This is true for the connections for the piezo tube as well.
The membrane was glued to a thick, circular metal disk which has a hole in the center so that the optical beam can pass through it. I will elaborate on the gluing method when discussing the measurement results for the Q-factor because apparently, as has been confirmed in other experiments, the gluing technique is important in determining the clamping loss and therefore the Q-factor. In the picture below, you can see how the membrane is glued to the metal disk. This is an example for one point gluing. We have also tried four point gluing to compare the results.

The glue we used for the membrane is a special Epoxy, EPO-TEK H77, which is thermally conductive and electrically isolating. Gluing was carried out by a cure schedule. For the first membrane, we used gluing to four edges and the glue was dropped carefully to the edges of the disk and then the membrane was put above. However, for the second membrane, we used only one point glue(which makes a considerable increase in Q-factor) and the gluing method was slightly different. The membrane was put on the disk and the glue was dropped from above to stick them. This might have helped the Q-factor increase slightly more as we believe. After the epoxy was dropped, the membrane and the disk had to be heated. The simple procedure we followed was to heat them at around 140°C for approximately one hour. The temperature was not increased to 140°C immediately but rather was ramped from a certain value to 140°C in a slow manner. The problem with the epoxy is that it is diffusive and while dropping it to the membrane, it is inevitable to prevent from leaking through the surface. This of course increases the contact area with the support and may increase the clamping loss.

Figure 5.6 A picture showing how our membrane was glued to the metal disk. As stated before, this metal disk was then screwed to the membrane mount in Fig 5.5. Looking carefully at the picture, one can see the viscous glue that has diffused between the membrane edge and the disk.

5.2.5 Vacuum chamber

The membrane's dynamics might be affected by the existence of the air surrounding it. This may introduce extra damping, namely air damping, which would change the Q factor and degrade the measurements. On the other hand air flow in a cavity is not preferable because it is well known that the air density fluctuations might deteriorate the nice optical mode inside the cavity. So especially due to the air damping concern, we operated the experiment in a vacuum chamber which can in principle reach a value of $\approx 10^{-7}$ Torr, already good enough for our purposes.

Cleaning the vacuum elements and assembly

Since we had an old vacuum chamber, we had to make sure that we removed all the contaminated dirt in the chamber and other elements that were suspicious. So if the element is thought to be dirty, it should be cleaned in ultrasonic bath with an ordinary soap solution. First, the bath is heated to 40°C and kept running for 1 hour. Then it should be rinsed using deionised water again in 40°C for 1 hour. This is a precleaning procedure before assembly. The second cleaning stage is wiping the element with spectroscopic grade acetone and finally by methanol. After those steps, the element can be assemblied. We also baked our vacuum chamber to remove contamination . We basically wrapped alimunim foil around the chamber and the ion pump, connected it to heat wires and heated with a heating cord.

Vacuum Pumping procedure

I will simply outline our vacuum procedure here. We used a turbo molecular pump and a diaphram roughing pump to back the performance of the ion pump. The pumping method is as follows; First the TMP(turbomolecular pump) connected to the chamber is turned on

Figure 5.7 The picture shows our vacuum chamber before we put our cavity and the membrane in it. There are several windows which provide optical and electronic access as well as connection to different types of vacuum pumps. Two of the pipes shown here are for connection to the turbomolecular pump and the ion pump.

and after 30 seconds the diagphram pump(DP) connected to the TMP is on. TMP reaches normal operation(56 RPM) and after some time when the Pirani gauge(between DP and TMP) reads 10^{-1} Torr we assume that vacuum level at the ion gauge is around such a value that we can safely operate the ion gauge to measure a lower vacuum level. Waiting for some time and reaching around 10^{-7} Torr, the ion pump is on. We read the vacuum level by a voltmeter and it can reach up to 10^{-9} Torr. Then the connection valve to the chamber is closed . TMP is shut down and DP is shut down 30 seconds later. Ion gauge is off. Sooner this part gets into equilibrium with atmospheric pressure and we can remove that part. So the ion pump by itself continues pumping the vacuum chamber. Without the backing pumps, it can achieve 10^{-8} Torr with an empty cavity and close to 10^{-7} Torr with our cavity and mounts installed.

5.2.6 Detection

I will be more clear about the detection part when I will be dealing with the measurement itself but it is worth noting here the elements we use. For detecting the transmitted and reflected light, we used homemade photodetectors. The reflection part requires a fast photodiode since we would like to see the membranes imprint (around MHz regime) by looking at the reflected beam from the cavity. The photodiode has a bandwidth of 20 MHz. For the thermal spectrum measurement we used an HP spectrum analyzer. For the ringdown measurement we rather needed a lock-in detection where we selected out a single frequency(namely the membrane's eigenfrequency). The circuit is also a home-made one which can show two outputs, cosine and sine component of the signal. The bandwidth of

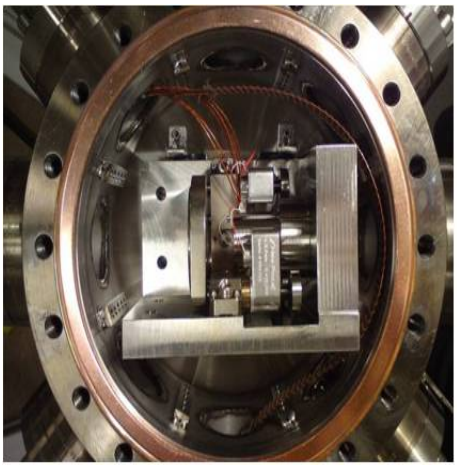

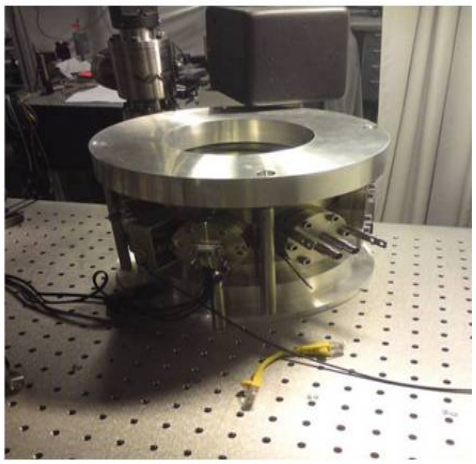

Figure 5.8 Top view of the vacuum chamber including the cavity and membrane mount assembled together (left). Since the cavity should be isolated from unwanted vibrational noise from the environment, we rather need a stable vacuum chamber. The ion pump can also introduce some vibrations that directly couple to the chamber. This structure where the chamber is pressed from above by a heavy metal disk seems to be a nice solution for this. The ground disk can be screwed to the optical table providing stronger support (right).

the circuit was limited by 2 MHz and within the circuit we used a low pass filter of 500 Hz. We amplified that signal(gain 20) after the lock-in circuit and used a function operator which would give square summation, therefore the power of the signal. This was then fed to an oscilloscope to see the real time decay of the mechanical signal. The switching circuitry will be explained in the measurement part.

Chapter 6

Characterization of SiN membranes

Characterization chapter will deal with the measurements of our two SiN membranes and the results together with their comparison. Both membranes are supposed to be identical in dimension, mass etc. We have measured the eigenfrequencies and Q-factors of these two membranes for several modes. Especially for the Q-factor measurements, they yielded different results due to our different way of gluing of the membrane to the mounting structure.This chapter can be regarded as the highlight of the thesis and as we will see in detail, we were able to note quite nice Q-factors (exceeding 10^6 at 300K). Characterization process is substantial for us in terms of understanding how we can improve the mechanical properties of our membrane for the future experiments. We hope to characterize more samples in the future as time permits.

6.1 Measurements with the first SiN membrane

6.1.1 Thermal spectrum measurement

I shall first start with the experiments for the characterization of the first SiN membrane. Our first goal was simply to get a signal at the spectrum analyzer without any external excitation, namely due to the thermally-induced displacement at room temperature. The experimental scheme is the one depicted in Fig 5.1 in the Experimental Setup chapter. We used a HP8561b spectrum analyzer which has a resolution bandwidth of 10 Hz.

Cavity mode-matching

Before the thermal spectrum measurement, we had to mode-match the probing light to the cavity formed by our membrane and the curved mirror. For this purpose, we monitored the transmitted light from the cavity on the scope. Since our cavity had already low finesse, mode-matching was not extremely difficult. We monitored our membrane by placing a CCD camera in front of the vacuum chamber window and this helped us locate the position of the beam with respect to the membrane. We also put another CCD to see the transmitted beam out of the cavity. By using mirrors, we tried to align the beam so that a

good mode-matching could be achieved. We used the membrane mount motors to tilt the membrane and seek the perpendicular situation since the membrane should stay vertical with respect to the beam. Once we realized that the alignment was correct by seeing a nice and bright Gaussian mode, we switched the method to monitoring the transmission on a photodector and therefore on a scope. By playing with the alignment slightly, we tried to attain a nice transmission curve and eliminate other modes so that we would dominantly have the $TEM_{0,0}$ Gaussian mode. In the meanwhile, we were using the signal generator to drive the piezotube attached to the mirror, in order to scan the cavity length.

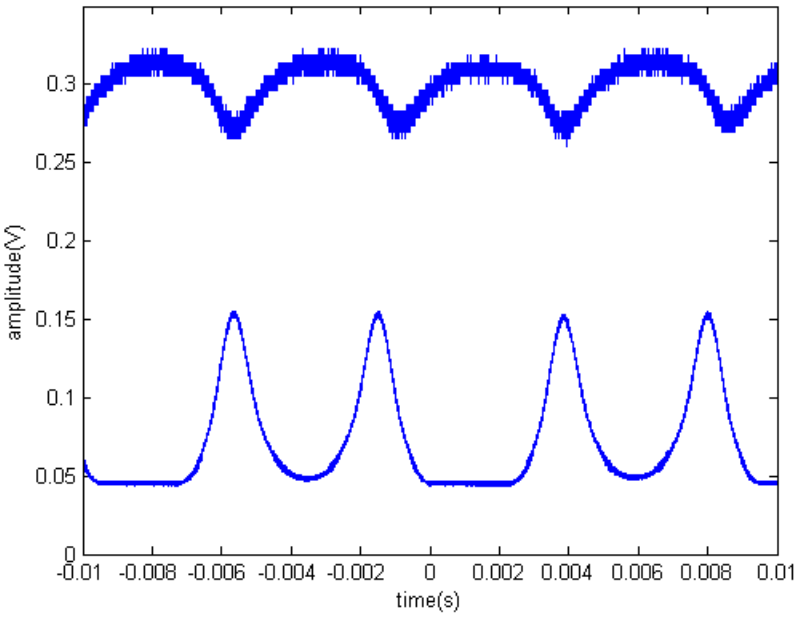

Figure 6.1 The curve below shows the transmission from the cavity while it was being scanned by the piezo-driver. We achieved mode-matching to the Gaussian mode by aligning the mirrors and by checking this transmission curve. The curve above shows the corresponding reflection signal from the cavity, detected by another photodiode which would later on be used to monitor membrane's fluctuations.

Detecting the mechanical signal

After having mode-matched our 810 nm probe light($\approx$ 1 mW) to the cavity, we stopped cavity scanning and chose a specific point for the probe light to stay. This is the steepest slope point, where the fluctuations of the mirror cause the largest amplitude-modulation of the cavity's transmission and reflection. This amplitude modulation is expected to be at the membrane's eigenfrequency of the spesific vibrational mode. We should remind ourselves that the cavity finesse is quite bad, so we do not have a very strong signal enhancement. The naive idea in the thermal spectrum measurement was then to extract the information of the membrane's motion from the photodetector at the reflection path of the cavity and hope to see a strong discernible peak at the corresponding mechanical frequencies. The fast

photodetector(20MHz bandwidth) was used for this purpose and the output after being amplified was sent directly to the spectrum analyzer. We used averaging of 20 to increase the signal-to-noise ratio. We were able to see 6 thermal peaks which were of mechanical origin, namely coming barely from membrane's thermally induced vibrations. The results are shown in Fig 6.2 and one has to be careful at some point because it is possible to misjudge whether a signal comes from membrane or some other noise source. One immediate

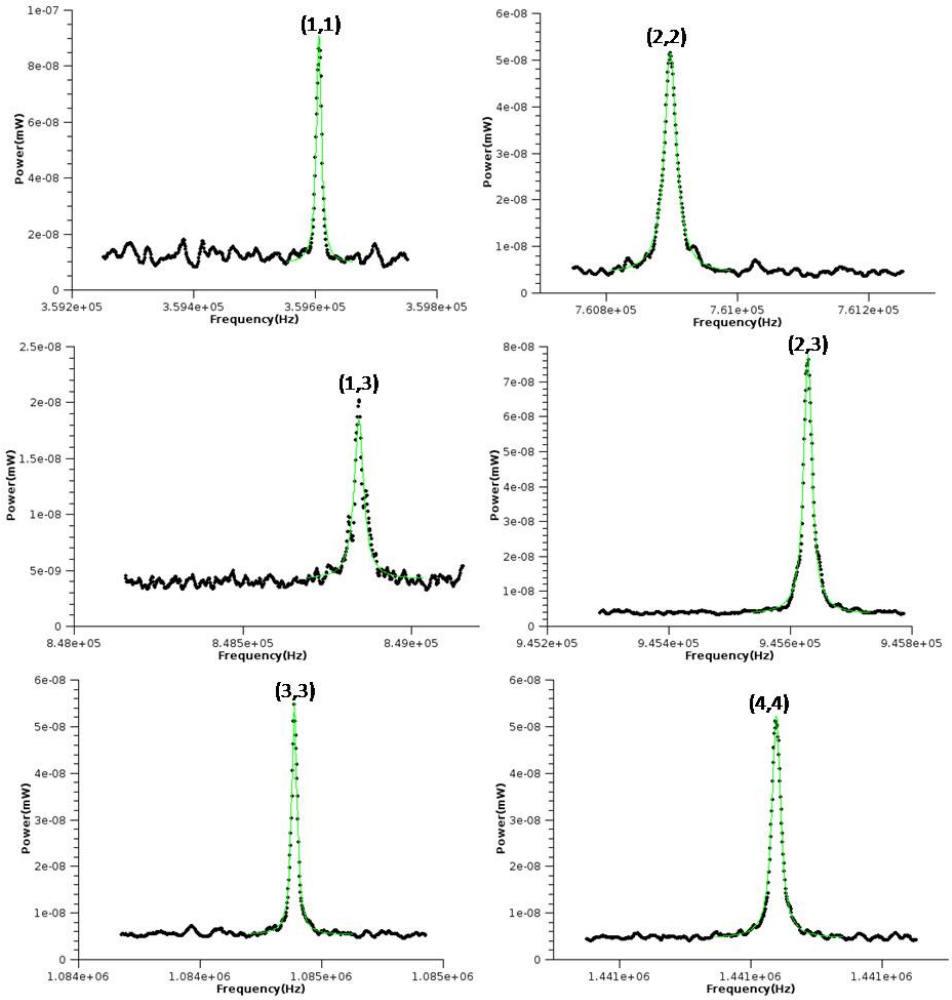

Figure 6.2 The spectrum analyzer data from 6 mechanical peaks of the membrane. The green lines are the Lorentzian fit functions to the resonance lines.

test is to compare these frequencies with the theoretically expected ones and this would give a rough clue about the origin of the signal. But a more strict and necessary proof of whether the signal is of mechanical origin comes from the following test. Apart from staying at slope position, we also looked at the signal at the off-resonance position. This ensures that the signal now does not contain any cavity-enhanced effect, stemming from mechanical fluctuations. So in principle this mechanical signal should dissappear at this operating point. And this is exactly what we observed. We did this test for all the 6 peaks

and all of them dissapeared at the off-resonance point strongly suggesting that they are of mechanical origin instead of noise. (See one example in Fig 6.3)

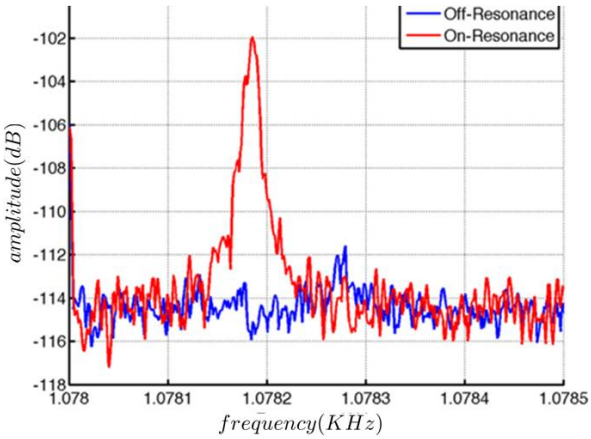

Figure 6.3 The signal from one of the mechanical modes of the membrane. As can be seen, one trace recorded the signal when the probe position was at off-resonance point and the other trace recorded it when it was on the slope. It is obvious from the picture that the signal disappears in the off-resonance case suggesting strongly that the signal is of mechanical origin.

Now I shall elaborate on the 6 peaks individually. What we expect theoretically is that the response of the mechanical resonator to thermally-induced forces will be a Lorentzian function centered at the mechanical resonance frequency. That is precisely what we observed for each peak. Fig 6.2 shows the mechanical peaks and their fits to a Lorentzian of the form,

$$fitfunction = y_0 + \frac{2A}{\pi}\frac{\gamma}{(4(\omega-\omega_c)^2+\gamma^2)} \tag{6.1}$$

where the ω_c is the center frequency and γ is the width at half maximum.

The direct spectrum analyzer data is on dB scale so I converted the data to linear scale(in units of power). The Lorentzian model fits quite well with the spectrum data, however there are some problems with this method when it comes to determining the widths of those peaks. The width information is crucial because one can deduce the Q-factor and also the effective temperature by using that information. So let us think about the limitations of that method. First of all, thermal gradients and instabilities may affect the results. The thermal changes in the environment might alter the membrane's tensile stress and therefore it is probable that the eigenfrequency shifts accordingly. We had beforehand actually observed noticable frequency shifts with the course of time when we had our heat producing elements like amplifiers closer to our experimental setup. Since we do averaging for the spectrum analyzer data and accumulation takes some time, we in principle might have added up small thermal shifts during the measurement that would broaden the resonance linewidth. The other important thing is that since the probe position might deviate from the slope due to slow frequency drifts with respect to the cavity resonance and since we might have intensity drifts as well, the power exerted on the membrane can change and cause small eigenfrequency shifts which we again accumulate in the width. Thus a more precise measurement would

require intensity lock and slope-position lock to stay at the same probing point. Yet another limiting factor is of course the resolution bandwidth of the spectrum analyzer. The best performance our device could achieve was 10 Hz and this might limit the precision. This limitation is more obvious when we consider a high Q-factor mechanical mode. In principle, by dividing the center frequency to the width estimated from the Lorentzian fits, one can calculate the Q-factor. However, we are usually dealing with really high Q resonators(10^5 or 10^6) and this translates into the fact that the resonance linewidths are quite narrow for some modes(a few Hz or even less). Since our spectrum analyzer can not afford that precision, thermal spectrum measurements underestimate the Q-factor when we are talking about high Q modes. This is exactly the case we observed and I shall return to that point in detail. Let us, for now, look at the results from the analysis of the Lorentzian fits and I shall later compare them with the more reliable ringdown results.
First thing worth to note is that the optical signal strength(probe light) coming from each mechanical mode basically depends on two factors. If we go back to the thermally induced displacement, it was shown to be scaling with the inverse of frequency so it is larger for lower order modes. The second determining factor for the signal strength is the spatial overlap between the optical beam(which is roughly focused around the center of the membrane) and the membrane's displacement profile for the spesific mode. Now let us go to the stage which we are more interested in and show the Qf results in a table. Here we estimate the frequency from ω_c of the Lorentzian fit and the Q-factor just from dividing this frequency by the width which is again estimated from the fit. The mode numbers I provide here depend on the eigenfrequency model for our membrane and I will talk about it in detail when we determine the frequencies more precisely for the ringdown measurements. The table will

Mode	Frequency	Q-factor
(1,1)	359.60 kHz	3.6×10^4
(2,2)	760.89 kHz	3.4×10^4
(1,3)	848.84 kHz	2.5×10^4
(2,3)	945.62 kHz	5.8×10^4
(3,3)	1.08455 MHz	1.0×10^5
(4,4)	1.44083 MHz	0.9×10^5

Table 6.1 The table here shows the results of the thermal spectrum measurement for the first membrane.

be useful in comparing these results with the ringdown measurements. Our fundamental frequency turns out to be around 360 kHz and this value makes sense when we consider the stress value of the membrane. By using the equation 4.14 and inserting the density of $\rho = 2.7g/cm^3$ for our membrane of dimensions 1mm×1mm, we get the tensile stress value of $\approx$ 700MPa. This is actually lower than what we expected because our membrane is supposed to be in stoichometric form yielding high stress of around 900 MPa. So we think that our first membrane might be slightly deformed and we owe the discrepency(although not so large) between the eigenfrequency model and data to this deformation. However, for the second membrane we will later see that experimental data perfectly fits theory. We will, after the ringdown data analysis, also see that Lorentzian fit method is quite good in estimating low Q- factors (10^4), but it is not so reliable in estimating high Q-factors of (for

example the fundamental mode) due to the limited resolution bandwidth.

6.1.2 Ringdown measurements with the first membrane

As I stated before, the thermal spectrum measurement has some limitations especially when we are dealing with high Q-factors as in our case. Therefore, for better frequency and Q-factor determination, we had to perform a ringdown experiment for each of the 6 peaks. The experimental scheme is as outlined in Fig 5.2. Since we did not use a piezo crystal attached to the member, we had to excite the membrane's mechanical resonances by some other means. Therefore our ringdown method(in terms of excitation) is different from the similar experiments done by other groups [22, 25]. For this purpose, apart from the 1mW probe light, we used another laser source to excite the membrane's mechanical modes by the help of radiation pressure. Although when performing this optical excitation method we had to be careful about some points which I will touch upon, it can be said that it is a nice alternative where one does not need a piezo for exciting the membrane. One can in this way avoid the extra noise or the complexity that the piezo might bring.
Preparing the experiment is almost the same procedure with the thermal spectrum measurement so I shall not repeat those again. The naive idea behind ringdown is that we excite a specific mechanical mode of the membrane which means that during this time, the membrane builds up power for the oscillation and then we abruptly cut off the excitation so that the amplitude decays through a lossy mechanism(the physics of which I shall touch upon when elaborating on the results) which comes from damping. In principle, damping may stem from a combination of many effects like air pressure, interaction with the intrinsic defect centers of the material, clamping loss due to the coupling to the support, thermoelastic damping etc [26]. Under certain conditions usually one of the effects strongly dominates the damping. In the end, what we are interested in, is this damping time from which we can calculate the Q-factor.

Exciting the mechanical modes of the membrane

This session is the key part for the ringdown experiment. We utilize the radiation pressure from the 852 nm TiS laser to hit the membrane and excite it. We at least needed power on the order of a few mW to make sure that the radiation pressure exerts a sufficient energy for excitation. As can be seen from the figure of the setup, this excitation beam is on purpose misaligned with respect to the cavity. The reason is simply that we do not want this beam to be accidentally collected on our detector. Otherwise through scattering and getting converged by the lenses, this signal can sneak through our detector which would jeopardize the reliability of the measurement since it is modulated at the same frequency as the mechanical signal. To avoid the aforementioned situation, we carefully tested that we eliminated such a fake signal.
The next step is to use the EOM to make this laser beam modulated at the frequency of mechanical oscillation so that we can have an exciting force of sinosoidal form. For this purpose, we aligned the polarization of the incoming beam to the axis of the cystal of the EOM by using waveplates to maximize the amplitude modulation. The figure below shows how we checked the amplitude modulation before we started the experiment. We used 15 percent modulation of our mean light power.

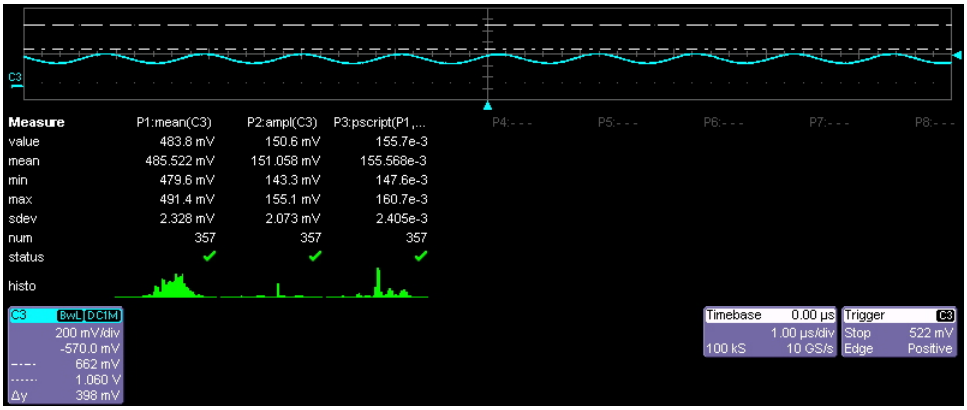

Figure 6.4 Oscilloscope data ensuring that we appropriately modulate our laser beam. Before we started the experiment we had to make sure that we had the proper amount of amplitude modulation so that we could excite the membrane sufficiently.

Detection of the mechanical ringdown

The amplitude modulation for the EOM is controlled by a signal generator and the other port of the generator is used to provide a signal for the local oscillator input port of our lock-in detection circuit. So the idea is to excite the membrane at the mechanical frequency and get a response exactly at the same frequency which will be contained in the reflected light from the cavity. Then this reflected light signal is fed to the lock-in circuit and multiplied with the local oscillator signal which is also adjusted to be at the same mechanical frequency. Therefore, by using the lock-in circuit, we detect only the frequency of interest, namely making the measurement bandwidth narrower. In principle, we can also adjust the relative phase of the local oscillator and the excitation signal to be zero and this usually has to be carried out in an empirical way until we reach a nice looking signal. The result is a cosine and sine signal(both 500 Hz low-pass filtered) which is then, through electronic manipulation, converted to square summation (power) . Finally it is fed to an osciloscope to see the real-time ringdown.

Switching

Switching is definitely a crucial part of the experiment. Not only modulating the excitation light is sufficient, but also one should be able to switch it on/off properly. We actually encountered some problems regarding this issue throughout the measurement and it would be better to give some details here which, I believe, is important in understanding the experiment.
The first method we tried for switching was to use a mechanical shutter. The idea was that we would modulate the excitation laser all the time and then just cut this light on and off by moving the mechanical shutter. However, it turned out to be a bad idea as can be seen in the Fig 6.5. Although we were able to see a signal that looked like a ringdown of the

mechanical mode, it contained a ringing effect which made the measurement problematic. The naive reason behind this, lies in the switching method. By using the mechanical shutter, we had full power during the excitation time and no power during decay time. This caused a problem because the radiation pressure itself exerts a force on the membrane and changes its tensile stress, consequently altering the eigenfrequency. And if there is a huge difference in light power during on/off times(which is the case in the mechanical shutter) then we would have some difference between the driving frequency and the real membrane frequency. It is highly probable this gives rise to a beating effect which results in the ringing we observe as shown here.

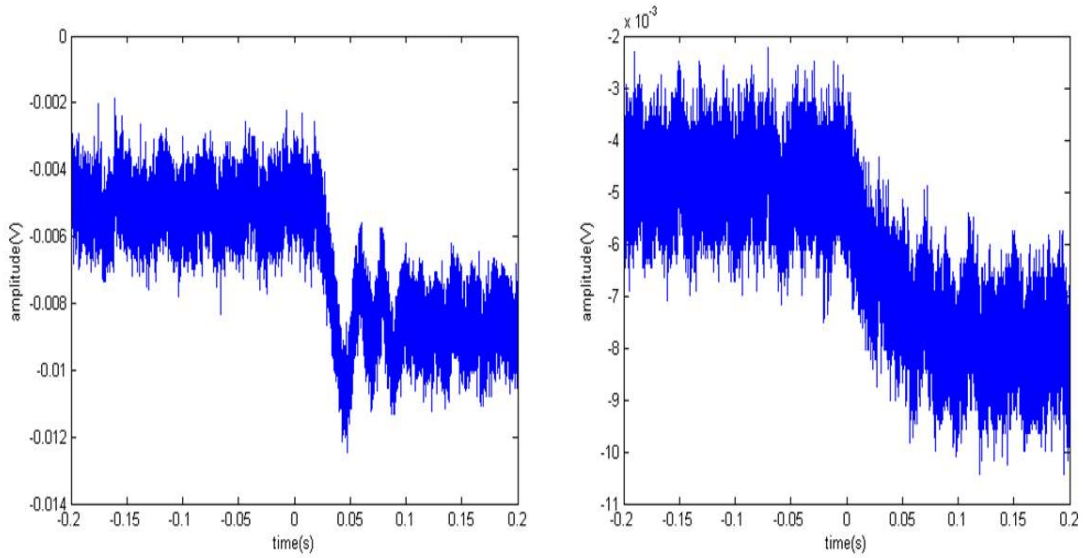

Figure 6.5 The figure (left) shows the scope signal in the case of using the mechanical shutter for switching purpose. There is a ringing effect due to the frequency shift between the real eigenfrequency and the excitation frequency. However, as seen in the other figure (right), if we change the switching method where we use the signal generator without cutting the light off totally, as opposed to the case with the mechanical shutter, we can remove this unwanted effect. The excitation pump power was around 10 mW.

Modifying the switching method

After having failed with the mechanical shutter method, we removed it and tried to control the switching by some other means. The basic idea was to keep the mean power of the excitation light always at a certain level and on top of that add modulation which would be switched on and off continuously. In this case, even if the modulation is off during the decay period, the mean radiation pressure is still there, keeping the eigenfrequency of the membrane around the same value. And it turned out that this method worked out well and removed the ringing effect. The switching method was briefly as follows; we modulated the EOM through the function generator, but before feeding the sinosoidal signal from the generator(adjusted to be at the mechanical frequency) to the EOM, we fed it to a mixer.

We also used another function generator to create a TTL pulse(square) and fed it to the mixer as well. The resulting signal after the mixer could be fed to the EOM and used to switch the modulation on/off without changing the mean radiation pressure.

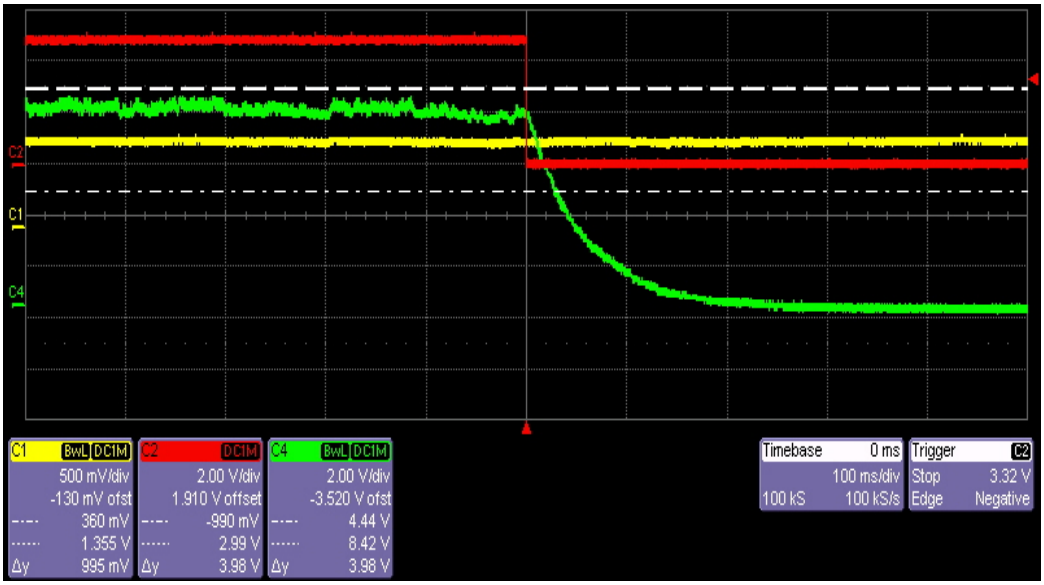

Figure 6.6 The figure shows the direct signal on the oscilloscope which captures one excitation and decay event(fundamental mode around 360 kHz). The yellow signal comes from the transmission of the cavity and this gives information about where our probe light sits. In all of the measurements we kept an eye on this signal by changing the offset of the piezo and trying to hold the yellow line in the middle which corresponded to the slope position. The red signal is the trigger. As it cuts off the excitation, the ringdown immediately starts(green signal-mechanical) and we measure the decay time to estimate the Q-factor.

Scanning and finding the right frequency of excitation

Another important issue is to excite the membrane at the right frequency so that we match the resonance. This is not so easy as well. We firstly located the peaks roughly by using the spectrum analyzer. This gives a helpful picture of where we should start scanning the eigenfrequency of excitation. One can alternatively use the function generator's sweeping properties to make an automatic scan of the excitation frequency and see if there is a resonance matching around the specified span. But in the end, we had to stop the sweep and manually seek the resonance frequency by hand. We had to do this carefully for each peak until we saw a nice ringdown signal which means that we matched the correct resonance frequency. However, temperature shifts in the environment, changes in the probe position and intensity drifts are possibly responsible for shifting the membrane's eigenfrequency, so some of the times it was tricky to stay exactly at resonance. But this is a matter of patience and prudence rather than a limitation of the method as it is in the thermal spectrum measurement. The trigger of switching was controlled by the function generator and we could

adjust the duration of open(modulation on) and closed(modulation off) times. This is also important because it takes some time for the membrane to build up power and also one has to adjust the closed time so that it is possible to see the whole decay. The same trigger was used to see the signal on the scope. One other thing to mention is that as I stated before, radiation pressure can change the membrane frequency for a noticable amount. If one changes the pump power, he also has to change the excitation frequency because the eigenfrequency would no longer be the same. That is what we observed when we varied the pump power at 10mW, 15 mW and 20 mW and each time we saw the ringing effect if we did not readjust the excitation frequency. I would roughly say that a 1 mW power change could cause shifts on the order of 10 Hz. Finally, after making all the carefull adjustments, we were able to see nice ringdown results at 20mW pump power. Figure 6.6 is one example showing the signal with the trigger on the scope.

Eigenfrequencies and Q-factor results

As I have stated before, we were able to see 6 clear thermal peaks in the spectrum analyzer and this time we measured the eigenfrequencies and the Q-factors by ringdown method. Instead of showing all the results in 6 figures, I will just show one example of a nice ringdown fit(fundamental mode) together with a one in which the signal to noise ratio was low, therefore yielding a bad ringdown data(Fig 6.7). It will be useful for us to compare those two modes and elaborate on the reasons for the differences. First of all, we expected that it would be easier to excite the fundamental mode relative to the others due to its spatial property which makes it well-coupled to the excitation beam that was focused roughly at the center. Secondly, Q-factor is also a determining factor in the amplitude of the response because as I have shown before, radiation force effect is enhanced linearly by the Q-factor, therefore making it easier to excite. Apart from these, the response to an external force scales inversely with ω^2, thus for lower order modes one should expect to see a stronger response. The amplitude of the 360 kHz mode was quite high with respect to the others and we were able to see a very nice ringdown due to the high signal-to-noise ratio. On the other hand, there is a challenge that is strongly pronounced when one has a large Q-factor; one has to be very precise in matching the resonance frequency for the very fact that the resonance linewidth is very narrow in high Q resonators. This is also what we observed during the experiment. For high Q-factor modes, we had to make small touches for the frequency change, on the orders of less than Hz level. The other figure beside the fundamental mode shows the (1,3) modes's ringdown and as one can see the signal-to-noise ratio is not so good and one can estimate from the time scale that the Q-factor would be on the order of 10^4 which makes sense when compared with the thermal spectrum data as in Table 6.1.

Before I go deeply into the Q-factor results and comments on it, I would like to elaborate on the eigenfrequency determination. The eigenfrequencies we found experimentally by the ringdown method were ; 359.514 KHz(1,1) , 760.805 KHz(2,2), 849.074 KHz(1,3) , 945.827 KHz(2,3) , 1.084521 MHz(3,3) and 1.4408383 MHz(4,4) starting from lower order modes to higher order ones. The results will also be shown in a table with the corresponding Q-factors. As you might remember, we had a simple model for estimating our eigenfrequencies and what we now have to do is to fit this experimental data to the simple model. We used Mathematica to search for the best fit to the data. The fitting idea was simply as follows; the fundamental mode frequency was the fit parameter to adjust and the other modes can

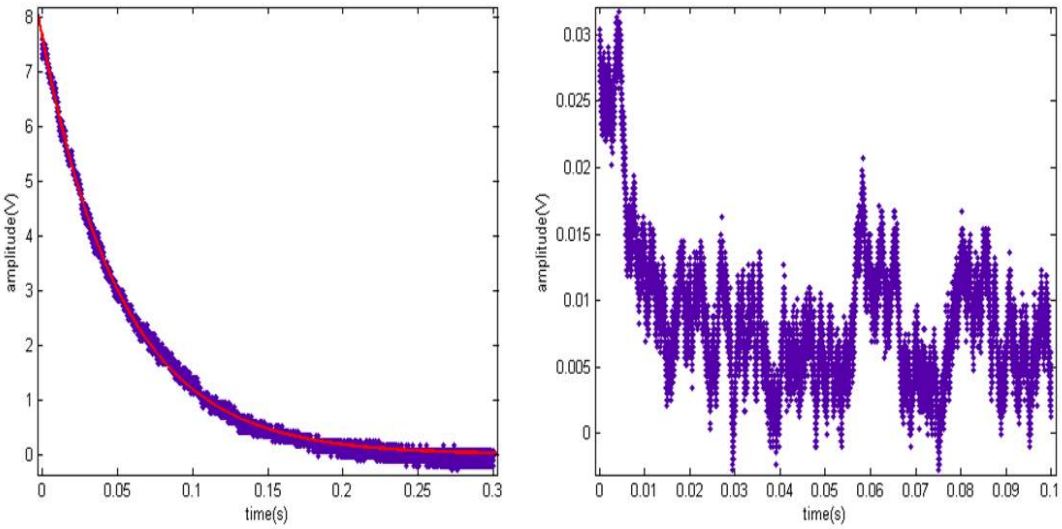

Figure 6.7 The figure shows the signals from two of the six mechanical modes. The figure on the left is a fit to the ringdown data of the (1,1) mode at around 360 kHz and the figure on the right shows the signal from the (1,3) mode at roughly 850 kHz.

easily be calculated given that we know the fundamental one. Then each of the 6 experimental values were substracted from the theoretical prediction and we used the least square method which minimizes the sums of the squares of the residuals. Based on this method, we have the most appropriate model for the eigenfrequencies(Hz) as below. Columns and rows corresponds to the mode numbers, i.e diagonals being (1,1), (2,2) etc.

$$\begin{bmatrix} 366508 & 579501 & 819538 & 1.06855 \times 10^6 & 1.32146 \times 10^6 \\ 579501 & 733017 & 934417 & 1.159 \times 10^6 & 1.39562 \times 10^6 \\ 819538 & 934417 & 1.09953 \times 10^6 & 1.2958 \times 10^6 & 1.51115 \times 10^6 \\ 1.06855 \times 10^6 & 1.159 \times 10^6 & 1.2958 \times 10^6 & 1.46603 \times 10^6 & 1.65944 \times 10^6 \\ 1.32146 \times 10^6 & 1.39562 \times 10^6 & 1.51115 \times 10^6 & 1.65944 \times 10^6 & 1.83254 \times 10^6 \end{bmatrix}$$

Red colored values are the theoretical predictions for the 6 of the modes we found experimentally. As can be seen, the agreement in the (1,1) , (3,3) and (4,4) modes are such that the errors are between 1 and 2 percent for all the three modes. There is a larger discrepancy for the other modes. For example the (2,2) mode at 760 kHz has an error of around 4 percent with respect to the fit model estimation. The discrepancy in general is not so large but we expected to see a much better agreement. We owe this difference to the possible deformation of our SiN membrane(might come from an artifact due to gluing as our first trial). This deformation might introduce a difference and inhomogenity in the tensile stress, therefore changing the eigenfrequency by some amount. And this effect may show difference from mode to mode. As we will see later, our second membrane's eigenfrequencies will show excellent fit with theory so this strengthens our suspicion that the first membrane had some deformation. For the eigenfrequency determination, one should be aware of the

small effect of the radiation pressure as well. In principle these frequencies are not the exact, bare eigenfrequencies because we inevitably apply radiation pressure to excite the membrane, so slighty shifting the eigenfrequency. But this effect accounts for much smaller errors than the ones we already have in this membrane(from our empirical knowledge, 20 mW optical power is expected to give a shift of around 200 Hz).
Now let us have a look at the frequency-Q factor table. The approximate Q-factor values are found from the decay time information and the most remarkable result showed a Q-factor of the order of 10^5 with this membrane.

Mode	Frequency	Q-factor
(1,1)	359.514 kHz	1.2×10^5
(2,2)	760.805 kHz	3.8×10^4
(1,3)	849.074 kHz	$\approx 10^4$
(2,3)	945.827 kHz	1.0×10^5
(3,3)	1.084521 MHz	1.4×10^5
(4,4)	1.4408383 MHz	1.1×10^5

Table 6.2 The table here shows the results of the ringdown measurement for the first membrane.

The highest Q-factor we achieve is with a higher order mode(3,3) around 1.4×10^5. This makes sense because we expected that the higher order modes would be less affected from the coupling to the mounting structure than the lower order modes(in case mounting is the limiting factor in Q). This is naively due to the fact that as the number of nodes for the mechanical modes increases, the center of the membrane is better protected from coupling to the support. The second thing to note is that the diagonal modes(in general) might tend to have higher Q-factors than the off-diagonals. This has also been observed as a general trend in similar experiments [25]. However, one needs more data points to make conclusive remarks(other mechanical peaks were not so easy to find), so a more reliable discussion should be made on rather the second membrane since we could achieve more data points for the second one. We should remind ourselves that these results are for the first membrane which was glued on four points from the edge to the metal disk. We think that this might have been the main reason why we could not reach Q-factors on the order of 10^6 with this gluing method. The relatively small Q value of (2,2) diagonal mode is worth to note. The frequency error in this mode was also relatively higher, so the deformation might also have contributed to the degradation of the Q-factor.

Before closing this section for the first membrane, I shall as a final point comment on the comparison between the thermal spectrum results and the ringdown results regarding the Q-factor determination. The comparison results make quite a lot sense when we think of the limitations of the thermal spectrum method. The thermal spectrum results agree well with the ringdown method for the low Q value modes as expected. For example, thermal peaks predict a Q value of 3.4×10^4 for the 760 kHz mode and the ringdown estimates a Q value of 3.8×10^4 yielding a consistent result within ≈ 10 percent error. But as we hypothesized before, the thermal width measurment is incompetent in estimating the high Q values because of the narrow linewidth requirement. For example, it underestimates the Q factor as 3.6×10^4 for the fundamental mode whereas the ringdown method predicts a

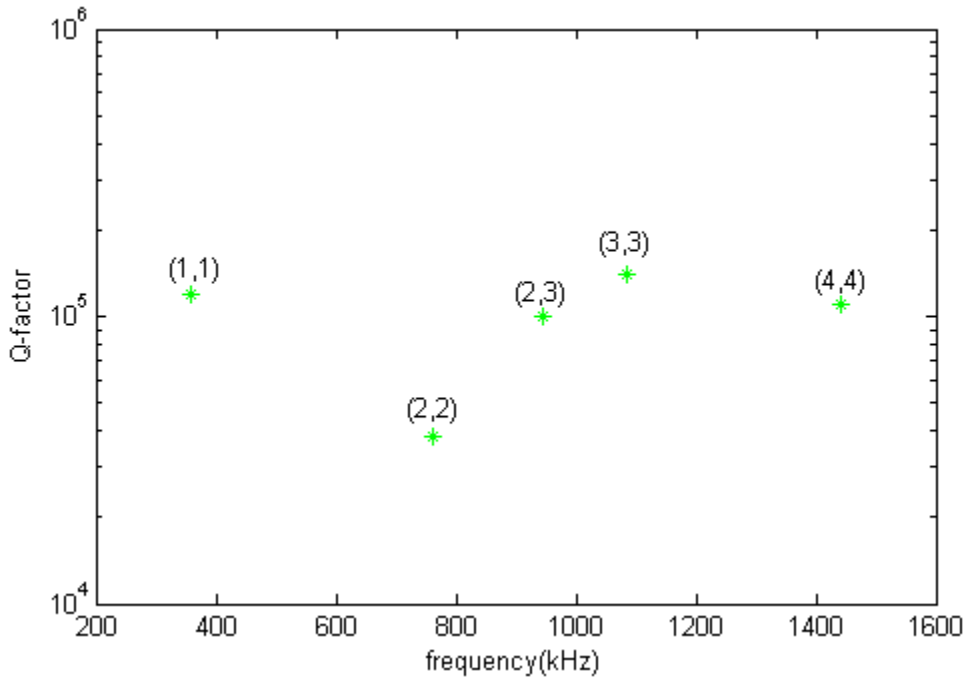

Figure 6.8 The figure shows the trend for the Q-factor of 5 modes (except the bad ringdown at 850 kHz) starting from lower order modes.

more reasonable result of 1.2×10^5. In this case,the discrepancy between two measurement methods exceeds ≈ 50 percent. The thermal method also underestimates the Q for (2,3), (3,3) modes($\approx$ 40 and 30 percent error respectively) but is closer to be correct(within 20 percent) in predicting the Q value of (4,4) mode which has a relatively high width ($\approx$ 14 Hz). On the whole, we can say that the ringdown method gives a more reliable estimate of the Q-factor especially when we are dealing with the membranes with very high Q-factors.

6.2 Measurements with the second SiN membrane

Here I shall give the results for the second membrane just as we did for the first one. Since all the measurement methods are the same, I see no reason to bother the reader by explaining them again. Therefore in this part, I will directly give the results and just outline the differences from the measurements done with the first membrane.

6.2.1 Thermal spectrum measurement

Our main goal was to proceed to the Q-factor measurements of the second membrane as fast as possible, so this time we used the thermal spectrum data just to roughly locate the eigenfrequencies. We were able to identify 9 mechanical peaks for which we could later perform the ringdown measurement.

6.2.2 Ringdown measurements with the second membrane

Having known roughly the eigenfrequencies of the 9 modes of mechanical origin, we did the ringdown measurement in the same way as described with the first membrane as in 6.1.2. This time we could observe really high Q-factors ($\approx 10^6$) making also the ringdown measurement quite challenging. The reason, as might be guessed, is that now the linewidths were extremely narrow and we had to scan the excitation frequency delibaretely to match with resonance of the corresponding eigenfrequency.
But before going to the analyis of the Q-factor results, we shall again elaborate on the eigenfrequencies and how the data fits with theory for this second membrane.

Eigenfrequency model

The precise eigenfrequency values of the 9 modes we found by the ringdown is as follows; 411.661 kHz (1,1) , 651.140 kHz (1,2) , 823.4582 kHz (2,2) , 920.725 kHz (3,1) , 1.235291 MHz (3,3) , 1.301977 MHz (4,2) , 1.567806 MHz (5,2) , 1.6470293 MHz (4,4) and finally 1.8637615 MHz (5,4) . These will be more clear when I will show them with their corresponding Q-factors in the following part but for now, let us again show the eigenfrequency model(in units of Hz) that fits best to this experimental data.

$$\begin{bmatrix} 411717 & 650982 & 920628 & 1.20035\times10^6 & 1.48447\times10^6 \\ 650982 & 823435 & 1.04968\times10^6 & 1.30196\times10^6 & 1.56777\times10^6 \\ 920628 & 1.04968\times10^6 & 1.23515\times10^6 & 1.45564\times10^6 & 1.69755\times10^6 \\ 1.20035\times10^6 & 1.30196\times10^6 & 1.45564\times10^6 & 1.64687\times10^6 & 1.86413\times10^6 \\ 1.48447\times10^6 & 1.56777\times10^6 & 1.69755\times10^6 & 1.86413\times10^6 & 2.05859\times10^6 \end{bmatrix}$$

Now the difference from the first membrane is that we have almost excellent agreement with theory. As you might remember, for the first membrane there were errors of almost up to 4 percent , but this time we have errors as small as $\approx 1\times10^{-4}$ for all the modes. This relatively higher precision we think, is due to the fact that this second membrane was not deformed as the first membrane. Our claim can further be strengthened by noting that the tensile stress value we get from the fundamental mode frequency of around 411 kHz is estimated to be $\approx 900MPa$ which makes perfect sense with the data provided for high-stress membranes(Norcada). On the whole, our experimental frequencies for the eigenmodes of the membrane to a high precision agree with the very simple theoretical model of a rectangular drum.

Q-factor measurement results

Instead of putting all the ringdown graphs, I shall again show 2 of them by comparing the two. The mode around 1.235 MHz has a quite high Q-factor and the response we get from that mode is very good in terms of SNR. For example the mode at 1.567 MHz is an off-diagonal mode and the Q-factor is lower with respect to the 1.235 MHz. As can be seen in Fig 6.9, the graph on the right shows a worse SNR and a faster decay time meaning higher loss.

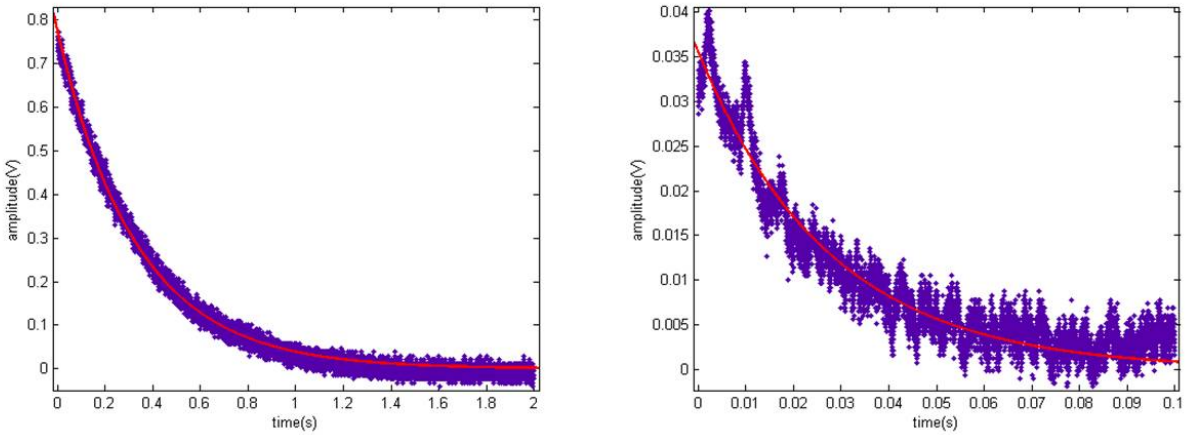

Figure 6.9 A very clear ringdown signal of the second membrane from a diagonal high Q mode at 1.235 MHz (left). Signal from an off-diagonal mode at 1.567 MHz(right). Power of the excitation laser was around 30 mW for all the measurements.

Mode	Frequency	Q-factor
(1,1)	411.661 kHz	3.3×10^5
(1,2)	651.140 kHz	0.82×10^5
(2,2)	823.4582 kHz	3.9×10^5
(3,1)	920.725 kHz	1.5×10^5
(3,3)	1.235291 MHz	2.6×10^6
(4,2)	1.301977 MHz	bad SNR
(5,2)	1.567806 MHz	2.7×10^5
(4,4)	1.6470293 MHz	2.2×10^6
(5,4)	1.8637615 MHz	8.2×10^5

Table 6.3 The table shows the results of the 9 ringdown measurements for the second membrane. Two of the outstanding results with Q-factors exceeding 10^6 are shown in red.

For this membrane we have more data points then the first one (Table 6.3), so the general trend will be more clear. One outstanding result is the very high Q-factor of the (3,3) diagonal mode which actually was one of the main goals for us to achieve. This Q-factor suggests that this mode of the SiN membrane is a nice candidate for future quantum optics experiments. Actually a better figure of merit for mechanical resonators is the Qf product, so having high frequency(preferably MHz range) is a feature as important as having a high Q. We could not go beyond 2 MHz because our detection circuit was limited at that bandwidth. This is definitely a matter of improving the detection circuit and one can in principle measure the higher order modes.
Figure 6.10 strongly suggests that the diagonal modes tend to have higher Q-factors than the off-diagonal ones with our mounting method. The naive explanation behind this might be that if we think in terms of the spatial profiles of the modes, one would imagine that

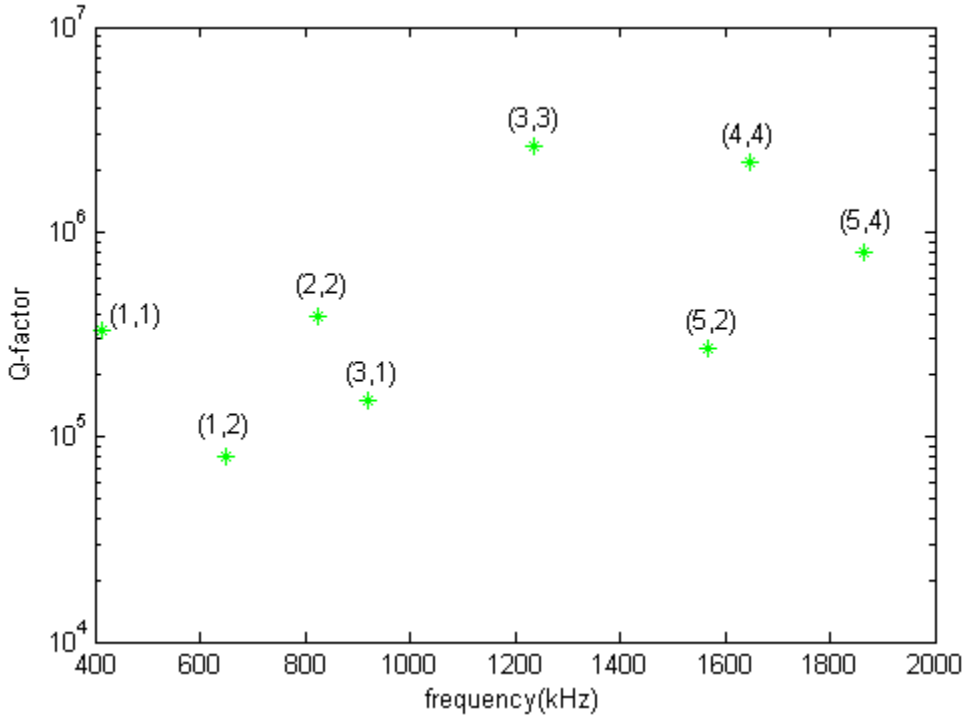

Figure 6.10 The graph shows all the Q-factors for the second membrane with respect to their frequencies and mode numbers taken from Table 6.3.

the diagonal modes(bearing symmetric nodal points) are less susceptible to coupling to the mounting structure with respect to the off-diagonal ones. One thing to note here is that in a similar experiment reported in [22], all the modes had relatively closer Q-factors(not a strong difference for being higher or diagonal mode) and this was mainly due to the fact that the mounting method was based on clamping the membrane with a tweezer rather than gluing it to a surface as in our case and as in [25]. So in that specific condition, it is highly probable that the Q-factor was mainly limited by the intrinsic loss [26] of the material or thermoelastic damping [27] since it does not depend significantly on the geometry of the mode and the support structure. For our case, one other general trend(which is apparently less pronounced compared to the diagonality trend) is that as we go to the higher modes we seem to observe larger Q-factors as I stated before. But it does not follow strictly necessary, because just as we observed in the first membrane, here as well, (4,4) mode has a lower Q-factor than the (3,3) mode. So the trend may be broken beyond a certain frequency limit. This point is yet to be elucidated. It can be said that there is a combined effect of the general trends, so it is tricky to set forth a smooth a priori account of the Q-factor without applying detailed models. In this regard, it would be nice for our future goals to work on simulations of possible loss mechanisms that would predict a Q value for a certain mode within a given set of parameters and geometry. Our results strongly suggest that the main loss mechanism relevant in our case is the coupling to the support structure and this might be modelled by a perturbative phonon tunneling [28] approach for different geometries of clamping, given that we come up with designs of small contact points to the support

structure. One supportive argument for clamping dominated loss in our case is that even for the second, high Q membrane, we observed strong geometry dependance of the Q-factor for different modes. For example, there is almost a difference of a factor of 30 between (1,2) mode and (3,3) mode which hints that damping is still to a large extent determined by the spesific mode's coupling to the support structure. Another argument that strengthens the aforementioned claim comes from Zener's theory for thermoelastic damping. Thermoelastic damping might be an important damping mechanism for microsize resonators at room temperature. Zener's theory predicts a thermoelastic damping limited Q-factor depending on the parameters given by the following formula [29],

$$\frac{1}{Q} = \frac{E\alpha^2 T}{C_v} \frac{\omega\tau}{1+(\omega\tau)^2} \tag{6.2}$$

where E is the Young's modulus, T is temperature, C_v is the heat capacity at constant volume, α is the thermal expansion coefficient and ω is the frequency of the resonator mode. Here τ represents the relaxation time which is given by,

$$\tau = \frac{C_v b^2}{\kappa\pi^2} \tag{6.3}$$

where b is the thickness of the resonator and κ is the thermal conductivity.
As can be seen from the formula, thermoelastic damping is determined by the thermoelastic parameters of the material and the eigenfrequency of the specific mode. If I insert the parameters for our SiN membrane, I get a Q value which is on the order of 10^8 for the $\approx$1 MHz mode. Since we have observed Q-factors which are almost two orders of magnitude smaller than this value, we can say that our damping is not at the thermoelastic limit yet.

6.3 Comparison of the first and second SiN membrane in terms of Q-factor

An important task for us would be to set forth the differences in the Q-factor results for the two SiN membranes. As I have stated before, for the first membrane , we glued it from four edges to the metal disk wheras for the second one we used only one glue point from the edge. We thought that this would be crucial for decreasing the coupling to the mounting structure(therefore increasing the Q) as has been tested in a similar setup before (in various ways) [25]. The results we found are also consistent with those results and we have reached almost the same Q-factors. A nice way would be to compare our two membranes on a graph as in Fig 6.11 to see the effect of different way of gluing.

What is clear in the comparison of the two membranes is that the Q-factors for all the modes have increased when we used one point gluing instead of four. This effect is more pronounced for the (3,3) and (4,4) modes yielding an improvement of almost a factor of 20 . One can critisize the comparison I made hereby, on the ground that one should in principle do the experiment with four point gluing and one point gluing on the same membrane. Yet insofar we believe to have kept the conditions and parameters approximately the same for the two membranes, one can say that this huge difference of the Q- factor comes to a large extent from the difference of the gluing method, also in consistency with what other groups have observed. It turns out to be that at room temperature and at this low level of air

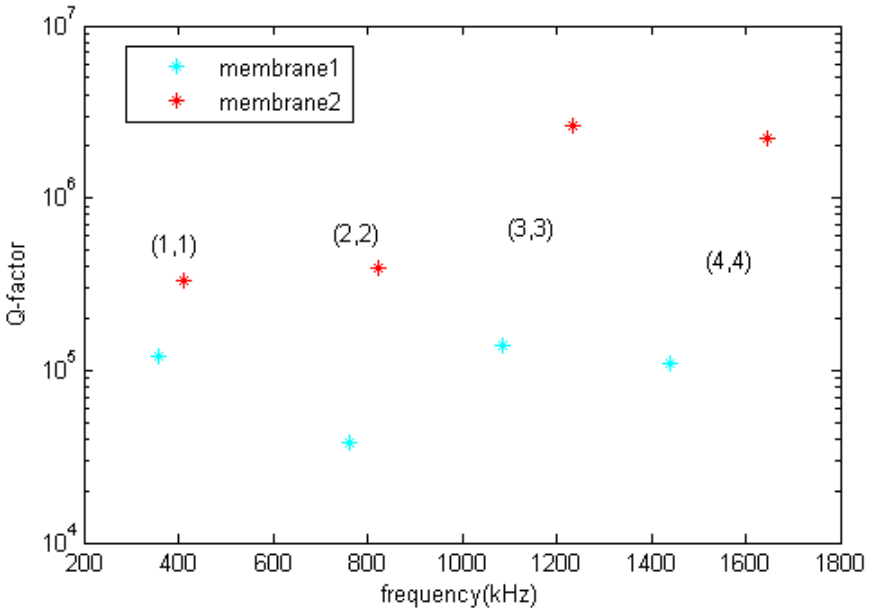

Figure 6.11 The figure shows the comparison of the Q-factors for our two SiN membranes. Since we did not have as many points for the first membrane as the second one, the comparison is done with the 4 diagonal modes. The blue asterix corresponds to the first membrane whereas the red one corresponds to the second membrane.

pressure, the dominant damping mechanism is the coupling to the support structure and this can, to a considerable extent, be avoided by applying the principle of having the least surface area contact with the substrate.

6.4 Discussion and concluding remarks

As has been stated before, our main concern was to reach impressive Q-factor values for our SiN membranes at room temperature. We can safely say that we have promising results showing Q-factors exceeding 10^6 with frequencies in the MHz range. We have made a comparison of two SiN membranes where we have seen that the second one showed a better Q-factor, dominantly due to gluing method. The results, overall, show that our damping is clamping loss dominated. We are at the same time planning to try different geometries in the fabrication process, for example making thinner and smaller contact points on the nodes of the relevant mechanical mode to be used, in order to reduce clamping loss and increase the Q-factors. This would definitely call for a more thorough theoretical analysis of mechanical modes and the damping mechanism behind. Having improved these already promising Q-factors, we can use the membranes for our future experiments, hopefully in pursuit of quantum signatures. Apart from damping considerations, we have also seen that the thermal spectrum and width measurement is limited in reliability with respect to the ringdown technique in terms of determining the Q-factor.
A discussion may arise on the methods carried out in our experiments and whether more

improved or sophisticated techniques could have been used. This of course very much depends on the goal of the experimenter. We were mainly interested in estimating the order of magnitude of the Q-factor of our membranes and whether they are promising to be used in our future experiments. For our purposes, I would say that the current setup has done its job. However, one could have been interested in, for example, a more precise frequency or Q-factor determination. As for the thermal spectrum measurement, it is obvious that this would firstly require a spectrum analyzer with a better resolution bandwidth. On top of that, due to the reasons I mentioned about the eigenfrequency shift, one should think of an intensity stabilization and slope position lock. Yet another improvement of the system would include a temperature stabilization method for the membrane. This would definitely reduce the effects of the thermal gradients in the environment which would cause unwanted shifts in membrane's eigenfrequencies. The aforementioned improvements would also help a lot in the ringdown experiment, making it easier for the experimenter to match the mechanical resonance and stay at this point during a ringdown decay. Otherwise, it is possible to encounter sudden bumps or ringing effects in the signal while recording the amplitude decay(within lets say 1 second) which might deteriorate the decay fit. For our measurements, we were successful in suppressing this to a large extent by trying the ringdown many times and selecting the best looking signal. This makes the job tedious when one aims to characterize a huge number of samples. Along with these modifications, we should also have a more practical way of changing many samples in a rather shorter time, in order to have more conclusive judgements about the general trends with those membranes.

Chapter 7

First results with the GaAs membrane and prospects

In this chapter, I would like to introduce to the reader the first, preliminary characterization results of our GaAs(Gallium Arsenide) membrane. The reason why we are interested in GaAs apart from SiN, is simply because that GaAs has many desirable and interesting electro-optical properties which I will shortly touch upon throughout the section. At the time this thesis was about to be handed in, we were continuing the experiments with this material and encountered some supposedly cooling effects of which we have no full understanding yet. So the short discussion I will conduct in this chapter, will be mainly based on the mechanical Q-factor data we have been able to confirm so far(we were able to see a Q-factor exceeding 10^6 for a particular mode). And the other aim of the chapter is to give the reader a taste of the interesting properties of this material and outline the prospects for our future experiments with GaAs.

7.1 Properties of GaAs

GaAs is a compound consisting of Gallium and Arsenide and it is known to be a III/V semiconductor. It has found place in various applications, especially in the field of optoelectronics due to its desirable properties. A review paper [30] can be referred to as a fundamental source of reference for the properties of GaAs. First thing to note would be that GaAs is a direct bandgap semiconductor with an energy gap of $\approx 1.42eV$ at room temperature. Bearing this feature, GaAs has some advantages over the most prominent semiconductor Silicon which is an indirect gap material. This means that GaAs is much more efficient when used as a light emitting diode or a diode laser [31]. Compared to Silicon, it also has a higher electron mobility and drift velocity which allows it to be used as a transistor operating at very high speeds [32]. GaAs is also less sensitive to heat and less susceptible to radiation damage which makes it suitable for space-based applications. On top of these, one of the most interesting properties of GaAs is that it has a strong piezoelectric behavior [33] which means that the mechanical degree of freedom can be coupled to the charge distribution on the structure.
Having been an attractive center of research in the field of optoelectronics, GaAs recently started to be investigated also by the quantum optics community, especially as a mechan-

ical resonator. In this regard, mechanical properties of GaAs resonators, namely their Q-factors, has become an interesting matter for exploration. However, Q-factors of high frequency GaAs oscillators have not yet been reported to reach very impressive results (less than the order of 10^5) for room temperature. According to a recent experiment where the micromechanical resonator(MHz regime) was a AlGaAs monocyrstalline heterostructure, the reported Q-factor at 20 K was around 80 000 [34]. The microresonator was at the same time a high-reflectivity Bragg reflector that is proposed to be used as an end mirror in a cavity optomechanical setup. So the idea is to be able to fabricate a high frequency GaAs mechanical resonator which has an impressive Q-factor. One other interesting paper [35] is related to the piezoelectric properties of GaAs and it was shown that by shining light(above bandgap) on the GaAs, one can excite charge carriers which causes a change in the damping(therefore Q-factor) through the piezoelectric effect.

7.2 Mechanical Q-factor of the GaAs membrane

I would rather keep this section shorter than the chapter on the results of the SiN membrane because the idea behind measuring the mechanical Q-factor is basically the same. Therefore, I will concentrate on the differences we observed during the experiments due to the features of the GaAs.
First of all, I shall start with the properties of our GaAs membrane. These membranes were fabricated by our collaborators at the DTU Photonics group. The GaAs membrane we used for characterization, is a low stress intrinsic semiconductor (i type) with dimensions around 1.36 mm (width) , 1.91 mm (height) and 160 nm (thickness).

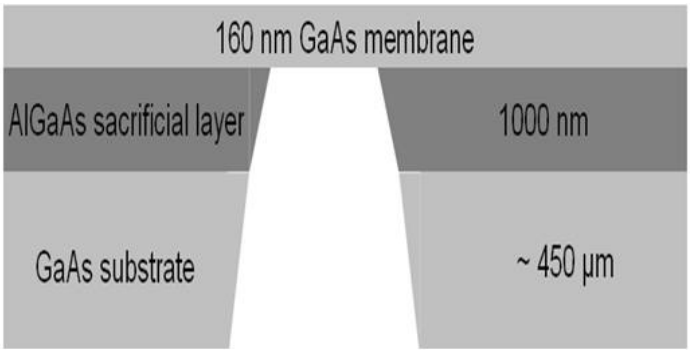

Figure 7.1 The sketch shows the growth of the GaAs membrane on the substrate layers.

The mounting method is again the same(gluing from the edges), however this time our support structure around the GaAs layer is rather large and the substrate was glued on 3 points to the metal disk mount. The experiment was first done by shining our 810 nm probe light on the GaAs and we tried to see the thermal peaks at room temperature as we had done with the SiN membranes before. However, while mode-matching to the cavity and looking at the transmission signal, we realized that the signal beared sort of chaotic oscillations which made the measurement very difficult when the probe power was around a few hundred μW. We think this complication comes from the fact that we shine light

that is above bandgap and we induce charge-carrier excitation. Currently, we are trying to figure out what type of physical mechanism underlies the interesting behaviour we have seen. Upon realizing the complication with above bandap light, we switched to a case where we used below bandgap probe light (975 nm) at 1mW power as in Fig 7.2. This time we simply shined this probe light in a misaligned manner onto the membrane and detected the reflected light by using a home-made split-diode detector. As the membrane fluctuates and the reflected beam moves accordingly, the two split diodes start to get different amounts of light on them and their differential current reveals the information about membrane's mechanical motion. Then we fed this signal to the spectrum analyzer to see the thermal peaks at room temperature.

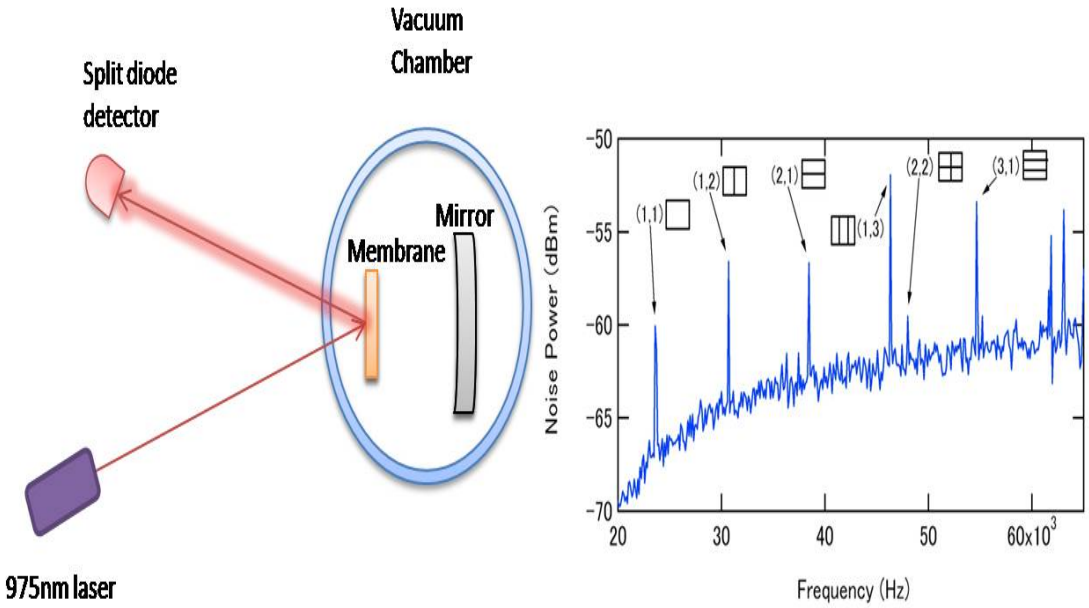

Figure 7.2 The sketch shows a simplified version of our setup for the thermal spectrum of the GaAs membrane(left). A broad spectrum was recorded and the mechanical peaks are pointed with their corresponding mode numbers(right).

As can be seen from Fig 7.2, we had clear mechanical signals from our GaAs membrane. This actually makes sense when we compare it to the SiN membrane, because the fundamental frequency of GaAs membrane seems to be much lower. As a result, the spring constant is smaller which means that under the same conditions and the same force, the displacement response of the resonator should be larger. As for the mechanical eigenfrequencies, it is challenging to achieve impressive agreement with theory. The main reason behind this, is simply that our GaAs membrane(as a first fabrication trial) is not purely a rectangle, it has rather an elliptical shape. The other thing is that the membrane bears some crystal cavern features. In summary, the boundary conditions and the stress value are not well-defined for this sample, however we hope to clarify these points soon by using a better model for this membrane.

At that point, let us continue with the ringdown measurements with this membrane. For this purpose, we had slight differences from the SiN membrane measurements but the idea

of lock-in detection and switching mechanisms are basically the same. The simplified experimental setup is depicted in Fig 7.3. Here the strong(1mW) probe light comes from below-bandgap light source of 975 nm whereas this time the excitation light is $30\mu W$ at 810 nm wavelength. We made sure, by changing the piezo voltage, that this light was at off-resonance point in order to avoid cavity-originated effects. The excitation light was modulated by an AOM in this case.

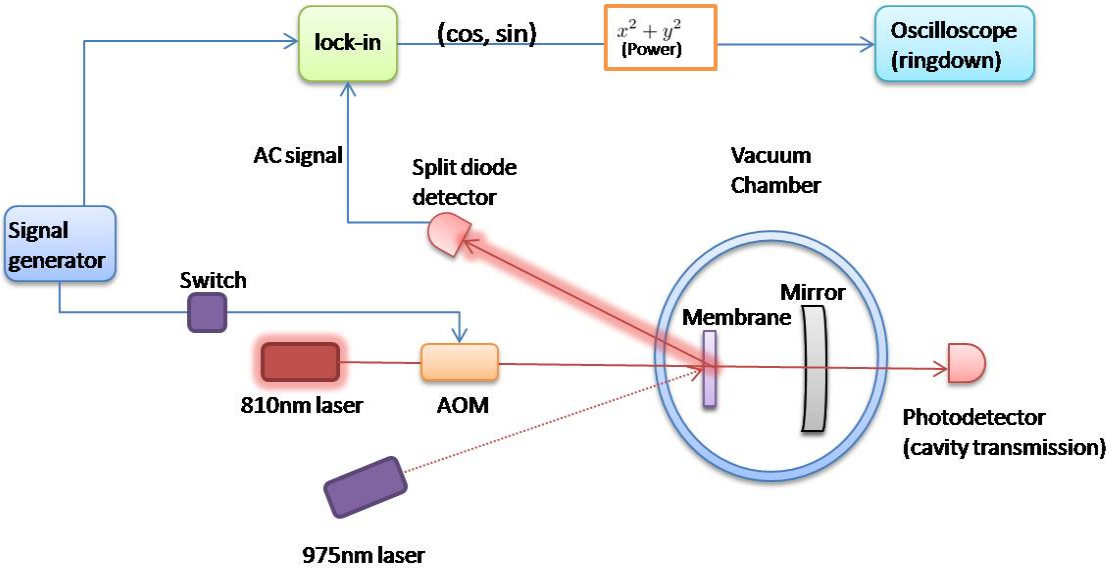

Figure 7.3 Experimental setup for the ringdown measurement of the GaAs membrane.

Table 7.1 shows the eigenfrequencies of several modes of the membrane and their corresponding Q-factors. The Q-factors for all modes seem to be close to each other and we have achieved to see Q-factors exceeding the order of 10^5, the best one being 59.5 kHz(3,1) mode with a Q-factor of 2.3×10^6 .

Mode	Frequency	Q factor
(1,1)	23.4 kHz	0.50×10^6
(1,3)	45.5 kHz	0.56×10^6
(2,2)	47.5 kHz	0.53×10^6
(3,1)	59.5 kHz	2.3×10^6
(3,3)	72.2 kHz	0.48×10^6

Table 7.1 The results of the 5 ringdown measurements for our GaAs membrane.

Q-factor results look promising when we consider the results achieved with GaAs so far. However, one thing to note is that our fundamental eigenfrequency is quite low, so it would be a nice question to ask what would happen if we measured eigenfrequencies of MHz range. One of the next steps in prospect is to make changes in the dimensions and introduce extra stress during the fabrication process to increase the fundamental mechanical frequency. As

for observing relatively high Q-factors with our current GaAs membrane, one of the possible reasons behind this might be that, as stated before, the substrate around GaAs was quite large and since the gluing points are far away from the membrane itself, this might have helped reducing the damping significantly. The fact that the Q-factor of different modes are close to each other also suggests that the effect of mounting on Q-factor is eliminated to a large extent. One problem we encountered with the GaAs membrane was that, compared to the SiN case, it was rather challenging to keep the ringdown signal free of bumps. One of the possible reasons is that the radiation-pressure change due to the shift of the slope position and intensity drifts of the 1 mW light source apparently have a larger effect on the GaAs membrane since it has a lower spring constant. Thus for the GaAs membrane we had to implement intensity stabilization for the laser power and slope-lock method to stay at the right detuning point. We realized that implementing these improvements helped in increasing the reliability of the Q-factor measurement for the GaAs membrane and removed most of the unwanted behaviour in the ringdown signal. Apart from these considerations, we have to make a thorough investigation of the absorption properties of GaAs depending on the wavelength and measure the finesse of the cavity to characterize the optical cavity as a whole. Further study on the eigenfrequency model(taking into account the imperfections of the GaAs crystal) will shed light on the clarification of eigenmode numbers and the observed eigenfrequencies.

7.3 Future goals with the GaAs membranes

GaAs looks to be a promising material due its unique optoelectronic and piezoelectric properties and given that one can realize high mechanical Q-factors with GaAs membranes, hopefully in the MHz frequency regime, it can be regarded as an interesting tool in prospective quantum optomechanics experiments. Furthermore, there is a possibility of controlling the Q-factor and the damping mechanism by manipulating carrier excitation and this may result in realizing an effective cooling mechanism for GaAs membranes. Apart from that, optical refrigeration has drawn great attention so far and physicists have been trying to find a way of cooling a semiconductor by just shining light on it. GaAs, in this sense, bears the possibility of being cooled from room temperature down to 10 K without need of any cryogenics [36]. However, this has hitherto proved to be very challenging. If cooling can be achieved in an efficient way and combined with radiation-pressure cooling in an optomechanical setup, it will pave the way for new directions to follow with various applications.

Chapter 8

Conclusion and Outlook

The field of cavity optomechanics is currently regarded to be one of the hottest research topics. Many groups, working especially on Gravitational Wave Detection, are aiming to reach unprecedented position sentivities with large scale cavity optomechanical setups. Thermal noise of the mirrors and residual classical noise coming from various sources pose strong challenges in reaching further higher sensitivities. Current systems are striving to approach a stage where the dominant noise is expected to show quantum behaviour at the Heisenberg limit and schemes that can go even below the SQL have already been proposed. On the other hand, Quantum Optics groups have been in great competition during the last few years in order to achieve ground-state cooling of a mechanical resonator. Along with the strong optomechanical interaction realized in high-finesse cavities, ground-state cooling will for the first time pave the way for observing truly quantum behaviour of a macroscopic object and will render the chance of full quantum control over such a large scale [37]. Future expectations include the utilization of nanomechanical sytems in Quantum Information protocols as well. Nanomechanical systems have been recently proposed to be used in the development of hybrid sytems for quantum teleportation [38]. Apart from the technical opportunities, reaching such a quantum noise dominated regime will shed light on philosophical concerns like the boundaries between the quantum and the classical world and possible decoherence mechanisms. From all aspects, implementation of new optomechanical schemes where coupling between the mechanical resonator and light is strong enough and the mechanical Q-factor is large, proves to be of paramount significance for future considerations.

In this regard, we are interested in the membrane-inside-cavity setup [13] which uses the advantage of seperating the mechanical and optical merits to different elements, therefore making it easier to realize both high mechanical Q and high finesse at the same time. Apart from this consideration, not only cooling but also successful elimination of classical noise is required in order to be able to reach a quantum-noise limited regime. Therefore, we aim to operate around the linear coupling regime and realize a highly sensitive displacement measurement by utilizing a two-color probing scheme that would cancel the classical noise to a large extent. On top of that, if we can achieve to integrate a radiation-pressure cooling strategy as well, the proposed setup would be a promising candidate to get closer to the long-time desired goal.

Bearing in mind all these goals and concerns, we started characterizing high Q-factor mi-

cromechanical resonators made of SiN and GaAs that are planned to be used in our future experiments and this turned out to be the core part of the master thesis. For this purpose, we basically realized a Fabry-Perot configuration with the membrane being one of the end mirrors and measured the eigenfrequencies and Q-factors of the membrane, by performing an optical readout of its fluctuations and using an excitation method for the ringdown via optical means instead of a piezo-drive. Mechanical ringdown measurements turned out to yield more reliable results compared to the thermal spectrum measurements due to the narrow linewidth requirement dictated by the large Q-factor of the resonators. Q-factor results, exceeding 10^6 for SiN membranes at frequencies in the MHz range (room temperature), are quite promising for the future, given that we come up with new geometrical designs in order to reduce coupling to the support structure more effectively. As far as GaAs is concerned, we were able to see an unprecedented Q-factor(on the order of 10^6) for a particular mode($\approx$ 60kHz) which means a Qf product of $\approx 10^{11}$Hz at 300K, so the next step would be to investigate whether we can see such impressive values for higher frequency resonators as well. Apart from the mechanical quality considerations, as I have outlined in the short chapter dedicated to GaAs, it is a semiconductor with many desirable unique properties which we can exploit in our future optomechanical experiments.
On the whole, the master thesis has culminated in promising results for the mechanical characterization of our membranes and in addition to that, the experiments conducted so far, gave us the first chance of gaining experience to explore those interesting membranes before we go to the long-term experiments in mind.

Bibliography

[1] B. E.A.Saleh and M.C.Teich, *Fundamentals of Photonics*, 1st ed. (John Wiley and Sons Inc, 1991), pp. 310–323.

[2] T.J.Kippenberg and K.J.Vahala, "Cavity Optomechanics: Back-action at the Mesoscale," Science **321,** 1172–1176 (2008).

[3] http://www.ligo.caltech.edu/ .

[4] S.Groeblacher, K. Hammerer, M. R. Vanner, and M. Aspelmeyer, "Observation of strong coupling between a micromechanical resonator and an optical cavity feld," Nature **460,** 724–727 (2009).

[5] C.Genes, D.Vitali, P.Tombesi, S.Gigan, and M.Aspelmeyer, "Ground-state cooling of a micromechanical resonator: Comparing cold damping and cavity-assisted cooling schemes," Physical Review A. **77** (2008).

[6] S. Groeblacher, J. Hertzberg, M. Vanner, G. Cole, S.Gigan, K. C. Schwab, and M. Aspelmeyer, "Demonstration of an ultracold micro-optomechanical oscillator in a cryogenic cavity," Nature Physics **5,** 485–488 (2009).

[7] A. Schliesser, O. Arcizet, R. Rivire, G. Anetsberger, and T. Kippenberg, "Resolved-sideband cooling and position measurement of a micromechanical oscillator close to the Heisenberg uncertainty limit," Nature Physics **5,** 1–6 (2009).

[8] D.Kleckner and D.Bouwmeester, "Sub-kelvin optical cooling of a micromechanical resonator," Nature **444,** 75–78 (2006).

[9] A. D. OConnell *et al.*, "Quantum ground state and single-phonon control of a mechanical resonator," Nature **464,** 697–703 (2010).

[10] H. J. Kimble, Y. Levin, A. B. Matsko, K. S. Thorne, and S. P. Vyatchanin, "Conversion of conventional gravitational-wave interferometers into quantum nondemolition interferometers by modifying their input and/or output optics," Phys. Rev. D **65** (2001).

[11] V.Braginsky, Y.I.Vorontsov, and K.P.Thorne, "Quantum nondemolition measurements," Science **209,** 547–557 (1980).

[12] A. Heidmann, P. Cohadon, and M. Pinard, "Optomechanical characterization of acoustic modes in a mirror," Physical Review A. **68** (2003).

[13] J. D. Thompson, B. M. Zwickl, A. M. Jayich, F. Marquardt, S. M. Girvin, and J. G. E. Harris, "Strong dispersive coupling of a high-finesse cavity to a micromechanical membrane," Nature **452,** 72–75 (2008).

[14] M.Hossein-Zadeh and K.J.Vahala, "Observation of optical spring effect in a microtoroidal optomechanical resonator," Optics Letters **32,** 1611–1613 (2007).

[15] F.Marquardt and S.M.Girvin, "Optomechanics," Physics **2** (2009).

[16] A.M.Jayich, J.C.Sankey, B.M.Zwickl, C.Yang, J.D.Thompson, S.M.Girvin, A.A.Clerk, F. Marquardt, and J.G.E.Harris, "Dispersive optomechanics: a membrane inside a cavity," New Journal of Physics **10** (2008).

[17] G.Brooker, "Modern Classical Optics," Oxford University Press (2003).

[18] E. D.Black, "An introduction to Pound Drever Hall laser frequency stabilization," American Journal of Physics **92,** 79–87 (2001).

[19] K. Borkje, A. Nunnenkamp, B. M. Zwickl, C. Yang, J. G. E. Harris, and S. M. Girvin, "Observability of radiation pressure shot noise in optomechanical systems," arXiv:1004.3587v1 (2010).

[20] http://www.norcada.com/index.php .

[21] http://mathworld.wolfram.com/WaveEquationRectangle.html .

[22] B. M. Zwickl, W. E. Shanks, A. M. Jayich, C. Yang, A. C. B. Jayich, J. D. Thompson, and J. G. E. Harris, "High quality mechanical and optical properties of commercial silicon nitride membranes," Applied Physics Letters. **92** (2008).

[23] C. Vallance, "Innovations in cavity ringdown spectroscopy," New J. Chem **29,** 867 – 874 (2005).

[24] D. Osborn, J.Bood, and A.McIlroy, "Ultra-Sensitive absorption measurements using Cavity-Enhanced Frequency Modulation Spectroscopy," Laser applications to chemical, security and environmental analysis (LACSEA) (2006).

[25] D.J.Wilson, C.A.Regal, S.B.Papp, and H.J.Kimble, "Cavity Optomechanics with stoichiometric films," Physical Review Letters **103** (2009).

[26] P. Mohanty, D. A. Harrington, K. L. Ekinci, Y. T. Yang, M. J. Murphy, and M. L. Roukes, "Intrinsic dissipation in high frequency micromechanical resonators," Physical Review B. **66** (2002).

[27] R.Lifshitz and M.L.Roukes, "Thermoelastic damping in micro and nanomechanical systems," Physical Review B. **61,** 5600–5609 (2000).

[28] G. Cole, I.W.Rae, K.Werbach, M. Vanner, and M.Aspelmeyer, "Minimization of phonon tunneling dissipation in mechanical resonators," arXiv:1007.4948 (2010).

[29] C. Zener, "Internal Friction in Solids II. General Theory of Thermoelastic Internal Friction," Physical Review Letters **53,** 90–99 (1938).

[30] J.S.Blakemore, "Semiconducting and other major properties of gallium arsenide," J. Appl. Phys **53** (1982).

[31] S.Prasad, "Optoelectronics A deep-level LED," Nature Materials **2,** 359–360 (2003).

[32] C.Y.Chang and F.Kai, *GAAS High Speed Devices*, 1st ed. (Wiley Interscience, 1994), p. 1.

[33] J.Soderkvist and K.Hjort, "The piezoelectric effect of GaAs used for resonators and resonant sensors," Journal of Micromechanics and Microengineering **4,** 28 (1994).

[34] G.D.Cole, I.Wilson-Rae, M.R.Vanner, S.Groblacher, J.Pohl, M.Zorn, M.Weyers, A.Peters, and M.Aspelmeyer, "Megahertz monocrystalline optomechanical resonators with minimal dissipation," Micro Electro Mechanical Systems (MEMS) IEEE 23rd International Conference pp. 847–850 (2010).

[35] H.Okamoto, D.Ito, K.Onomitsu, T.Sogawa, and H.Yamaguchi, "Controlling Quality Factor in Micromechanical Resonators by Carrier Excitation," Appl. Phys. Express **2** (2009).

[36] M.S.Bahae and R.I.Epstein, "Optical Refrigeration," Nature Photonics **1** (2007).

[37] M.Aspelmeyer and K.Schwab, "Focus on Mechanical Systems at the Quantum Limit," New Journal of Physics **10** (2008).

[38] K. Hammerer, M. Aspelmeyer, E. S. Polzik, and P. Zoller, "Establishing Einstein-Poldosky-Rosen Channels between Nanomechanics and Atomic Ensembles," Physical Review Letters **102** (2009).

Appendix A

Derivation of the optomechanical coupling term

To obtain the interaction term that couples the mechanical oscillator motion to light, we assume a simple cavity geometry where one of the end mirrors(representing the mechanical resonator) is free to move. Normally in case of no length change, the Hamiltonian reads as this simple form,

$$H = \hbar\omega_c a^\dagger a \tag{A.1}$$

where ω_c is the cavity resonance frequency and $a^\dagger, a$ correspond to the photon creation and annihilation operators. ω_c can in principle be simply written in the well-known form for a Fabry-Perot cavity as $\omega_c = n2\pi c/2L$. Now introducing a small change δx to the total length of the cavity(L) due to the fluctuations of the end mirror, the Hamiltonian takes the form ,

$$H = \hbar\frac{2\pi c}{(2L + 2\delta x)} n a^\dagger a \tag{A.2}$$

With a bit of manipulation, it can be wrtitten as,

$$H = \hbar\omega_c \frac{1}{(1 + \frac{\delta x}{L})} a^\dagger a \tag{A.3}$$

Now we make the simple assumption that the perturbation is small so $1/(1+\delta x/L)$ becomes $\approx 1 - \delta x/L$, then the Hamiltonian reads as,

$$\begin{aligned} H &= \hbar\omega_c(1 - \frac{\delta x}{L}) a^\dagger a \\ &= \hbar\omega_c a^\dagger a - \hbar\omega_c \frac{\delta x}{L} a^\dagger a \end{aligned} \tag{A.4}$$

At this point we switch to the quantized picture and the displacement is written in a way as is usually done,

$$\delta x = \sqrt{\frac{\hbar}{2m\omega_m}}(b + b^\dagger) \tag{A.5}$$

where m is the effective mass of the mechanical resonator and b and $b^\dagger$ represent the annihilation and creation operators for phonon modes. Then the second term in the Hamiltonian which adds as a perturbation to the bare resonant term, can be written as,

$$H_{coupling} = -\frac{\hbar\omega_c}{L}\sqrt{\frac{\hbar}{2m\omega_m}}a^\dagger a(b+b^\dagger) \tag{A.6}$$

For simplicity we shall write $(b+b^\dagger)$ as the operator $\hat{x_m}$. We also make another assumption, namely that our light field is strong(which can be perfectly realized in experiment) and the operator for photon number can be written as a steady state term plus fluctuations $a^\dagger a = (\sqrt{n}+a_c^\dagger)(\sqrt{n}+a_c)$. Then to linearize the whole term, we neglect the nonlinear terms which come from the multiplication of fluctuations with each other. Finally we reach the rather intuitive form as follows,

$$H_{coupling} = -\frac{\hbar\omega_c}{L}\sqrt{\frac{\hbar}{2m\omega_m}}(n\hat{x}+\sqrt{n}(a_c+a_c^\dagger)\hat{x_m}) \tag{A.7}$$

We can at this point define the light position operator as $\hat{x_c} = a_c + a_c^\dagger$. The first term of the Hamiltonian is the mean displacement term. We are interested in the second term which couples the two quadratures for light and the mechanical resonator. Then I write the coupling Hamiltonian only consisting of this interesting term,

$$H_{coupling} = -\frac{\hbar\omega_c}{L}\sqrt{\frac{\hbar}{2m\omega_m}}\sqrt{n}\hat{x_c}\hat{x_m} \tag{A.8}$$

where our effective coupling constant g appears to be,

$$g = \frac{\omega_c}{L}\sqrt{\frac{\hbar}{2m\omega_m}}\sqrt{n} \tag{A.9}$$

That is actually the single photon coupling enhanced by the intracavity cavity field amplitude.

Appendix B

Shot-noise limited sensitivity

This appendix is intended to clarify how one can reach the shot noise limited sensitivity for the PDH detection scheme we will apply. We start with the two mirror cavity reflected power spectrum [18],

$$F(\omega) = \frac{r(exp(\frac{i\omega}{fsr}) - 1)}{1 - r^2 exp(\frac{i\omega}{fsr})} \tag{B.1}$$

Now we insert $\delta\omega$ instead of ω because the resonant term yields 1 in the exponential , giving no change. We are only interested in the small perturbation term for the frequency that stems from the membrane motion. Also using the approximation $e^x \approx 1 + x$ for small x, we get for the reflection function,

$$\begin{aligned} F &= \frac{r(1 + \frac{i\delta\omega}{fsr} - 1)}{1 - r^2(1 + \frac{i\delta\omega}{fsr})} \\ &= \frac{r\frac{i\delta\omega}{fsr}}{1 - r^2 - r^2\frac{i\delta\omega}{fsr}} \end{aligned} \tag{B.2}$$

We have to make yet another assumptions to make the expression look simpler. First of all $r \to 1$ and for high finesse cavities, the finesse reads $\mathcal{F} \approx \pi/(1-r^2)$ and reminding ourselves that $fsr = \delta\nu\mathcal{F}$ where $\delta\nu$ is the linewidth of the cavity, we reach for the reflection function,

$$F = \frac{\frac{ri\delta\omega}{fsr}}{\frac{(1-r^2)fsr - r^2 i\delta\omega}{fsr}} = \frac{ri\delta\omega}{\pi\delta\nu - r^2 i\delta\omega} \tag{B.3}$$

$$\approx \frac{i\delta\omega}{\pi\delta\nu - i\delta\omega} \tag{B.4}$$

And as a final remark we can claim that $\delta\omega \ll \delta\nu$ since the frequency detuning is definitely small with respect to the cavity linewidth , so the reflection function becomes as promised,

$$F \approx \frac{i\delta\omega}{\pi\delta\nu} \tag{B.5}$$